LIFE-CYCLE ASSESSMENT OF EMERGING GREENHOUSE GAS MITIGATION STRATEGIES IN THE ENERGY SECTOR

by

Kerry Elizabeth Kelly

A dissertation submitted to the faculty of
The University of Utah
in partial fulfillment of the requirements for the degree of

Doctor of Philosophy

Department of Civil and Environmental Engineering

The University of Utah

May 2015

The University of Utah Graduate School

STATEMENT OF DISSERTATION APPROVAL

The dissertation of **Kerry Elizabeth Kelly**

has been approved by the following supervisory committee members:

David W. Pershing	, Chair	**1/5/2015** Date Approved
JoAnn S. Lighty	, Member	**1/5/2015** Date Approved
John D. McLennan	, Member	**1/5/2015** Date Approved
Brian J. McPherson	, Member	**1/5/2015** Date Approved
Geoffrey D. Silcox	, Member	**1/5/2015** Date Approved

and by **Michael Barber**, Chair/Dean of the

Department/College/School of **Civil and Environmental Engineering**

and by David B. Kieda, Dean of The Graduate School.

ABSTRACT

With numerous options for mitigating CO_2 emissions, the need to address global climate change, and limited financial resources, it is essential to evaluate greenhouse gas (GHG) mitigation strategies to prioritize investments of time and capital. This research adopts a life-cycle approach toward this prioritization for three GHG mitigation strategies: (1) aqueous CO_2 mineralization, (2) oxyfiring for unconventional transportation fuels, and (3) underground coal thermal treatment (UCTT). As this research moves from strategy (1) to strategy (3), it progresses from using literature data to close collaboration with other researchers to design and perform experiments and simulations needed to assess GHG impacts. The evaluation of each strategy includes quantitative consideration of all major energy and GHG flows and a qualitative consideration of other potential barriers, i.e., resource availability and hazardous byproducts.

Commercial-scale, aqueous CO_2 mineralization involves the reaction of CO_2 with an industrial caustic or a waste containing a reactive metal oxide to form a solid mineral carbonate. The evaluation revealed that once the full-life cycle material and energy balance are considered, this technology has limited applicability at the large scale. The industrial caustic pathway has a high energy penalty (50 to > 100%) and produces toxic byproducts (chlorine gas). The reactive metal oxide/waste pathway has a lower energy penalty (10 to 20%), but its applicability is limited by the availability of wastes

containing reactive metal oxides.

Oxyfiring with CO_2 capture is one of the most promising CO_2 mitigation strategies for the fossil energy sector. Chapter 3 discusses whether oxyfiring with CO_2 could help fuels derived from oil sand and shale meet a low-carbon fuel standard. The results showed that this strategy is feasible, but it will likely place these fuels at a competitive disadvantage.

UCTT is a novel technology to heat coal in situ and produce a lower carbon content, higher heating value syngas or liquid fuel. Results indicate that UCTT has a limited potential for CO_2 mitigation because of the large energy "losses" to the coal in situ caused by the large volumes of coal that are heated to low temperatures, resulting in limited product.

I would like to dedicate this thesis to Adel F. Sarofim (deceased) and JoAnn S. Lighty who graciously, but persistently, encouraged me to pursue a PhD and enthusiastically supported me over the years. I'd also like to thank my husband, Ross Whitaker, who made me laugh when I was discouraged and even helped refresh my memory on solving differential equations.

TABLE OF CONTENTS

LIST OF TABLES

LIST OF FIGURES

ACKNOWLEDGMENTS

Many thanks to the committee members for their thoughtful contributions to this work, with particular thanks to President Pershing who continued to carve time out of his busy schedule after becoming president of the university. I would also like to thank several faculty members for their assistance: Dr. Eddings for his guidance on the UCTT experiments and their interpretation, Dr. Deo for his expertise on subsurface processes, Dr. Silcox for his guidance on heat transfer, Dr. Wendt for his expertise on oxyfiring, and Dr. Smith for his advice on yield models, encouragement, and flexibility. Thanks to Dr. Hradisky who patiently helped verify the results of the UCTT energy balance with his more sophisticated simulations and who taught me a few things about numerics, and thanks to Dr. Fry for helping us fix reactor leaks on the weekend. Finally, without Dr. Sarofim's encouragement, I would likely not have pursued a PhD. I regret that I could not finish in time for you to be here.

Several students deserve credit for their contributions including Jonathan Wilkey for his work on our oxyfiring paper and Ding Wang for his extensive experimental contributions UCTT studies. In addition, two undergraduate students, Jesse Dumas and Colin Young, assisted with my work.

Thanks to my husband, Ross Whitaker, for his encouragement and ability to make me laugh, and even technical advice – the advantage of being married to a professor. Thanks to my Dad, Tom Kelly, and my Mom, Gail Kelly (deceased), for their support.

I also wanted to thank my Grandmother, Grace Kelly, who graduated from the University of Illinois in microbiology during the depression, lived to 100 years old, and always encouraged her granddaughters to excel in science. I'm happy to be your third granddaughter with a PhD.

Some portions of this work were supported by the Department of Energy under Award Number DE-FE0001243, DE-NT0050015, and DE-NA0000740. The views and opinions of authors expressed herein do not necessarily state or reflect those of the United States Government or any agency thereof.

CHAPTER 1

INTRODUCTION

Life-cycle assessment (LCA) is an important tool for evaluation of the most promising emerging energy technologies. The example of corn ethanol illustrates the importance of considering a product's complete life cycle before implementing policies to encourage its adoption. Initially, conversion of petroleum-based transportation fuels to corn ethanol was encouraged, in part, because of corn ethanol's perceived reduction in GHG emissions. However, as researchers began considering the full life cycle of corn ethanol, they found relatively small reductions in greenhouse gas (GHG) emissions (Wang et al. 2007) or a net increase in GHG emissions (Searchinger et al. 2008). Incentives for corn ethanol production remain controversial, and the GHG emissions associated with land-use change continue to be debated (Carter and Miller 2012).

This research focused on the application of LCA to three emerging GHG mitigation strategies: (1) aqueous CO_2 mineralization, (2) oxyfiring for unconventional transportation fuels, and (3) underground coal thermal treatment (UCTT). As the research progressed from strategy (1) to strategy (3), the level of involvement increased in terms of experimental design, data collection, and simulation development. Commercial-scale, aqueous CO_2 mineralization (strategy 1) is discussed in Chapter 2 and involves the reaction of CO_2 of with an industrial caustic, i.e., NaOH, or a waste

containing a reactive metal oxide, i.e., coal fly ash or cement-kiln dust, to form a solid mineral carbonate. The process has the potential to produce beneficial byproducts and permanent CO_2 storage. Oxyfiring with CO_2 capture (strategy 2) is one of the most promising CO_2 mitigation strategies for the fossil energy sector, and its evaluation for use with unconventional petroleum resources is discussed in Chapter 3. Instead of combusting a fuel in air, the fuel is combusted in oxygen, and the energy-penalty associated with air separation is an important consideration. UCTT (strategy 3) is a novel technology to heat coal in situ and produce a lower carbon content, higher heating value syngas or liquid fuel. The evaluation grew out of close collaboration with the experimentalists to access the energy and GHG balances of a potential full-scale process.

1.1 Goals

The goals of this research were to:

- Estimate the life-cycle energy requirements and GHG emissions for several emerging greenhouse gas mitigation strategies;
- Identify critical process steps for each strategy, understand the sensitivity of each evaluation to the underlying assumptions, and determine likely bounds on associated GHG emissions and energy requirements;
- For the UCTT evaluation and through close collaboration with experimentalists, design experiments, and identify and collect key experimental results; and
- Suggest opportunities for reducing the GHG emissions and energy requirements of a UCTT process.

1.2 LCA background

LCA is a technique to assess the comprehensive environmental impacts associated with a product, process, or service, by:

- Compiling an inventory of relevant energy and material inputs and environmental releases;
- Evaluating the potential environmental impacts associated with inputs and releases; and
- Interpreting the results to help make a more informed decision (US EPA 2006).

It is a systematic approach to evaluating environmental burdens from different stages/locations. A product's life cycle refers to the major activities in the course of its lifetime, and it is divided into the following stages: material extraction, product manufacture, use, maintenance, and final disposal. LCA helps avoid shifting environmental burdens from one stage to another. Figure 1.1 illustrates a product's typical life cycle, its life-cycle stages, and its inputs and outputs. This research employs different system boundaries for each of the strategies evaluated, and these are discussed in Chapters 2 - 4.

An LCA has four interdependent steps (ISO 14040 and ISO 14044):

- Goal, definition, and scoping – This step includes the development of an explicit goal for the study and its audience. It also includes the definition of: the functional unit or basis (which will enable the comparison with other alternatives), the system boundaries, the assumptions, and the methods to partition the environmental burdens of a process with multiple

products (Rebitzer et al. 2004).

- The life-cycle inventory – This step includes an accounting of the flows to and from the product system such as water, energy, and raw materials, as well as releases to air, land, and water. It is typically the most labor-intensive step of an LCA, and it can be challenging because of the lack of publicly available data and lack of detail about the conditions and underlying assumptions in the available data. This research focuses primarily on energy and GHG inputs and outputs, although it does identify other significant environmental burdens.
- Impact assessment – This step evaluates the importance of the inventory results. This research focuses primarily on energy and GHG emissions; consequently, the assessment is more straightforward than attempting to compare the other more disparate impacts, such as water consumption and releases of ozone-depleting chemicals.
- Interpretation – This step includes the evaluation of the results and impact assessment, such as the identification of data gaps, weaknesses, sensitivity, and consistency with other studies.

There are typically two types of LCAs, a process-based LCA (EPA 2006) and an economic input-output-based LCA (Henrickson et al. 2006). The process-based LCA is well suited to individual or developing processes, and is adopted in this research. However, this type of LCA can be labor intensive, and an alternative is the economic input-output-based LCA, which considers the entire economy and industry sectors. It uses economic input-output data produced by national governments to quantify material

and energy consumed as well as releases by industry sectors to estimate life-cycle impacts.

1.3 Application of LCA to energy systems

LCA has been applied to numerous commonly used and emerging energy-related technologies. Examples include conventional sources of crude oil (Gerdes and Skone 2009), Canadian oil sands (McKellar et al. 2009), transportation fuel from algae (Frank et al. 2012) and oil shale (Brandt 2009), and electricity generation (Spath et al. 1999, Stoppato 2008). One of the most well-known LCA tools in the US is Argonne National Laboratory's publicly available GREET model (ANL 2014). This model is used to evaluate well-to-wheel and well-to-tank criteria-pollutant and GHG emissions associated with advanced vehicle technologies, new transportation fuels, and related energy processes (e.g., Frank et al. 2012; Clark et al. 2012). GREET is intended to reflect US average conditions, crude inputs, and energy requirements.

For emerging energy-related technologies, the results of LCAs can be highly uncertain, but as processes become better defined, uncertainty decreases. For example, McKellar et al. (2009) compare several well-to-tank LCAs for Canadian oil sands and for oil shale. Ex situ production of reformulated gasoline from Canadian oil sands generates 27 – 35 g CO_2 e/MJ, whereas production of the same product from oil shale generates 46 – 180 g CO_2 e/MJ fuel. It can also be challenging to compare the results of different LCAs for the same product because study boundaries (what activities are and are not included) and functional units often differ. However, LCA can be a useful tool in the evaluation of an emerging energy technology because it can identify potential barriers to

the process and opportunities for process improvement, as well as helping to prioritize different technologies.

1.4 References

ANL (Argonne National Laboratory). 2014. The Greenhouse Gases, Regulated Emissions, and Energy Use in Transportation (GREET) Model, GREET 1 2014.

Brandt A.R. 2009. Converting oil shale to liquid fuels with the Alberta Taciuk processor: energy inputs and greenhouse gas emissions. Energ. Fuel 23, 6253-6258.

Carter, C.A., Miller, H.I. 2012. Corn for food, not for fuel. *New York Times*. July 30, 2012.

Clark, C.E., Han, J., Burnham, A., Dunn, J.B., Wang, M. 2012. Life-Cycle Analysis of Shale Gas and Natural Gas. Technical Report ANL/ESD/11-11. Energy Systems Division, Argonne National Laboratory.

Frank, E.D., Elgowainy, A., Han, J., Wang, Z. 2013. Life cycle comparison of hydrothermal liquefaction and lipid extraction pathways to renewable diesel from algae. Mitig. Adapt. Strat. Gl. 18(1), 137-158.

Gerdes, K.J., Skone, T.J. 2009. An Evaluation of the Extraction, Transport and Refining of Imported Crude Oils and the Impact on Life Cycle Greenhouse Gas Emissions. Technical Report for the US Department of Energy, DOE/NETL-2009/1362.

ISO 14040. 2006. Environmental management – Life cycle assessment – Principles and framework. International Organisation for Standardisation (ISO): Geneve, Switzerland.

ISO 14044. 2006. Environmental management – Life cycle assessment – Requirements and guidelines. International Organisation for Standardisation (ISO): Geneve, Switzerland.

Hendrickson, C.T., Lave, L.B., Matthews, H.S. 2006. Environmental Life Cycle Assessment of Goods and Services: An Input-Output Approach. Resources for the Future Press: Washington, ISBN 1-933115-24-6.

McKellar, J.M., Charpentier, A.D., Bergerson, J.A., MacLean, H.L. 2009. A life cycle greenhouse gas emissions perspective on liquid fuels from unconventional Canadian and US fossil sources. Int. J. of Global Warm. 1(1/2/3), 160-178.

Rebitzer, G., Ekvall, T., Frischknecht, R., Hunkeler, D., Norris, G., Rydberg, T., Schmidt, W.P., Suh, S., Weidema, B.P., Pennington, D.W. 2004. Life cycle

assessment part 1: framework, goal and scope definition, inventory analysis, and applications. Environ. Int. 30, 701-720.

Searchinger, T., Heimlich, R., Houghton, R.A., Dong, F., Amani, E., Fabiosa, J., Tokgoz, S., Dermot, H., Yu, T.H. 2008. Use of U.S. croplands for biofuels increases greenhouse gases through emissions from land-use change. Science 319 (5867), 1238-1240.

Spath, P.L., Mann, M.K., Kerr, D.R. 1999. Life Cycle Assessment of Coal-fired Power Production. Technical Report NREL/TP-570-25119 for US Department of Energy, National Renewable Energy Laboratory: Golden, CO.

Stoppato, A. 2008. Life cycle assessment of photovoltaic electricity generation. Energy 33, 224-232.

US Environmental Protection Agency (US EPA) 2006. Life Cycle Assessment: Principles and Practice. National Risk Management Research Laboratory. Technical report EPA/600/R-06/060, Office of Research and Development: Cincinnati, OH.

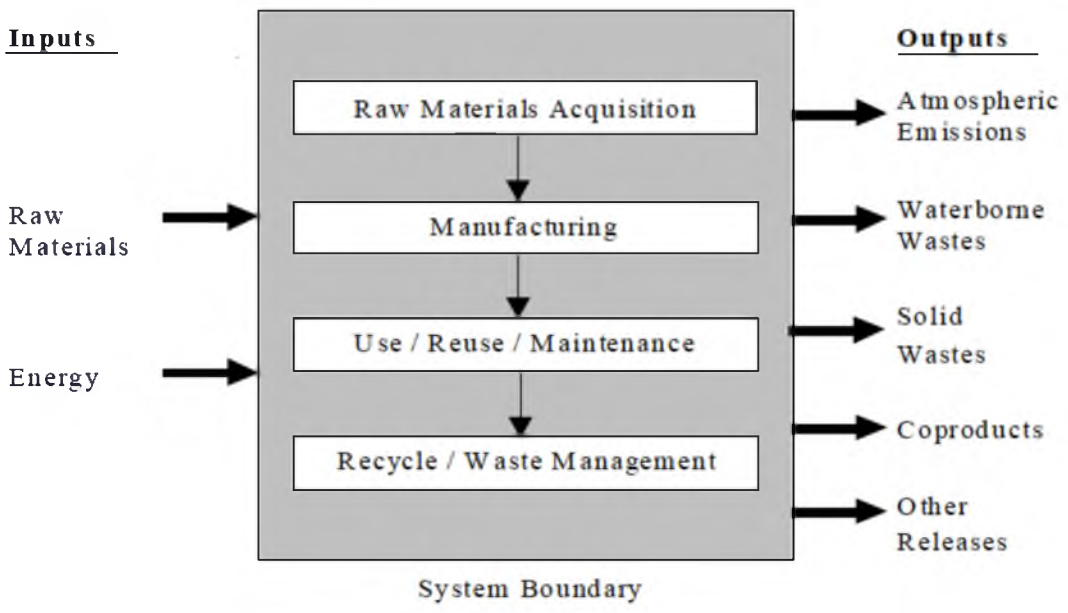

Figure 1.1 Typical cradle-to-grave life-cycle stages (EPA 2006).

CHAPTER 2

AN EVALUATION OF EX SITU, INDUSTRIAL-SCALE AQUEOUS CO_2 MINERALIZATION

International Journal of Greenhouse Gas Control 5 (2011) 1587–1595. An Evaluation of Ex Situ, Industrial-Scale Aqueous CO_2 Mineralization. K.E. Kelly, G.D. Silcox, A.F. Sarofim, D.W. Pershing

International Journal of Greenhouse Gas Control 5 (2011) 1587–1595

Contents lists available at SciVerse ScienceDirect

International Journal of Greenhouse Gas Control

journal homepage: www.elsevier.com/locate/ijggc

An evaluation of ex situ, industrial-scale, aqueous CO_2 mineralization

K.E. Kelly[a,*], G.D. Silcox[b], A.F. Sarofim[b], D.W. Pershing[b]

[a] Institute for Clean and Secure Energy, 380 INSCC, 155 South 1453 East, University of Utah, Salt Lake City, UT 84112, USA
[b] Department of Chemical Engineering, Institute for Clean and Secure Energy, 155 South 1453 East, University of Utah, UT 84112, USA

ARTICLE INFO

Article history:
Received 17 May 2011
Received in revised form 7 September 2011
Accepted 26 September 2011
Available online 20 October 2011

Keywords:
Mineral carbonation
CO_2 mineralization
Permanent carbon sequestration
Beneficial use of CO_2

ABSTRACT

It is essential to objectively evaluate the many CO_2 mitigation strategies in order to prioritize investments of capital and research. Aqueous CO_2 mineralization is one potential strategy to permanently sequester CO_2, without the associated long-term monitoring and liability issues. Investigators are studying and optimizing aqueous CO_2 mineralization for the production of inorganic carbonates and are scaling up some of these processes. This paper adopts a life-cycle approach toward the evaluation of energy requirements and discusses other potential barriers for three CO_2 mineralization pathways: industrial caustics, naturally occurring minerals, and industrial wastes. This analysis is based on CO_2 capture from a 1 GW coal-fired power plant using one of the three mineral mineralization pathways. The investigators utilize consistent system boundaries and process-modeling assumptions, standard engineering calculations to estimate energy requirements, and publicly available data for upstream energy requirements and for the production of products/co-products. The results suggest that some industrial wastes show promise for CO_2 mineralization, but their availability is limited. The other pathways currently have large energy penalties and face other significant barriers, such as the production of large quantities of potentially hazardous waste and large-scale mining.

1. Introduction

The United States (US) produced 5839 million tonnes CO_2 in 2008 (EIA, 2009), and carbon capture and storage (CCS) is one of several proposed strategies for reducing US and world greenhouse gas emissions (EPRI, 2009). It entails capturing a relatively pure CO_2 stream from an industrial source, such as a fossil-fuel power plant, transporting it to a storage location, and the long-term storage of the CO_2, in locations such as deep geological formations (IPCC, 2005). CCS offers the potential for continued use of fossil fuels with reduced CO_2 emissions, and a variety of CCS demonstration projects are currently underway (Herzog, 2011). However, the sequestration of CO_2 in geological formations faces a number of challenges including public perception, the potential for CO_2 escape, the requirement for long-term site monitoring and liability (Wilson et al., 2008; Herzog, 2011; IPCC, 2005). Consequently, aqueous mineral carbonation has been proposed as a strategy to permanently sequester CO_2 and even to potentially produce beneficial products, without the associated long-term monitoring and liability issues.

Several research groups are studying and optimizing aqueous-phase CO_2 mineralization for the production of inorganic mineral carbonates and are beginning to scale up the some of these proposed processes (Gerdemann et al., 2007; Reddy et al., 2010; EPRI, 2007). Some of these results have attracted industry and government investment. For example, the US DOE recently invested $119 million to test innovative concepts for the beneficial use of CO_2 including inorganic mineral carbonates, building materials, and soil amendments (US DOE, 2010a,b). Zevenhoven et al. (2006) discuss the use of anthropogenic CO_2 emissions as resources for the production of mineral carbonates and other beneficial products, and summarize the world markets for a number of inorganic carbonates.

Given the variety of options for mitigating CO_2 emissions, the need for rapid action to address global climate change, and limited financial resources, it is essential to objectively evaluate these options and to prioritize investment strategies. One challenge in evaluating CO_2 mineralization is that few studies report mass and energy balances or discuss potentially significant environmental impacts, such as large-scale mining disposal of the resulting solid material (CSLF, 2010). This paper takes a step toward this evaluation and presents preliminary bounds for an energy balance for three CO_2 mineralization pathways: industrial caustics, naturally occurring minerals, and industrial wastes. It attempts to apply consistent system boundaries and to fairly evaluate process products and co-products for an industrial-scale CO_2 mineralization process.

* Corresponding author. Tel.: +1 801 587 7601; fax: +1 801 585 1456.
E-mail address: Kerry.kelly@utah.edu (K.E. Kelly).

1750-5836/$ – see front matter © 2011 Elsevier Ltd. All rights reserved.
doi:10.1016/j.ijggc.2011.09.005

1.1. Industrial caustics

Two CO_2 mineralization processes have recently been proposed that are based on the industrial caustic sodium hydroxide. One yields sodium bicarbonate (EPRI, 2007) and is given by reactions (1) and (2), where the $\Delta H_{reaction}$ at standard temperature and pressure is presented in parentheses.

$$CO_2 + H_2O \rightarrow H_2CO_3 \quad (1)$$
$$\underline{H_2CO_3 + NaOH \rightarrow NaHCO_3 + H_2O} \quad (2)$$
$$CO_2 + NaOH \rightarrow NaHCO_3 \quad (-101\ kJ/mol)$$

The other involves a brine solution containing calcium and/or magnesium ions and yields calcium or magnesium carbonates as shown in the following reaction (Constantz, 2009).

$$CO_2 + 2NaOH + Ca^{2+} \rightarrow CaCO_3 + H_2O + 2Na^{+} \quad (-196\ kJ/mol) \quad (3)$$

In order for reaction (3) to proceed to an appreciable extent, the pH must be greater than 9 in a brine solution (Druckenmiller and Maroto-Valer, 2005).

Reactions (1)–(3) are exothermic and proceed rapidly to completion. However, they both rely on sodium hydroxide, which is produced by the energy-intensive chlor-alkali reaction process:

$$NaCl + H_2O \rightarrow 0.5Cl_2 + 0.5H_2 + NaOH \quad (+223\ kJ/mol) \quad (4)$$

Because these mineralization processes are being commercialized, publicly available material and energy data are limited. However, this pathway can be evaluated using publicly available life-cycle inventory data and some estimates of theoretical minimum work requirements.

1.2. Naturally occurring minerals

Naturally occurring mineral silicates are another pathway to CO_2 mineralization, as initially discussed by Seifritz (1990), Dunsmore (1992), and Lackner et al. (1995). Olivine, serpentine, and wollastonite are naturally occurring magnesium silicate compounds that react exothermically with CO_2 to form carbonates. These minerals are available in sufficient quantities to allow for CO_2 mineralization of current fossil-fuel reserves (Zevenhoven et al., 2006; IPCC, 2005), and these ores are inexpensive, approximately $20/tonne (Gerdemann et al., 2007). One example of this reaction (for a pure form of olivine, fosterite) is given by:

$$Mg_2SiO_4 + 2CO_2 \rightarrow 2MgCO_3 + SiO_2 \quad (-95\ kJ/mol) \quad (5)$$

Although the reaction of CO_2 with magnesium silicates is exothermic, it occurs slowly in nature, over a period of thousands of years. In order to identify more favorable kinetic conditions, Gerdemann et al. (2007) performed over 700 kinetic studies of mineral carbonation of olivine, serpentine, and wollastonite at varying temperatures, partial pressures of CO_2, solution chemistries, particle sizes, and pretreatment conditions. For the most promising conditions, they performed a feasibility study using ASPEN to estimate capital and operating costs. Huijgen et al. (2006) also performed process modeling for mineral carbonation of wollastonite ($CaSiO_3$) to estimate energy requirements and net CO_2 reduction. These studies concluded that mineral carbonation with naturally occurring minerals can be part of an integrated strategy for carbon sequestration.

1.3. Industrial wastes that contain reactive oxides

A number of industrial wastes contain significant fractions of reactive metal oxides, in particular CaO and MgO, that will react to form mineral carbonates as in the following example:

$$CaO + H_2O \rightarrow Ca(OH)_2 \quad (6)$$
$$\underline{Ca(OH)_2 + CO_2 \rightarrow CaCO_3 + H_2O} \quad (7)$$
$$CaO + CO_2 \rightarrow CaCO_3 \quad (-179\ kJ/mol)$$

These reactions of CO_2 with metal oxides are exothermic. Consequently, some industrial wastes have been proposed for their potential in CO_2 mineralization including coal fly ash (Soong et al., 2006; Fernández Bertos et al., 2004; Montes-Hernandez et al., 2009; Reddy et al., 2010), steel/iron/blast furnace slag (Huijgen et al., 2006; Stolaroff et al., 2005; Eloneva et al., 2008), waste cement (Stolaroff et al., 2005; Iizuka et al., 2004), asbestos mine tailings, electrical arc furnace waste, cement kiln dust (Huntzinger et al., 2009; Gunning et al., 2010), lime kiln dust, paper ash, bauxite residue (Sahu et al., 2010; Bonenfant et al., 2008; US DOE, 2010c) and others. Gunning et al. (2010) studied 10 sources of industrial waste for suitability for CO_2 mineralization. The majority of these studies were performed at the laboratory scale, although Reddy et al. (2010) studied mineral carbonization of fly ash at the pilot scale. Fernández Bertos et al. (2004) and Gunning et al. (2010) found that the most reactive wastes tended to be those containing high concentrations of CaO, MgO, Na_2O, and K_2O. The theoretical maximum CO_2 uptake capacity of a waste can be estimated from the chemical composition of the waste using the Steinour formula (Steinour, 1959), in which the concentration of each species of interest is entered as a weight percent.

$$CO_2(\%) = 0.785(CaO - 0.7SO_3) + 1.091MgO + 2.09Na_2O + 0.93K_2O \quad (8)$$

2. Materials and methods

The following analysis is intended to provide bounds for energy use and is based on publicly available data. The basis for this evaluation is a theoretical 1 GW coal-fired power plant emitting 8×10^6 tonne CO_2/yr, which is captured by one of the three mineral carbonation pathways. The coal for this theoretical plant has a heating value of 30,000 kJ/kg, an ash content of 10% and a carbon content of 72.5%. The plant is 35% efficient, which is slightly higher than the 33% average efficiency of coal-fired power plants in the US (EIA, 2010). Several of the proposed pathways produce potentially valuable products/co-products, and this analysis includes an energy value for the products and co-products.

The evaluation includes major energy-consuming processes for each pathway, such as separation of CO_2 from the power plant flue gas, pumping of the liquids and slurries, compressors, mixers, and heaters. The blower energy requirement is not included because it is insignificant compared to other processes. For processes that are common across the three pathways, Table 1 summarizes assumptions associated with the low and high estimates. Assumptions that are only relevant to a single pathway are discussed in the each of the following sections. This analysis is a gate-to-gate estimation; it begins with flue gas entering the process and continues through the production of products or materials for disposal. It does not include the energy associated with the operation of the coal-fired power plant, mining of coal, the construction of the power or mineral carbonation plants, or the transportation of products.

Table 1
Assumptions used to obtain energy requirements for high and low cases that are common to more than one pathway.

Unit	Low	High
CO_2 separation	16.7% energy penalty[a]	16.7% energy penalty[a]
Pump	80% efficiency	80% efficiency
Compressor	Isothermal, 80% efficiency	Adiabatic, 80% efficiency
Mixing	10 rpm, N_p = 0.31, 80% efficiency, impeller diameter 1/4 of reactor dimension, assuming a cube	30 rpm, N_p = 1.27, 80% efficiency, impeller diameter 1/4 of reactor dimension, assuming a cube
Heating	80% efficiency	80% efficiency

N_p: Power number of the impeller.
[a] Katzer et al. (2007), assumes a sub-critical pulverized coal power plant using amine scrubbing for 90% CO_2 separation.

2.1. Industrial caustics and brine

Fig. 1 illustrates a simplified flow diagram of a theoretical industrial caustic pathway for the production of both calcium/magnesium carbonates and sodium bicarbonate. It shows the processes, inputs, products, and system boundaries that are included in the analysis. The analysis assumes complete conversion of the CO_2 to either calcium/magnesium carbonates or sodium bicarbonate. This pathway does not require the separation of CO_2 from flue gas.

One challenge for the evaluation of this pathway is the allocation of energy requirements between sodium hydroxide and the three potential co-products from the chlor-alkali process: hydrogen, chlorine, and hydrochloric acid. This can done on a monetary value basis (Guinée, 2002). Because of the massive scale of CO_2 emissions, the adoption of this process for even one large coal-fired power plant could drastically reduce the monetary value of chlorine and hydrochloric acid. The production of 1 mol of sodium bicarbonate requires 1 mol of sodium hydroxide, and the production of 1 mol of calcium/magnesium carbonates requires 2 mol of sodium hydroxide. This results in the production ½–1 mol of chlorine gas (Cl_2) (or 1–2 mol of hydrochloric acid) for each mole of CO_2 mineralized. Consequently, the CO_2 emissions from a 1 GW coal-fired plant (8×10^6 tonne CO_2/yr) would result in chlorine production equaling 12–24% of world Cl_2 demand (World Chlorine Council, 2011). Widespread adoption of this pathway would generate vast quantities of chlorine or hydrochloric acid wastes.

The lower bound of energy required to produce sodium hydroxide is based on a Gibbs free energy minimum work calculation and the allocation of energy between sodium hydroxide, chlorine, hydrogen, and hydrochloric acid (see Supplementary data, Sections S.1 and S.2, for details). Briefly, the production of sodium hydroxide to mineralize all of the CO_2 from the theoretical 1 GW plant requires a minimum of 2.4 GW of energy. This energy can be allocated to the two products of value (sodium hydroxide and hydrogen). One kg of product from the chlor-alkali process contains approximately 0.523 kg sodium hydroxide, 0.464 kg chlorine gas, and 0.0131 kg hydrogen gas. Sodium hydroxide has a value of approximately $440/tonne (ICIS, 2011), and hydrogen has a value of approximately $18,500/tonne (National Hydrogen Association, 2010). Allocating the minimum work to sodium hydroxide yields 1.17 GW of energy required for the theoretical 1 GW power plant.

Alternatively, the hydrogen and chlorine gas can react to form hydrochloric acid and produce energy:

$$H_{2(g)} + Cl_{2(g)} \rightarrow HCl \quad (9)$$

On the 1 GW basis, this reaction releases 1.5 GW and results in a net minimum energy requirement of 0.9 GW (details in Supplementary data, Section S.1). Hydrochloric acid is a waste and assumed to have no value. In fact treatment and disposal of this waste would incur a cost.

For sodium hydroxide production, the upper bound of the life-cycle energy requirement is 6.9 MJ/kg chlor-alkali product (US DOE, 2011a), and this was apportioned on the same mass-adjusted monetary value basis as described for the minimum work calculation (see Supplementary data, Section S.2). This results in an upper-bound energy requirement of 3.4 MJ/kg sodium hydroxide (1.5 GW for the 1 GW power plant).

The same procedure is applied to estimate the energy requirements for the production of sodium bicarbonate to produce sodium hydroxide (Supplementary data, Section S.4).

The brine flowrate is another key factor in the evaluation of this pathway. It affects the energy requirements for mixing and pumping as well as the size of process equipment. The required brine flowrate is based on the concentration of alkali-earth ions (Ca^{2+} and Mg^{2+}) in Dead Sea brine (4.59 and 1.76 wt%, respectively, low-energy estimate, Ma'or et al., 2006) and in seawater (0.04 and 0.13 wt%, respectively, high-energy estimate, Snoeyink and Jenkins, 1980). All of the calcium and magnesium ions are assumed to react to form products. The reactor volume is estimated using a range of liquid residence times from 5 to 30 min. The pumping requirement is based on head losses equivalent to 10 m (low) and 100 m (high).

Drying of the carbonate product is assumed to utilize low-grade heat from the power plant and to require no additional energy. The energy value for calcium/magnesium carbonates produced via this pathway is estimated at 0.073 MJ/kg based on the energy requirements for limestone mining, crushing and transportation (US DOE, 2011b).

Drying of the sodium bicarbonate product is also assumed to utilize low-grade heat from the power plant. In order to assess the value of the sodium bicarbonate product, one can consider its manufacturing process. Sodium bicarbonate is commonly produced in conjunction with soda ash. In the US, soda ash and sodium bicarbonate are typically produced from natural sources, and in Europe and Asia the Solvay process is typically employed. The lower-bound energy value for this product is estimated using a minimum work calculation for sodium bicarbonate production by the Solvay process (Supplementary data, Section S.5) to be 0.225 MJ/kg (58 MW on the 1 GW plant basis). The upper-bound energy value for the sodium bicarbonate product is estimated from the average energy required to mine and purify potash, soda ash and borate (0.33 MJ/kg, US DOE (2002) and 85 MW on a 1 GW plant basis). The world market for sodium bicarbonate is approximately 2.5 million tonnes/yr (Eurasian Chemical Market, 2011), and its current applications include cleaning productions, animal feed, cooking, pharmaceuticals, specialty chemicals, and fire suppression (SRI, 2009). The theoretical 1 GW power plant would produce of 6.4 million tonnes/yr of sodium bicarbonate, which would exceed current world demand. The adoption of this process for one or more power plants would likely reduce the world price for sodium bicarbonate, and this product is assumed to be a waste with no value. However, it possible that additional or expanded beneficial uses for this product could be identified, and Section S.5 illustrates how the energy value for sodium bicarbonate is estimated.

2.2. Naturally occurring minerals

Fig. 2 shows a simplified process diagram for this pathway. In order to achieve reasonable reactions rates and conversions, this pathway requires the separation of CO_2 from a flue gas stream as input and a reaction at elevated temperature and pressure. Huijgen et al. (2006) and Gerdemann et al. (2007) estimate process energy requirements for mineral carbonization with wollastonite and olivine, two of the most promising mineral silicate candidates. They assume that the mining and product disposition occurs onsite.

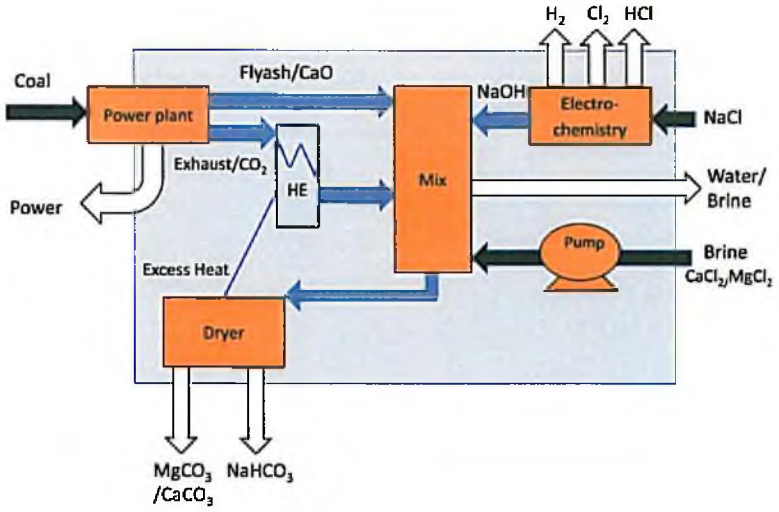

Fig. 1. Simplified process flow diagram for the production of $Ca/MgCO_3$ or $NaHCO_3$ from industrial caustics. It shows the processes evaluated (noted as orange boxes), material inputs (black arrows), products (white arrows) and system boundaries that are included in the analysis. HE: heat exchanger. (For interpretation of the references to color in this figure legend, the reader is referred to the web version of the article.)

Table 2
Reaction conditions based on experimental studies.[a,b].

	$CaSiO_3$ (wt%)	Mg_2SiO_4 (wt%)	Temperature (°C)	L/S	P (bar)	Residence time	Carb (%)	Tonne ore/tonne CO_2 seq
Olivine		100	185	3.33	152	2 h	100	1.8
Wollastonite	84.4		200	2.5	35.5	2–30 min	75	4.5

L/S: liquid to solid ratio on a mass basis.
[a] Huijgen et al. (2006).
[b] Gerdemann et al. (2007).

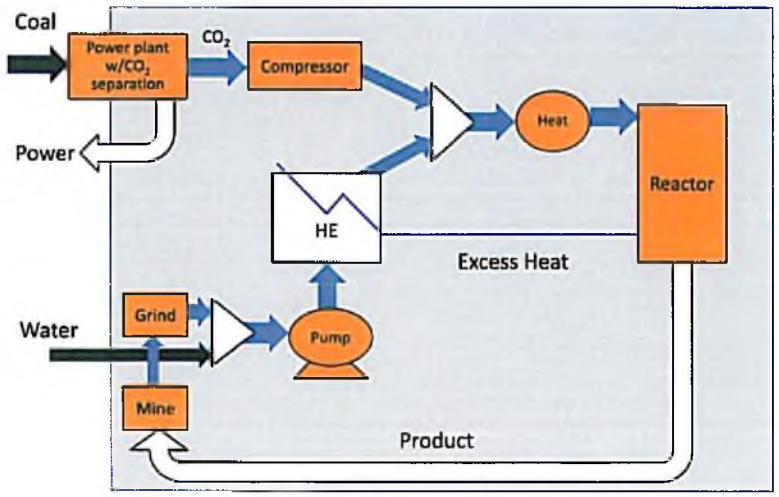

Fig. 2. Simplified process flow diagram showing mineral carbonation with naturally occurring minerals (based on Huijgen et al., 2005). It shows the processes evaluated (noted as orange boxes), material inputs (black arrows) products (white arrows) and system boundaries that are included in the analysis. HE: heat exchanger. (For interpretation of the references to color in this figure legend, the reader is referred to the web version of the article.)

Their estimates include crushing/grinding, pumping, compression, heating, and other ancillary processes. Both studies identify grinding as an important process step and a major contributor to the overall energy requirement for this pathway. Their analysis did not include mining of the mineral, transportation, or CO_2 separation. Table 2 shows the key conditions of their theoretical mineral carbonation processes.

For the same process conditions, our estimates of energy requirements for compression, pumping and heating agree within 10% of Huijgen's results (Huijgen et al., 2006). The wollastonite energy requirements are then adjusted to achieve 100% carbonation, assuming that additional material will be pumped, heated, and reacted, and the compressed gas is recycled with minimal additional energy required. The olivine process energy requirements are estimated using the same assumptions. For both processes, we assume that excess energy from the power plant or the mineralization system is used to heat the slurry to 185 °C. Achieving higher temperatures, requires supplemental heat. For the wollastonite process, Huijgen's estimates include energy recovery from the carbonation step (Eq. (5)), but it is unclear whether this energy could be easily recovered (Huijgen et al., 2006).

To facilitate comparison of this pathway with other pathways, we included two potentially significant process steps, CO_2 separation and mining, within the system boundaries (Fig. 2). We assume a uniform energy penalty of 167 MW for separation of CO_2 from the flue gas (Katzer et al., 2007). For mining energy requirements, the lower estimate is based on limestone mining 12.3 kWh/tonne ore mined (79.7–199 MJ/tonne CO_2 sequestered), and the upper estimate is based on copper mining of 22.2 kWh/tonne ore mined (144–360 MJ/tonne CO_2 sequestered) (US DOE, 2002).

2.3. Industrial wastes

Although numerous industrial wastes have been proposed for CO_2 mineralization, most have been investigated only at the laboratory scale (i.e., Baciocchi et al., 2010; Fernández Bertos et al., 2004; Gunning et al., 2010; Huntzinger et al., 2009; Montes-Hernandez et al., 2009). Table 3 presents annual US production of several wastes that contain calcium and magnesium oxides and their concentration ranges. This list is not exhaustive but provides an indication of the scale of potentially useful wastes in the US. This analysis focuses on two wastes, fly ash and iron slag, for which process or pilot-scale data are available. For both wastes, we assumed that the carbonated mineral is disposed on site and does not require transportation. Table 4 provides the process conditions. The energy requirements are adjusted to 100% carbonation for comparison purposes.

2.3.1. Iron slag

The conditions are based on the work of Huijgen et al. (2006) who evaluated the mineral carbonation of steel slag experimentally and via ASPEN process modeling. The slag contains 56.8% $CaSiO_3$, 7.7% $CaCO_3$, and 35.5% FeO. Their process requires grinding of the slag to an average particle size <38 μm, mixing the slag with water (5:1 or 2:1, L/S, liquid to solid ratio on a mass basis), preheating the mixture, and pumping the mixture into a heated pressure vessel (35.5 bar and 200 °C). The difference between the low and high cases is a L/S ratio of 2:1 and 5:1, respectively. This process requires CO_2 separation.

2.3.2. Fly ash

The estimates are based upon the recent pilot study of CO_2 mineralization using a slipstream of the flue gas from the Jim Bridger power plant, which contains 12–13.6% CO_2 (Reddy et al., 2010). The flue gas passes through a 3.7 m high fluidized-bed reactor containing fly ash from the plant; the reactor operates at 60 °C and at a gas flowrate of 0.142 m^3/s. The fly ash contains 3.85% MgO and 7.5% CaO. The authors report that after 1.5–2 h of reaction, the mineralization capacity of the ash is not fully depleted. Our estimate did not include energy for solids handling.

3. Results

Table 5 summarizes the range of energy requirements for each pathway for CO_2 capture from a theoretical 1 GW power plant. It does not include energy recovery from the carbonation reaction.

3.1. Industrial caustics and brine

The net energy penalty for producing the sodium bicarbonate product via the industrial caustic pathway ranges from 45% to 78%. The main difference between the lower and upper bound energy requirement is the sodium hydroxide production estimate, with the lower estimate based on the minimum work calculation (Supplementary data, Section S.1) and the upper estimate based on life-cycle data for sodium hydroxide production (US DOE, 2011a).

The production of calcium/magnesium carbonates via the industrial caustic pathway has a large energy penalty, greater than 90% using a minimum-work calculation for sodium hydroxide production and a brine concentration corresponding to that in the Dead Sea. The upper-bound energy requirement bound is based on publicly available life-cycle energy requirements for sodium hydroxide production (US DOE, 2011a) and brine concentration corresponding to that in seawater.

3.2. Naturally occurring mineral pathway

Table 5 shows energy requirements for two of the more promising magnesium silicates for mineral carbonation, olivine (based on Gerdemann et al., 2007) and wollastonite (based on Huijgen et al., 2006). Both of these pathways require CO_2 separation, mining and grinding of the ore, reaction at elevated temperature and pressure, and relatively long reaction times. This results in an energy penalty of 55% (low estimate for olivine) to greater than 100% (wallastonite).

3.3. Industrial wastes

The two wastes included in this analysis use quiet different process to achieve mineralization and illustrate the wide range of energy penalties. The Fe slag is ground and reacts with CO_2, which has been separated from flue gas, at elevated temperatures and pressures (Huijgen et al., 2006). The process is designed to achieve 67% carbonation in 2 h. However, when one includes the energy required to mine the ore and to separate CO_2 from the power plant's flue gas, this process would have more than a 100% energy penalty.

The CO_2 mineralization process with fly ash described by Reddy et al. (2010) employs a fluidized bed, flue gas, and operates at lower temperatures and near ambient pressure. This process achieves approximately 30% carbonation in a few seconds. Its energy penalty is the most favorable among those evaluated, ranging from 9 to 22%.

4. Discussion

4.1. Industrial caustics and brine

The energy balance for the production of sodium bicarbonate is more favorable (45–78% penalty) than that for the production of calcium or magnesium carbonates (90–100+% penalty), primarily because sodium bicarbonate requires half the amount of sodium hydroxide (or other industrial caustics) compared to calcium or

Table 3
Annual production of selected US wastes that contain reactive oxides.

Waste	US production (tonne/yr)	Composition range (%)	Composition average (%)	Average (tonne/yr)[a]	Average plant (tonne/yr)[b]
Lime kiln dust	3.0×10^{6}[c]				
CaO			50[c]	1.5×10^{6}[d]	4.0×10^{4}
Fly ash	1.2×10^{8}[e]				
CaO		1–40[f]	16[g]	1.9×10^{7}	2.4×10^{4}
Cement kiln dust	1.4×10^{7}[h]				
CaO		11–45[i]	28	3.8×10^{6}[j]	2.8×10^{4}
MgO		0.4–2[i]	1	1.6×10^{5}[j]	1.2×10^{3}
Red mud[k]	7.8×10^{6}[k]				
CaO		2–8[k,l]	5	3.9×10^{5}[k]	7.8×10^{3}
Na_2O			6	4.7×10^{5}[k]	9.4×10^{3}
Steel slag	8.1×10^{6}[m]				
CaO		38–42[n,o]	40	3.2×10^{6}[o]	2.8×10^{4}
MgO		8–9[n,o]	9	6.9×10^{5}[o]	5.9×10^{3}
Iron slag	9.1×10^{6}[p]				
CaO		32–52[n,p]	42	3.8×10^{6}	2.9×10^{4}
MgO		5–15[n,p]	10	7.1×10^{5}	5.5×10^{3}

[a] Average composition multiplied by the US production.
[b] Average US tonne/yr of reactive component divided by the number of plants in the US.
[c] Schlag and Funada (2009).
[d] Miller and Callaghan (2004).
[e] American Coal Ash Association (2008).
[f] National Research Council (2006).
[g] Weighted average of concentration range of lignite, bituminous, and subbituminous coal production (EIA, 2011).
[h] US EPA (2008).
[i] US EPA (1993).
[j] Portland Cement Association (2009).
[k] Red mud is also known as bauxite residue, USGS (2009a).
[l] Red Mud Project (2011).
[m] National Slag Association (2007).
[n] Joshi and Areniez (2011).
[o] USGS (2009b).
[p] Lewis (1992).

Table 4
Reaction conditions based on experimental studies.[a,b].

	Temperature (°C)	L/S	P (bar)	Residence time	Carb (%)	Tonne/tonne CO_2 seq
Fe slag	200	2.5	35.5	2–30 min	67	6.8
Fly ash	60	–	1.1	2–10 s	30	4.8

L/S: Liquid to solid ratio on a mass basis.
[a] Huijgen et al. (2006).
[b] Reddy et al. (2010).

magnesium carbonates. The production of sodium hydroxide is the main contributor to the energy penalty for this pathway. Eloneva et al. (2008) also identify the use of sodium hydroxide and the energy associated with its production as a key factor in an unacceptable energy penalty for a CO_2 mineralization process involving blast-furnace slag. Their process entails first leaching calcium from the slag using acetic acid and then adding sodium hydroxide to the solution to achieve a high enough pH to precipitate the mineral carbonates. It requires 3.5 kg of sodium hydroxide for every kg of CO_2 sequestered (or 3.85 mol NaOH per mol of CO_2 sequestered). It is possible that a naturally occurring alkaline brine could be available that would reduce the need for sodium hydroxide and the energy required for this pathway. However, naturally occurring brines with a pH above 9 are rare, and a pH above 9 is necessary

Table 5
Energy requirements in MW for mineral carbonation of 100% of the CO_2 emitted from a 1 GW power plant via several pathways. Values denoted with a positive (+) sign indicate energy credits.

	NaOH ($NaHCO_3$)	NaOH ($Ca/MgCO_3$)	Olivine	Wollastonite	Fe slag	Fly ash
Processes						
Mining	–	–	18–32	45–81	–	–
CO_2 separation	–	–	167	167	167	–
NaOH prod	450–775	900–1550	–	–	–	–
Compress	–	–	97–217	86–128	86–129	3–4
Fluid bed	–	–	–	–	–	89–216
Pumping	4	4–309	52[a]	21–43	40–65	–
Mixing	0–5	0–10	–	–	–	–
Grinding		–	219	328	276	–
Heating		–	–	385–1040	529–1428	–
Energy penalty	454–780	904–1870	553–687	1032–1659	1098–2065	92–220
Products	0	+1	–	–	–	–

[a] No range is shown because pumping energy primarily depends on pressure and L/S, and only one L/S is evaluated.

for reaction (3) to proceed to an appreciable extent. For example, a survey of over 2.5 million water samples available from the United States Geological Survey (USGS, 2011) reveals less than 1% have a pH of 9 or greater.

It is also possible that the production of calcium or magnesium carbonates could yield materials with cementitious properties (Fialka, 2010; Constantz et al., 2010), and materials with cementitious properties would have a greater energy value than those for $Ca/MgCO_3$. Because information on the cementitious properties of materials produced from this pathway is not publicly available, credits for it are not included in the analysis. Consequently, for the industrial caustic pathway to produce calcium or magnesium carbonates, the energy penalty is greater than 90%, even using a minimum-work calculation, and the energy value of this product is negligible compared to the energy required to produce it.

In addition, the brine source can play a significant role in the energy required for pumping and mixing. A brine with high concentrations of calcium and magnesium ions, such as the Dead Sea, would be more suitable than a brine with calcium and magnesium ion concentrations in the range of sea water.

As discussed in the approach section, the widespread adoption of this pathway would also result in the generation of large quantities of chlorine or hydrochloric acid wastes. For example, coal-fired power plants in the US generate 2125 million tonne/yr CO_2 (EIA, 2009); if all of the CO_2 from these plants were mineralized via this pathway it would produce over 30 times the world demand for chlorine (World Chlorine Council, 2011).

In summary, because the lower bound energy penalty is at least 45% and because of the chlorine/hydrochloric acid waste generation, the production of sodium bicarbonate via this pathway is only potentially viable on a small scale unless another source of alkalinity is available.

4.2. Naturally occurring mineral pathway

Table 5 shows that the energy penalty for this pathway is in the same range (55–100+%) as reported by Gerdemann et al. (2007) and IPCC (2005). The requirements for CO_2 separation and mineral grinding are important factors in the large energy penalty. The results presented here are for olivine and wollastonite, which have a more favorable energy requirement than the more-common serpentine, which requires additional energy to remove chemically bound water (Gerdemann et al., 2007). Khoo et al. (2011) performed a life-cycle evaluation of CO_2 mineralization using serpentine, another mineral silicate, and flue gas from a natural gas combined cycle power plant, and they report energy penalty of approximately 90–125%. Their evaluation includes the same processes considered in this evaluation as well as transportation, but their process takes place at atmospheric pressure and has minimal grinding energy requirements compared to those used by Gerdemann et al. (2007) or Huijgen et al. (2006).

In addition to the energy requirements, the mining of the mineral silicates is another potential barrier to the adoption of this pathway on a wide scale. Each tonne of CO_2 requires 1.8–4.5 tonne of ore (Gerdemann et al., 2007; Huijgen et al., 2006), depending on the type of ore. If adopted for coal-fired power plants in the US, the scale of mining would exceed that of coal mining in the US and would have similar environmental impacts, such as land disturbance (Gerdemann et al., 2007).

Because this pathway has only received attention relatively recently and has only been studied at the laboratory scale, room for improvement exists. For example, recent studies, such as those by Krevor and Lackner (2011) and Baldyga et al. (2010), have identified weak acids that enhance the dissolution of natural silicate minerals and could potentially improve reaction rates. Brent et al. (2011) propose the integration of mineral carbonation with power generation and other extraction/manufacturing processes involving magnesium silicates, such as the extraction of magnetite, nickel, and chromium from serpentine. This type of synergistic approach offers the potential to offset the energy penalty and costs associated with mineral carbonation using naturally occurring minerals. Another approach to offset the energy penalty with mineralization of naturally occurring minerals is presented by Werner et al. (2011) who propose direct mineralization of CO_2 in flue gas without the need for CO_2 capture, thereby avoiding the energy penalty associated with CO_2 capture.

This pathway requires process improvements to reduce the energy penalty before it could be considered feasible. In their cost evaluations of aqueous mineral carbonation, Huijgen et al. (2007) (wollastonite) and Khoo et al. (2011) (serpentine) also conclude that reducing energy demand for their proposed processes is important. Furthermore, the large-scale mining of magnesium silicates may limit the adoption of this pathway.

4.3. Industrial wastes

Table 5 shows that the energy penalty associated with CO_2 mineralization of iron slag is greater than 100%, making this process unlikely to be feasible. Heating, compression, CO_2 separation, and grinding are all significant contributors to this high energy penalty. Eloneva et al. (2008) also report on a related process, the mineralization of CO_2 with blast-furnace slag. As discussed in Section 4.1, their process is also unlikely to be feasible. It tends to produce more CO_2 than would be bound by the carbonation step, primarily due to the process's use of sodium hydroxide and its associated energy requirement (Eloneva et al., 2008).

The use of fly ash for CO_2 mineralization has low energy requirements, which makes this process attractive, but it may be difficult to achieve high levels of mineralization. However, Reddy et al. (2010) suggest that this type of process could be useful for reducing the need for CO_2 sequestration in underground saline aquifers. This process may also be useful in meeting greenhouse gas performance standards, like those adopted in California that require all new long-term commitments for baseload power generation have emissions no greater than a combined cycle gas turbine plant (1100 pounds of CO_2 per MWh) (California Public Utilities and Commission, 2007). Furthermore, the fly ash used in their study contains 7.5% CaO and 3.85% MgO, but some coals, such as lignites can produce ash containing up to 40% CaO (National Research Council, 2006), which could lead to greater extents of mineralization and potentially more rapid reactions. Finally, it may be possible to improve the reactivity of fly ash by grinding, thereby increasing the surface area and availability of reactive metal oxides. However, grinding fly ash would require additional energy, which would limit any potential benefits, as discussed for Fe slag and naturally occurring minerals.

The mineralization of CO_2 with fly ash could also help reduce the large quantity of fly ash that is currently disposed of, primarily in landfills. The US generates approximately 1.2×10^8 tonne/yr of fly ash, and 55% of this material is landfilled (American Coal Ash Association, 2008). Worldwide, approximately 70% of fly ash is landfilled (Montes-Hernandez et al., 2009). Reddy et al. (2010) estimate that 2 Gt of fly ash is available in US landfills.

Soong et al. (2006) also evaluated the mineral carbonation of fly ash with acidic waste brine from oil and gas recovery. Because this proposed process requires the addition of supplementary caustic (sodium hydroxide) to bring the mineral solution to a basic pH, the life-cycle energy requirements would not be as favorable as the fluidized-bed pilot process proposed by Reddy et al. (2010). In a related paper, Baciocchi et al. (2010) performed a laboratory evaluation of bottom ash from incineration of refuse-derived fuel at

moderate temperatures (30–50 °C) and pressures (1–10 bar). They were able to achieve 9% CO_2 uptake in approximately 10 h.

One challenge associated with using fly ash to mineralize CO_2 emissions from a power plant is that the power plant generates much more CO_2 than reactive fly ash constituents. For example, if the theoretical power plant is fired with a coal containing 10% ash with the same composition as reported by Reddy et al. (2010), it would generate over 100 times more CO_2 than could theoretically react with the reactive metal oxides in the fly ash. Supplementary data, Section S.6, contains the details of this estimate. It is possible that fly ash available in landfills or onsite could also be used in this mineralization process. Baciocchi et al. (2010) also reached a similar conclusion: mineralization using bottom ash from the incinerator they studied could only capture a maximum of 2% of the CO_2 emitted from that incinerator.

Other wastes show promise but need further study and optimization. Huntzinger et al. (2006) experimentally evaluated the mineral carbonation of cement kiln dust with the flue gas from a cement kiln and obtained 60% carbonation. Their process would have low energy requirements because it takes place at ambient temperatures and pressures, but their residence time (8 h) would need to be optimized to make the process industrially feasible.

In addition to the need for study and optimization, the greatest challenge to the adoption of this pathway is the availability of wastes containing reactive oxides (Table 3). The hypothetical 1 GW coal-fired plant would produce 8 million tonnes of CO_2 annually, which is a factor of 100 greater than the quantity of reactive oxides available from a typical plant, i.e., cement, lime, coal-fired power plant, etc. Likewise, US coal-fired power plants produce 2.1×10^9 tonnes CO_2 per year, and summing the available data in Table 3 shows annual production of approximately a factor of 100 less than CO_2 production. In addition, many industries that produce wastes with reactive metal oxides are looking to reduce these as a way to improve their profitability. For example, from 1990 to 2005, the US cement industry reduced the amount of landfilled cement kiln dust by 47% (Adaska and Taubert, 2008). In addition, new technology has allowed the use of previously landfilled cement kiln dust to be used as raw feedstock. However, Table 3 does not contain all wastes containing reactive oxides, and some waste materials are available in landfills.

The waste pathway may offer additional benefits including pH reduction, thereby converting some caustic hazardous waste to a non-hazardous classification, modification of material properties, and reduction of the potential for metals leaching from wastes (Fernández Bertos et al., 2004; Gunning et al., 2010). Thus, industrial wastes that contain reactive oxides and do not require energy-intensive grinding or reaction conditions show promise for CO_2 mineralization in some applications. Their use will vary with the individual waste properties and be limited by their availability. CO_2 mineralization via the waste pathway may first be applied in situations where carbonation offers additional benefits such as the ability for industry to meet emission targets or the ability to mitigate a waste stream, as also suggested by Gerdemann et al. (2007). Understanding and optimizing processes for CO_2 mineralization using industrial wastes may also lead to reduced energy requirements for the pathway of mineralization with naturally occurring minerals, which are much more widely available than wastes containing reactive metal oxides.

5. Conclusions

The challenge for the adoption of ex situ CO_2 mineralization on an industrial scale is to develop a process that is rapid, cost competitive, and energy efficient, and that does not generate other unacceptable environmental impacts. After considering the energy requirements associated with the most significant processes, the results of this study suggest that some industrial wastes, such as fly ash, show promise for CO_2 mineralization. However, their availability is limited, approximately two orders of magnitude less than that required to treat CO_2 emissions from US coal-fired power plants. CO_2 mineralization may first be applied to remediate wastes and to meet emission targets, such as California's greenhouse gas performance standards. Because waste composition and physical properties vary by plant, further evaluation and pilot testing of individual wastes would be required in order to better assess the feasibility of CO_2 mineralization for specific wastes.

The naturally occurring mineral pathway would need to be optimized to become more energy efficient in order for this process to become feasible. The energy penalties for grinding and for CO_2 separation are barriers to this process. Another significant barrier to this process is the need for large-scale mining of the minerals. The industrial caustic pathway is unlikely to be feasible beyond a very small scale because of the energy required to produce sodium hydroxide and the generation of potentially hazardous wastes in the form of chlorine or hydrogen chloride.

Acknowledgments

This research was sponsored by the National Nuclear Security Administration under the "Accelerating Development of Retrofitable CO_2 Capture Technologies through Predictivity" through DOE Research Grant #DE-NA0000740.

Appendix A. Supplementary data

Supplementary data associated with this article can be found, in the online version, at doi:10.1016/j.ijggc.2011.09.005.

References

Adaska, W.S., Taubert, D.H., 2008. Beneficial uses of cement kiln dust. In: 2008 IEEE/PCA 50th Cement Industry Technical Conference, Miami, FL, May 19–22, 2008.

American Coal Ash Association, 2008. 2008 coal combustion product (CCP) production & use survey report. http://acaa.affiniscape.com/associations/8003/files/2008_ACAA_CCP_Survey_Report_FINAL_100509.pdf (cited 04.04.11).

Baciocchi, R., Costa, G., Lategano, E., Marini, C., Polettini, A., Pomi, R., Postorino, P., Rocca, S., 2010. Accelerated carbonation of different size fractions of bottom ash from RDF incineration. Waste Management 30, 1310–1317.

Baldyga, J., Henczka, M., Sokolnicka, K., 2010. Utilization of carbon dioxide by chemically accelerated mineral carbonation. Materials Letters 64, 702–704.

Bonenfant, D., Kharoune, L., Sauve, S., Hausler, R., Niquette, P., Mimeault, M., Kharoune, M., 2008. CO_2 sequestration by aqueous red mud carbonation at ambient pressure and temperature. Industrial and Engineering Chemistry Research 47, 7617–7622.

Brent, G.F., Allen, D.J., Eichler, B., Petric, J.G., Mann J.P., Haynes, B.S., 2011. Mineral carbonation as the core of an industrial symbiosis for energy-intensive minerals conversion. Journal of Industrial Ecology, doi:10.1111/j.1530-9290.2011.00368.x.

California Public Utilities Commission, 2007. PUC sets GHG emissions performance standard. Docket R.06-04-009.

Constantz, B., 2009. Testimony Before the United States Senate Subcommittee on Energy and Water Development, a Committee within Senate Appropriations May 6, 2009.

Constantz, B., Ryan C., Cirdic, L., 2010. Hydraulic cements comprising carbonate compound composites. US Patent 7,735,274 B2.

CSLF (Carbon Sequestration Leadership Forum), 2010. CSLF Technology Roadmap, November 2010.

Druckenmiller, M.L., Maroto-Valer, M.M., 2005. Carbon sequestration using brine of adjusted pH to form mineral carbonates. Fuel Processing Technology 86, 1599–1614.

Dunsmore, H.E., 1992. A geological perspective on global warming and the possibility of carbon dioxide removal as calcium carbonate mineral. Energy Conversion Management 33 (5–8), 565–572.

Eloneva, S., Teir, S., Salminen, J., Fogelholm, C.-J., Zevenhoven, R., 2008. Fixation of CO_2 by carbonating calcium derived from blast furnace slag. Energy 33, 1461–1467.

EPRI (Electric Power Research Institute), 2007. Assessment of Post-combustion Capture Technology Developments, 1012796, EPRI, Palo Alto, CA.

EPRI (Electric Power Research Institute), 2009. The Power to Reduce CO_2 Emissions, the Full Portfolio. EPRI, Palo Alto, CA.

Eurasian Chemical Market Magazine, 2011. Sodium Bicarbonate Production and Market in CIS, 1 (49) January.
Fernández Bertos, M., Simons, S.J.R., Hills, C.D., Carey, P.J., 2004. A review of accelerated carbonation technology in the treatment of cement-based materials and sequestration of CO_2. Journal of Hazardous Materials B112, 193–205.
Fialka, J.J., 2010. Can 'green cement' make carbon capture and storage obsolete? New York Times August.
Gerdemann, S.J., O'Connor, W.K., Dahlin, D.C., Penner, L.R., Rush, L.R., 2007. Ex situ aqueous mineral carbonation. Environmental Science and Technology 41, 2587–2593.
Guinée, J.V., 2002. Handbook on Life-Cycle Assessment, Operational Guide to the ISO Standards. Kluwer Academic Publishers, Secaucus, NJ.
Gunning, P.J., Hills, C.D., Carey, P.J., 2010. Accelerated carbonation treatment of industrial wastes. Waste Management 30, 1081–1090.
Herzog, H.J., 2011. Scaling up carbon dioxide capture and storage: from megatons to gigatons. Energy Economics 4, 597–604.
Huijgen, W.J., Ruijg, G.J., Comans, R.N.J., Witkamp, G.J., 2006. Energy consumption and net CO_2 sequestration of aqueous mineral carbonation. Industrial Engineering Chemical Research 45, 9184–9194.
Huijgen, W.J., Comans, R.N.J., Witkamp, G.J., 2007. Cost evaluation of CO_2 sequestration by aqueous mineral carbonation. Energy Conversion and Management 48, 1923–1935.
Huntzinger, D., Gierke, J., Komarkawatra, S., Eisele, T., 2009. Carbon dioxide sequestration in cement kiln dust through mineral carbonation. Environmental Science and Technology 43, 1986–1992.
ICIS Indicative Chemical Prices, 20011. http://www.icis.com/StaticPages/a-e.htm (cited 15.04.11).
Iizuka, A., Fujii, M., Yamasaki, A., Yanagisawa, Y., 2004. Development of a new CO_2 sequestration process utilizing the carbonation of waste cement. Industrial Engineering Chemical Research 43, 7880–7887.
IPCC (Intergovernmental Panel on Climate Change), 2005. In: Metz, B., Davidson, O., de Coninck, H., Manuela Loos, A., Meyer, L. (Eds.), Special Report on Carbon Dioxide Capture and Storage. Cambridge University Press, UK.
Joshi, V.K., Arenicz, R.M., 2011. Use of Slag: A Direct Benefit to Our Environment. National Slag Association, MF 203-11.
Katzer, J., et al., 2007. The Future of Coal, Options for a Carbon-Constrained World. Massachusetts Institute of Technology, Cambridge, MA.
Khoo, H.H., Bu, J., Wong, R.L., Kuan, S.Y., Shatratt, P.N., 2011. Carbon capture and utilization: preliminary life-cycle CO_2, energy, and cost results of potential mineral carbonation. Energy Procedia 4, 2494–2501.
Krevor, S.C.M., Lackner, K.S., 2011. Enhancing serpentine dissolution kinetics for mineral carbon dioxide sequestration. International Journal of Greenhouse Gas Control 5 (4), 1073–1080.
Lackner, K.S., Wendt, C.H., Butt, D.P., Joyce, E.L., Sharp, D.H., 1995. Carbon dioxide disposal in carbonate minerals. Energy 20, 1153–1170.
Lewis, D.W., 1992. Properties and Uses of Iron and Steel Slags. National Slag Association, MF-182-6.
Ma'or, Z., Henis, Y., Alon, Y., Orlov, E., Sørensen, K.B., Oren, A., 2006. Antimicrobial properties of Dead Sea black mineral mud. International Journal of Dermatology 45 (5), 504–511.
Miller, M.M., Callaghan, R.M., 2004. Lime kiln dust as a potential raw material in Portland cement manufacturing. United States Geological Service, Report 2004-1336.
Montes-Hernandez, G., Pérez-López, R., Renard, F., Nieto, J.M., Charlet, L., 2009. Mineral sequestration of CO_2 by aqueous carbonation of coal combustion fly ash. Journal of Hazardous Materials 161, 1347–1354.
National Hydrogen Association, 2010. Hydrogen and fuel cells. US Market Report, National Hydrogen Association 1211 Connecticut Avenue NW Suite 600 Washington, DC 20036, USA.
National Research Council of the Academies of Science, 2006. Committee on Mine Placement of Coal Combustion Wastes. Managing Coal Combustion Residues in Mines. National Research Council, National Academies Press, Washington, DC.
National Slag Association, 2007. Iron and steel slag, industrial resources council meeting with EPA. http://www.epa.gov/osw/conserve/rrt/imr/irc-meet/06-slag.pdf (cited 30.03.11).
Portland Cement Association, 2009. Report on sustainable manufacturing. http://www.cement.org/smreport09/images/shared_images/SustainReport08.pdf (cited 24.03.11).
Reddy, K.J., Weber, H., Bhattacharyya, P., Morris, A., Taylor, D., Christensen, M., Foulke, T., Fahlsing, P., 2010. Instantaneous capture and mineralization of flue gas carbon dioxide: pilot scale study, Nature Precedings.
Sahu, R.C., Patel, R.K., Ray, B.C., 2010. Neutralization of red mud using CO_2 sequestration cycle. Journal of Hazardous Materials 179, 28–34.
Schlag, S., Funada, C., 2009. Lime/Limestone: Chemical Economics Handbook. SRI Consulting, Menlo Park, CA.
Seifritz, W., 1990. CO_2 disposal by means of silicates. Nature 345 (6275), 486.
Snoeyink, V.L., Jenkins, D., 1980. Water Chemistry. John Wiley & Sons, New York, 3 pp.
Soong, Y., Fauth, D.L., Howard, B.H., Jones, J.R., Harrison, D.K., Goodman, A.L., Gray, M.L., Frommell, E.A., 2006. CO2 sequestration with brine solution and fly ashes. Energy Conversion and Management 47, 1676–1685.
SRI (Stanford Research Institute), 2009. Chemical Economics Handbook, Sodium Bicarbonate. SRI International, Menlo Park, CA.
Steinour, H.H., 1959. Some effects of carbon dioxide on mortars and concrete-discussion. Journal of the American Concrete Institute, 905–907.
Stolaroff, J.K., Lowry, G.V., Keith, D.W., 2005. Using CaO- and MgO-rich industrial waste streams for carbon sequestration. Energy Conversion and Management 46, 687–699.
The Red Mud Project, 2011. http://www.redmud.org/home.html (cited 24.03.11).
US DOE (United States Department of Energy), 2002. Energy and environmental profile of the US mining industry. Prepared by BCS Inc. for the Office of Energy Efficiency and Renewable Energy.
US DOE, 2010a. Secretary Chu announces six projects to convert captured CO_2 emissions from Industrial Sources into useful products, July 22, 2010. http://www.netl.doe.gov/publications/factsheets/project/FE0002415.pdf.
US DOE, 2010b. Recovery Act, Innovative concepts for beneficial reuse of carbon dioxide. http://fossil.energy.gov/recovery/projects/beneficial_reuse.html.
US DOE, 2010c. Innovative carbon dioxide sequestration from flue gas using an in-duct scrubber coupled with alkaline clay mineralization, March 2011. http://www.netl.doe.gov/publications/factsheets/project/FE0002415.pdf.
US DOE, 2011a. Life cycle inventory database for alkalis and chlorine manufacture for 2003. http://www.nrel.gov/lci/.
US DOE, 2011b. Life cycle inventory database for limestone at the mine. http://www.nrel.gov/lci/.
US EIA (Energy Information Administration), 2008. Emissions of greenhouse gases report. Report DOE/EIA-0573, December 3, 2009.
US EIA (Energy Information Administration), 2010. Energy information adminstration, average operating heat rate for selected energy sources. http://205.254.135.24/cneaf/electricity/epa/epat5p3.html.
US EIA (Energy Information Administration), 2011. Coal production and number of mines by state and coal rank. Report No: DOE/EIA-0584 (2011), Release Date: October 1, 2010, Updated: February 3, 2011. http://www.eia.doe.gov/cneaf/coal/page/acr/table6.html.
US EPA (United States Environmental Protection Agency), 1993. Report to Congress (1993) – cement kiln dust waste.
US EPA (United States Environmental Protection Agency), 2008. Study on increasing the usage of recovered mineral components in federally funded projects involving procurement of cement or concrete to address the safe, accountable, flexible, efficient transportation equity act: a legacy for users, June 3, 2008.
USGS (United States Geological Survey), 2009a. Aluminum, statistics and information. http://minerals.usgs.gov/minerals/pubs/commodity/aluminum/mcs-2010-alumi.pdf (cited 24.03.11).
USGS (United States Geological Survey), 2009b. Iron and steel, statistics and information. http://minerals.usgs.gov/minerals/pubs/commodity/iron_&_steel/ (cited 24.03.11).
USGS (United States Geological Survey), 2011. USGS water data for the nation. http://waterdata.usgs.gov/nwis (cited 19.08.11).
Werner, M., Verduyn, M., van Mossel, G., Mazzotti, M., 2011. Direct flue gas CO_2 mineralization using activated serpentine: exploring the reaction kinetics by experiments and population balance modeling. Energy Procedia 4, 2043–2049.
Wilson, E.J., et al., 2008. Regulating the geological sequestration of CO_2. Environmental Science and Technology 42 (8), 2718–2722.
World Chlorine Council, 2011. Chlorine products and benefits. http://www.worldchlorine.org/products/index.html (cited 17.03.11).
Zevenhoven, R., Eloneva, S., Teir, S., 2006. Chemical fixation of CO_2 in carbonates: routes to valuable products and long-term storage. Catalysis Today 115, 73–79.

CHAPTER 3

OXYFIRING WITH CO_2 CAPTURE TO MEET LOW-CARBON FUEL STANDARDS FOR UNCONVENTIONAL FUELS FROM UTAH

International Journal of Greenhouse Gas Control 22 (2014) 189–199. Oxyfiring with CO_2 Capture to Meet Low-Carbon Fuel Standards for Unconventional Fuels from Utah.

International Journal of Greenhouse Gas Control 22 (2014) 189–199

Contents lists available at ScienceDirect

International Journal of Greenhouse Gas Control

journal homepage: www.elsevier.com/locate/ijggc

Oxyfiring with CO_2 capture to meet low-carbon fuel standards for unconventional fuels from Utah

K.E. Kelly[a,*], J.E. Wilkey[b], J.P. Spinti[b], T.A. Ring[b], D.W. Pershing[b]

[a] Institute for Clean and Secure Energy, University of Utah, 155 South 1452 East, UT 84112, USA
[b] Department of Chemical Engineering, Institute for Clean and Secure Energy, University of Utah, 155 South 1452 East, UT 84112, USA

ARTICLE INFO

Article history:
Received 5 October 2013
Received in revised form
28 December 2013
Accepted 7 January 2014

Keywords:
Oxyfuel combustion
Life-cycle analysis
Oil sands
Oil shale, Energy return on investment
Net energy return

ABSTRACT

The transportation fuel sector is under pressure to reduce its greenhouse gas (GHG) emissions as a result of low-carbon fuel standards (LCFSs), which have been passed by the State of California and the European Union. These standards will be particularly challenging for producers of oil sands, heavy oil, and other unconventional resources. Oxyfiring with CO_2 capture is a promising technology for reducing CO_2 emissions from the transportation fuel sector, but it requires a significant amount of energy to generate oxygen. This study examines the potential for oxyfiring to reduce life-cycle GHG emissions from transportation fuels derived from in situ and ex situ oil shale and ex situ oil sands in the Uinta Basin of Utah. It also examines the effect of oxyfiring with CO_2 capture on the net energy return (NER). The evaluation focuses on the fuel's life-cycle GHG emissions, and it includes resource extraction, upgrading, transportation and refining. The results suggest that oxyfiring could help some unconventional sources of crude oil, such as ex situ production of oil sands and oil shale, meet a LCFS. However, oxyfiring with CO_2 capture reduces NER.

1. Introduction

Concern over GHG emissions and the resulting legislation, i.e., low-carbon fuel standards (LCFS), is motivating the transportation-fuel industry to evaluate strategies to reduce its carbon footprint. The State of California enacted the first low-carbon fuel standard in 2007, which went into effect in 2011 (CARB, 2012). However this standard is currently being contested in court. A recent provisional ruling by California's state appeals court suggests that the LCFS will be allowed to stand. California's LCFS requires oil refineries and distributors to ensure that the mix of reformulated gasoline sold in the state does not exceed the limit of 89.06 g CO_2 e/MJ by 2020. California has additional standards for other transportation fuels. This is a well-to-wheel (WTW) life-cycle standard and is based on GHG emissions from extraction, processing, refining, distribution, and vehicle tailpipe emissions.

At the federal level, the US Energy Independence and Security Act of 2007, Section 526, prohibits any federal agency from entering into contract for procurement of an alternative or synthetic fuel produced from non-conventional petroleum sources unless the life-cycle GHG emissions associated with the "production and combustion of the fuel" are less than or equal to the equivalent petroleum fuel produced from conventional petroleum sources (93.3 g CO_2 e/MJ petroleum baseline) (US EPA, 2009). Other countries and provinces have also approved carbon-based fuel standards, including British Columbia Parliament (2008), the European Union (2008), and the United Kingdom Renewable Fuels Agency (2009).

Unconventional liquid transportation fuels typically require more energy to produce and consequently generate more GHG emissions than conventional transportation fuels. When comparing unconventional and conventional fuel sources, it is important to consider the entire fuel's life cycle as illustrated in Fig. 1, which shows GHG emissions from a typical fuel cycle for gasoline from a conventional source of crude oil. Fig. 1 also illustrates the well-to-pump (WTP) cycle, which includes raw material extraction, transportation, refining, and delivery to the pump, while the well-to-wheel (WTW) cycle also includes the fuel consumption and the resulting tailpipe emissions.

As the US moves toward more unconventional sources of crude oil, the baseline WTP GHG emissions of a barrel of crude oil is increasing (Gerdes and Skone, 2009). In addition, a good deal of variability exists in the WTP GHG profile depending on the source of crude and the processing methods. For example, crude oil produced from Canadian oil sands, oil shale, and California heavy oil all have greater WTP GHG emissions than US conventional crude oil. However, high WTP GHG emissions are not limited to

* Corresponding author at: 380 INSCC, 155 South 1452 East, University of Utah, Salt Lake City, UT 84112, USA. Tel.: +1 801 587 7601; fax: +1 801 585 1456.
E-mail addresses: kerry.kelly@utah.edu, kelly@eng.utah.edu (K.E. Kelly).

1750-5836/$ – see front matter © 2014 Elsevier Ltd. All rights reserved.
http://dx.doi.org/10.1016/j.ijggc.2014.01.002

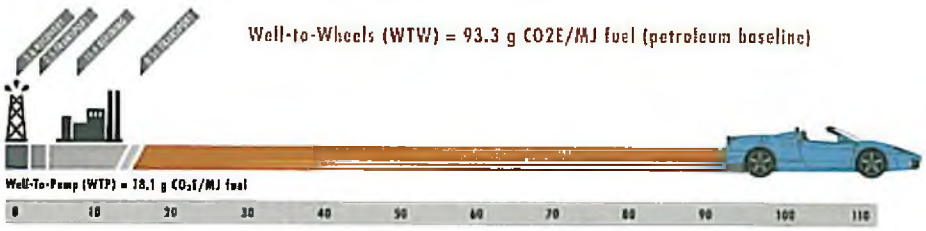

Fig. 1. WTP and WTW GHG emissions per lower heating value of conventional gasoline produced from conventional crude oil (MJ); data based on US EPA (2009). The GHG emissions in CO_2 equivalents include emissions of CO_2, CH_4, and N_2O.
Source: Reproduced from ICSE (2013).

unconventional fuels; Nigerian crude has twice the WTP GHG emissions of US conventional crude oil, primarily due the venting and flaring of nearly all of the co-produced natural gas (Gerdes and Skone, 2009).

Oxyfiring with CO_2 capture is one promising strategy for reducing GHG emissions from combustion sources (Allam et al., 2005; Buhre et al., 2005). Conventional combustion sources burn their fuel in air, resulting in a voluminous flue gas that is relatively dilute in CO_2 and expensive to capture (Singh et al., 2003). During oxyfuel combustion, a fuel burns in an environment of oxygen and recycled flue gas. It results in a less voluminous flue gas that contains primarily CO_2 and water, which is ready for sequestration. Thus, oxyfiring offers the potential for cost savings over post-combustion capture methods. However, the challenge with oxyfiring is the requirement for the generation of a pure, typically 95% pure, oxygen stream, which is energy intensive.

This study focuses on the use of oxyfiring with CO_2 capture in the production, upgrading and refining life-cycle stages of liquid transportation fuels from unconventional fuel resources, specifically oil shale and oil sands, in Utah's Uinta Basin. The objective is to evaluate the potential of oxyfiring to reduce life-cycle GHG emissions from these types of transportation fuels.

2. Material and methods

This study uses a simplified process model life-cycle assessment approach to determine WTP and WTW GHG emissions associated with the production of conventional gasoline from three potential scenarios in Utah's Uinta Basin: in situ oil shale, ex situ oil shale,

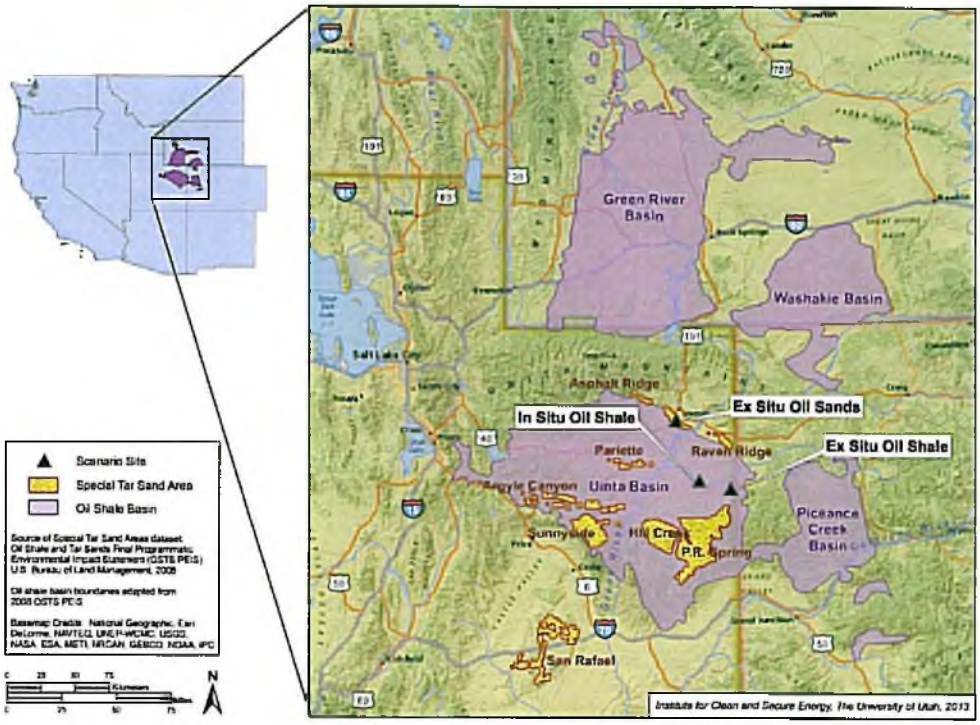

Fig. 2. Uinta Basin with locations of the oil sands and shale development scenarios noted.

Table 1
Summary of selected conditions, energy requirements, and emission factors for the baseline, sensitivity analysis and oxyfiring cases.

	Baseline GHG	Low GHG	High GHG	Oxy (1)	Oxy (2)	Oxy (3)
All scenarios						
Electricity	Utah mix[a]	53% efficient NGCC[b]	Utah mix[a]	Utah mix[a]	Oxyfired NGCC[c]	Oxyfired NGCC[c]
Air separation	200 kWh/ton O_2[d]	200 kWh/ton O_2[d]	200 kWh/ton O_2[d]	200 kWh/ton O_2[d]	268 kWh/ton O_2[e]	268 kWh/ton O_2[e]
Ex situ *shale*						
Retort process	Tosco II[f]	Tosco II[f]	Paraho[g]	Tosco II[f]	Tosco II[f]	Tosco II[f]
Shale richness	104 l/ton[h]	146 l/ton[h]	85.3 l/ton[h]	104 l/ton[h]	104 l/ton[h]	104 l/ton[h]
Material mined	79,650 ton/day	56,890 ton/day	99,790 ton/day	79,650 ton/day	79,650 ton/day	79,650 ton/day
Refining	9.57 g CO_2e/MJ[i]	7.73 g CO_2e/MJ[i]	11.4 g CO_2e/MJ[i]	9.57 g CO_2e/MJ[i,j]	9.57 g CO_2e/MJ[i,j]	5.74 g CO_2e/MJ[i,j]
In situ *shale*						
Project life	24 year[k]	40 year[k]	24 year[k]	24 year[k]	24 year[k]	24 year[k]
Initial permeability	20 mD	20 mD	1 mD	20 mD	20 mD	20 mD
Refining	8.67 g CO_2e/MJ[i]	7.00 g CO_2e/MJ[i]	10.3 g CO_2e/MJ[i]	8.67 g CO_2e/MJ[i,j]	8.67 g CO_2e/MJ[i,j]	5.20 g CO_2e/MJ[i,j]
Ex situ *sands*						
Bitumen	10% saturation	15% saturation	5% saturation	10% saturation	10% saturation	10% saturation
Refining	10.3 g CO_2e/MJ[i]	8.48 g CO_2e/MJ[i]	12.0 g CO_2e/MJ[i]	10.3 g CO_2e/MJ[i,j]	10.3 g CO_2e/MJ[i,j]	6.14 g CO_2e/MJ[i,j]

[a] EPA (2012).
[b] GHG emissions of 454 g CO_2 e/kWh (Spath and Mann, 2000).
[c] With CO_2 capture, GHG emissions of 12 g CO_2 e/kWh (Davison, 2007).
[d] Higginbotham et al. (2011).
[e] Amann et al. (2009).
[f] Weiss et al. (1982).
[g] Cleveland-Cliffs Iron Company (1976) and Fuel and Mineral Resources, (1983).
[h] Vanden Berg (2008).
[i] Gerdes and Skone (2009) and Brandt (2012).
[j] Allam et al. (2005).
[k] ICSE (2013).

and ex situ oil sands. All GHG emissions are presented on a basis of the lower heating value of conventional gasoline.

2.1. Uinta Basin resources

Utah's Uinta Basin (Fig. 2) is a major source of unconventional fuel resources in the form of oil sands and oil shale. The organic material in oil sands, bitumen, is extremely viscous with viscosities that exceed 10,000 centipoise at 16 °C. Oil shale is an immature petroleum source rock that contains organic matter in the form of kerogen; thermal treatment is required convert kerogen to oil and gas.

The Uinta Basin oil sands deposits contain an estimated 13.4 billion barrels of original oil in place (Oblad et al., 1987; Ritzma, 1979). Recent resource assessments estimate the Uinta Basin in-place oil shale resource at 1.32 trillion barrels (Johnson et al., 2010). Of this total, about 77 billion barrels of oil shale are located in deposits with an equivalent oil yield of at least 104 l/ton, are at least 1.5 m thick, are under less than 915 m of overburden, and are in areas available for oil shale development (i.e. BLM, state, private, or tribal lands without current conventional oil and gas resources) (Vanden Berg, 2008). Despite the size of these two resources, production of oil has thus far been limited to demonstration projects (Snarr, 2008; Nelson, 2012). As a result, this study utilizes potential development scenarios analyzed in a recent report (ICSE, 2013) rather than data from commercial operations.

2.2. Methodology overview

Fig. 2 shows a map of the Uinta Basin, the location for each of the scenarios, and the relationship of these resources to the refineries in Salt Lake City. The scenarios and associated processes are selected based on extensive discussions with industry and publicly available process information. The scenario locations are selected based on resource quality, availability, and access. Note that an in situ oil sands case is not included in this analysis because Utah's oil sands resources are not distributed in large contiguous deposits, as in Alberta, Canada, and consequently these resources may not be well suited to in situ production.

The following sections describe the life-cycle stages and processes included for each scenario. For all scenarios, construction and decommissioning of processes and land-use changes are not considered. None of the cases considered the potential for fugitive methane emissions associated with extraction of the ore or disposal of spent shale or tailings. Several subprocesses within the upgrading process (hydrogen production, hydrotreating, transportation, refining, air separation, and utilities (steam, water and electricity)) are common to all three scenarios and are described after the scenarios.

Because oil sands and shale are not produced commercially in Utah, there is a good deal of uncertainty associated with resource quality and the selection of extraction/processing methods. Consequently, we include a sensitivity analysis to provide a probable range of GHG emissions from each of these resources (Table 1). The parameters in the sensitivity analysis are selected based on conversations with industry experts and screening tests to identify which parameters affected GHG emissions most significantly. The baseline cases are based on currently available technology and good resource quality. The low-GHG case is based on current to near-term technology and good to optimistic resource quality. The high GHG cases have lower resource quality and more GHG-intensive processing.

In addition to a sensitivity analysis of the baseline conditions, we also consider a series of oxyfiring cases to reduce GHG: (1) oxyfiring with CO_2 capture in a natural gas combined cycle (NGCC) plant in the extraction and upgrading processes where possible (described for each scenario); (2) in addition to (1), oxyfiring with CO_2 capture for an NGCC plant generating the electricity required for the extraction and upgrading processes (Davison, 2007); (3) in addition to (1) and (2), oxyfiring with CO_2 capture in the refining stage (Allam et al., 2005). Table 1 summarizes the conditions and emission factors for each oxyfiring case. All of the baseline scenarios use a 24-year project lifetime.

2.3. In situ oil shale

Using data published by Vanden Berg (2008), we select a site in the Uinta Basin that had a 33 m thick, 104 l/ton oil shale deposit

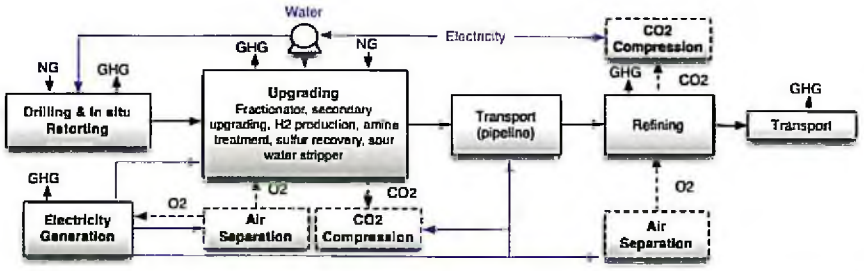

Fig. 3. Simplified process flow diagram for the Utah in situ shale scenario illustrating the processes considered in this evaluation. Dotted lines and boxes indicate processes that only apply to the oxycombustion cases.

under 330 m of overburden that will produce 50,000 barrel per day (BPD) at the end of the project lifetime (Fig. 2 and Fig. S-1). Average lifetime production from this scenario is approximately 16,500 BPD. Fig. 3 illustrates a simplified process flow diagram for the in situ extraction of oil shale. A brief process description follows; further scenario details can be found in ICSE (2013).

For the sensitivity analysis, shale permeability varies from 20 mD for the baseline and low GHG cases to 1 mD for the high GHG case. We also consider a project lifetime of 24 years for the baseline and high GHG cases, and a project lifetime of 40 years for the low GHG case.

Extraction. In the in situ extraction process, oil is produced from the oil shale by drilling pairs of horizontal wells, located 30.5 m apart, into the deposit as shown in Fig. S-2. The heating well, located in the center of the deposit, contains a mineral-insulated, electric heat-tracing line, which produces a constant heat flux to slowly heat the deposit. The constant heat flux from the heat tracing line gradually increases temperatures in the oil shale deposit to approximately 540 °C (below the thermal decomposition temperature of carbonate minerals, Campbell, 1978) over the course of 24 years. Kerogen (the organic material in oil shale) begins decomposing into oil and gas (e.g. in situ retorting) at temperatures greater than 210 °C. Oil and gas flow to the production well, which transports these fluids back to the surface for processing. Produced gas is separated from the oil and is used to reduce the amount the natural gas required to heat the formation.

Simulations of heating the oil shale formation were performed using STARS (CMG, 2013), a commercial reservoir simulation package, to obtain production rates of oil and gas as a function of time. By the end of the 24-year heating period, 34% of the kerogen in the deposit is converted to oil, gas, and coke, producing a cumulative 240 bbl/m of oil, 3670 m^3/m of gas, and requiring a total of 6.75×10^5 MJ/m of heat (units are per unit length of heated well).

The GHG emissions from drilling are based on a heater well length of 1750 m, a producer well length of 1765 m, and a total of 240 well pairs drilled over the 24-year life of the project, combined with diesel fuel consumption of 1.9 l/m drilled (Advanced Resources International, 2008).

Portable 2.5 MW reciprocating natural gas-fired generators provide the electricity required to power the heat tracing lines. The GHG emissions from the generators are based on a constant heat flux of 938 W/m and a generator efficiency of 46%. The GHG emissions and the energy associated with the consumption of all the natural gas (produced within the process and purchased) are included in the GHG and NER (net energy return) analyses. However, due to the distributed nature of the heating, oxyfiring with CO_2 capture is not feasible for the in situ retort process.

Upgrading. The produced oil is relatively high quality (35° API gravity) and requires only limited upgrading. As a result, the H_2 requirement is lower than that for the ex situ oil shale scenario. The raw shale oil from the producer well is fractionated into naptha and vacuum gas oil streams in an atmospheric distillation column. Each of these streams is hydrotreated (a form of secondary upgrading) to remove sulfur and nitrogen so that the final product, synthetic crude oil (SCO), is equivalent to a West Texas Intermediate crude oil; this requires 3.65 m^3 of hydrogen per barrel of produced oil. Other processes in this life-cycle stage include hydrogen generation by steam reforming, treatment of process water (sour water stripper), sweeting of produced gases (amine treatment unit), and sulfur recovery (Fig. 3). For the oxyfiring cases, we assume that oxyfiring with CO_2 capture can be applied to the boilers and process heaters in the hydrogen plant, hydrotreater and fractionator.

2.4. Ex situ oil shale

In the ex situ oil shale scenario, an oil resource with the same grade discussed in Section 2.3 is extracted by mining and surface retorting rather than drilling and heating the shale in place. A shallower location of the 104 l/ton shale is selected from Vanden Berg (2008) to the southeast of the location selected for the in situ oil shale case (Fig. 2 and Fig. S-3).

Fig. 4 shows a simplified process flow diagram for this scenario, which produces 50,000 BPD for 20 years, and it is followed by a brief description of each of the processes. Further details of the mining, pre-processing/upgrading, air separation, transport, and CO_2 compression can be found in ICSE (2013, chapter 6). For the sensitivity analysis, two retort processes are considered: the Tosco II (base and low GHG case) and the Paraho Direct (high GHG case). In addition, shale richness varied from 146 l/ton (low GHG cases) to 104 l/ton (baseline case) and 85.3 l/ton (high GHG case). The shale richness, in turn, greatly affects the quantity of material that must be mined, crushed and processed.

Extraction. For the base case (Tosco II retort), 79,650 tons per day of 104 l/ton oil shale is mined from a 15 m thick oil shale seam that runs at depths of 150–330 m. The seam is mined using the room and pillar method, wherein some material is left as pillars to support the mine roof. GHG emissions associated with mining and transport are based on the energy requirements for underground coal mining (US DOE, 2007), an adjustment for the difference in density of shale compared to coal, and the assumption that the energy is provided by diesel fuel (66 MJ/ton material moved). Mined shale is sent to a primary crusher and then conveyed to the surface where it undergoes secondary crushing; both crushers and the conveyor are electrically powered.

Retorting and upgrading. For the base case, the retort is based on the Tosco II process (Weiss et al., 1982). In the retort, heated ceramic balls at 700 °C are fed into a rotating retort drum with the crushed shale, where the ceramic balls act as a solid heat-transfer medium, raising the temperature of the shale to 480 °C. The retort requires 0.0544 kWh electricity and 170 MJ per GJ of gasoline.

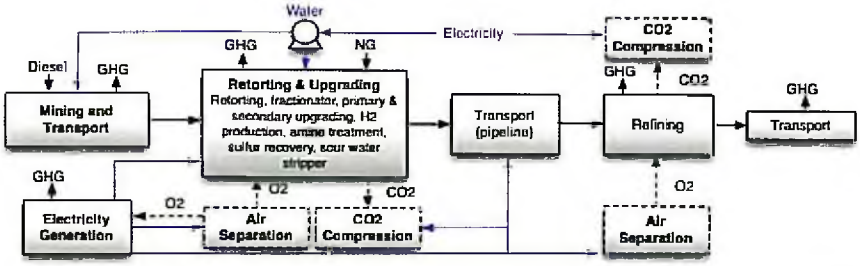

Fig. 4. Simplified process flow diagram for the Utah ex situ shale cases, showing the processes considered in this evaluation. Dotted lines and boxes indicate processes that only apply to the oxy-combustion cases.

The high GHG case is based on the Paraho Direct retort (Cleveland-Cliffs Iron Company, 1976; Fuel and Mineral Resources, 1983). For this case, the crushed and screened shale flows downward through the retort, where heat transfer is achieved by a counter-current flow of air and recycle gas injected from various locations along the retort. The downward movement of the shale is controlled by a grate, located at the bottom of the retort. The retort reaches a temperature of 649 °C, and the necessary heat is generated by combustion of the char remaining on the retorted shale and the recycle gas. At this temperature, a portion of the carbonate mineral in the shale decomposes and releases CO_2.

For both the Tosco II and Paraho Direct retorts, vapors from the pyrolysis of the organic material in the retort condense and flow to a fractionator, at which point the upgrading process begins and follows the same procedure described for in situ oil shale. However, the oil produced by surface retorting is of lower quality (20° API gravity) than that produced in situ. As a result, hydrotreating requires 57 m^3 of hydrogen per barrel of retorted oil. Oxyfiring with CO_2 capture can be applied to the boilers and process heaters in the retort, hydrogen plant, hydrotreater and fractionator.

2.5. Ex situ oil sands

One promising oil sand deposit in the Uinta Basin is Asphalt Ridge (Fig. 2). Blackett's (1996) survey of this deposit indicates that Asphalt Ridge contains 700–1048 million barrels of bitumen in place. The deposit ranges in thickness from 3 to 41 m, contains 6–15 wt.% bitumen, extends 19 km, and dips down from surface outcrops at angles of 8°–30°. Given the geometry of the deposit, production rates of 50,000 BPD are not economically feasible, and the ex situ oil sands process produces 10,000 BPD.

Fig. 5 illustrates a simplified process flow diagram for extracting oil from oil sands ex situ. It is followed by a brief description of each process. Further details can be found in ICSE (2013, chapter 8). For the sensitivity analysis, bitumen content ranged from 15 wt.% (low GHG case) to 10 wt.% (baseline) and 5 wt.% (high GHG case).

Mining, transport and bitumen recovery. Oil sand is mined using standard surface mining techniques (drilling, blasting, hauling, etc.) beginning at the outcrop and proceeding down-dip at the same angle as the deposit. Mining can continue this way until the stripping ratio (SR), the amount of overburden removed per unit of oil sand, reaches 4:1, which is the current economic limit for this type of mining. Assuming that the deposit contains 10 wt.% bitumen (base case), is 18 m thick, has a down-dip of 12°, and that the mine takes 20 years to reach an SR of 4:1, then 7.9 km of Asphalt Ridge would be mined to produce 10,000 BPD of oil for 20 years; the project lifetime is 24 years, which includes four years for permitting and construction.

During the extraction stage, GHG emissions result from the transport of oil sands and overburden as well as the production of hot water used to extract the bitumen from the sands. In order to meet the target production rate of 10,000 BPD, the mine must remove 12,510 ton/day of ore and an additional 12,510 ton/day of overburden on average (baseline). GHG emissions associated with transport of the oil sands were based on an energy consumption of 152 MJ/ton ore moved (Johnson et al., 2004), an average stripping ratio of 2:1, and the assumption that energy is provided by diesel. Oxyfiring with CO_2 capture can be applied to the heaters, which heat the water used to extract the bitumen.

Mined oil sands are hauled to an electrically powered grinding unit and then transported via conveyor belt to the bitumen-recovery process, which recovers 95% of the bitumen in the oil sand. Hot water (93 °C), citrus solvent, and oil sands are mixed together and pumped through a hydrocyclone train. Water is recovered from separated sands using dewatering screens and the damp (10 wt.% water) sands are disposed of as tailings. The extracted mix of bitumen, water, and solvent is decanted, separating the aqueous mixture into a water stream and a bitumen/solvent stream. Solvent is recovered from the bitumen in a distillation column and is also recycled through the hydrocyclone train.

Upgrading. Next, bitumen undergoes primary upgrading in a delayed coker, which thermally decomposes hydrocarbons in the bitumen (12° API gravity), creating lighter weight oils (25.8° API gravity), gas, and coke. The delayed coker requires 0.754 kWh of electricity and 8.38 MJ per GJ of gasoline produced. Gases produced in the delayed coker (5 wt.% of the product) are burned to recover their heating value after being treated to remove sulfur and nitrogen. Coke (12% of the product) is sold and is considered a co-product. GHG emissions are apportioned to the SCO and coke based on their value ($89/bbl SCO and $1.9/ton coke). The oil produced from the delayed coker is fractionated and hydrotreated to achieve the target syncrude quality of 32° API gravity. Hydrotreating requires approximately 11.7 m^3 of hydrogen per barrel of oil leaving the delayed coker. The remainder of the upgrading process is the same as that described for in situ oil shale. Oxyfiring with CO_2 capture is applied to the boilers and process heaters in the hydrogen plant, hydrotreater, and delayed coker.

2.6. Upgrading subprocesses

Hydrogen production, hydrotreating, amine scrubbing, fractionation, sour-water stripping, and sulfur recovery are common to several of the scenarios. Hydrogen production requires 0.164 kWh and 64.2 MJ of natural gas per kg of H_2 generated; it also generates a surplus of 90.3 kg of 600 psig steam per kg of H_2 generated, which is used to reduce steam requirements from other steps in the upgrading process. Table 2 shows the energy requirements from all sources for each of these subprocesses on a basis of unit energy of gasoline.

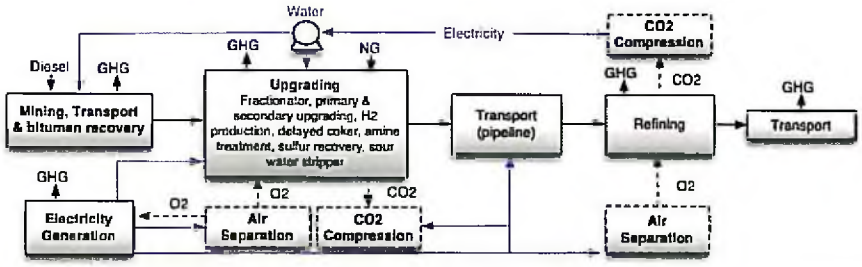

Fig. 5. Simplified process flow diagram for the Utah ex situ oil sand cases, indicating the processes considered in this evaluation. Dotted lines and boxes indicate processes that only apply to the oxy-combustion case.

2.7. Oxyfiring, air separation and CO_2 compression

CO_2 storage is feasible in the Uinta basin. Dooley et al. (2009) examined theoretical CO_2 storage capacity near the Uinta and adjacent Piceance Basins and found that there appears to be sufficient CO_2 storage capacity for large-scale production of transportation fuels from oil shale with carbon capture in the region, starting at 1 MM BPD in 2015 and increasing to 3 MM BPD by 2050.

When considering the cases with oxyfiring in the extraction through upgrading stages, the following processes could utilize oxyfiring: the hydrotreater and hydrogen plant (all scenarios), bitumen recovery (oil sands), delayed coker (oil sands), fractionator (all scenarios), and the surface retort (ex situ shale). The GHG emissions associated with oxyfiring (from the electrically powered air separation and compression of the CO_2) are included in this analysis. The separation of a 95% pure oxygen stream from air is an energy-intensive process, requiring 200 kWh/ton O_2 for a coal-fired power plant (Higginbotham et al., 2011) and 268 kWh/ton O_2 for a NGCC plant (Amann et al., 2009). The CO_2 compression system was designed to compress the flue gases from oxyfired equipment to a 99% pure CO_2 stream at its critical point (7.6 MPa and 2 °C), requiring 109 kWh of electricity, 28,500 l of cooling water, and 0.36 GJ of refrigeration per ton of CO_2 compressed.

It is also possible to capture approximately 40% of the CO_2 emissions from a refinery, specifically from the boilers and process heaters (oxy-case 3, Allam et al., 2005; van Straelen et al., 2010). In the Allam study, the power for air separation, CO_2 purification, compression and transport is provided by an oxyfired NGCC power plant with CO_2 capture. However, the refineries in Salt Lake City are relatively old and small, and they would be unlikely candidates for retrofitting with oxyfiring. Consequently, this is a less likely option for reducing WTW GHG emissions from a Utah transportation fuel produced in the Uinta Basin.

2.8. Transport

Energy is required to transport the SCO to the refinery and to transport the final product, gasoline, to the pump. The SCO is transported from the Uinta Basin to a refinery north of Salt Lake City by pipeline, which is assumed to follow the existing Chevron pipeline path as closely as possible. The total pipeline distance varies for each scenario: 245 km for ex situ oil sands, 256 km for in situ oil shale, and 285 km for ex situ oil shale. The electricity required to pump the crude includes the energy necessary to overcome inclination, friction and oil hold ups. The GHG emissions required to transport the final product to the pump is based on an average value for the United States of 0.51 g CO_2 e/MJ US EPA (2009).

2.9. Refining and oxyfiring in refineries

Refining GHG emissions vary with the crude's specific gravity and are based on the relationships developed by Gerdes and Skone (2009) and summarized in Brandt (2012). For the sensitivity the analysis, Table 1 presents the refining GHG emissions.

2.10. Utilities

Water. Water is pumped from the nearest river to each location along the shortest possible straight-line path. Electricity requirements for pumping water from the river to the site are calculated based on the friction losses and elevation changes along the path. This electricity for pumping water was apportioned to the

Table 2
Summary of energy requirements for upgrading subprocesses.

	Ex situ shale air-fired	Ex situ shale oxy-fired	In situ shale air-fired	In situ shale oxy-fired	Ex situ sand air-fired	Ex situ sand oxy-fired	Units
Hydrotreater							
Electricity	1.55	1.71	1.53	1.76	1.47	1.47	kWh/GJ product
Natural gas	35.9	30.8	33.8	33.3	37.2	36.6	MJ/GJ product
Fractionator							
Electricity	9.11E-02	9.11E-02	9.06E-02	9.06E-02			kWh/GJ product
Natural gas	19.2	19.2	19.1	19.1			MJ/GJ product
Steam: 50 psig	4.55	4.55	4.53	4.53			kg steam/GJ product
Amine treatment unit							
Electricity	2.79E-04	2.79E-04	2.96E-04	2.96E-04	1.21E-04	1.21E-04	kWh/GJ product
Steam: 50 psig	19.0	19.0	20.2	20.2	8.24	8.24	kg/GJ product
Sulfur recovery unit							
Electricity	6.79E-03	6.79E-03	7.22E-03	7.22E-03	2.94E-03	2.94E-03	kWh/GJ product
Sour water stripper							
Electricity	0.299	0.299	2.06E-02	2.06E-02	4.42E-02	4.42E-02	kWh/GJ product
Steam: 50 psig	17.0	17.0	1.17	1.17	2.51	2.51	kg/GJ product

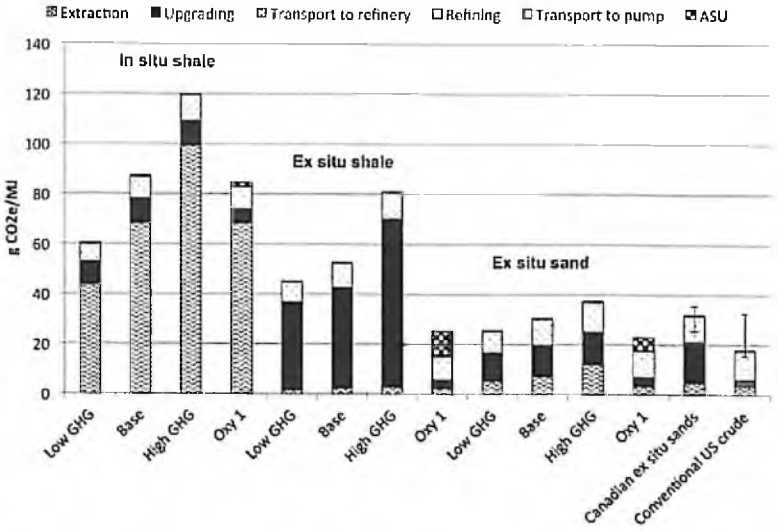

Fig. 6. Comparison of WTP GHG emissions for production of conventional gasoline from in and ex situ production of Utah oil shale, ex situ Utah and Canadian oil sands (ANL, 2012), and conventional crude oil (US EPA, 2009). The error bars on the Canadian ex situ sands show the range of values reported in McKellar et al. (2009) for reformulated gasoline, and the error bars for conventional US crude show the range of values reported in Gerdes and Skone (2009) for conventional gasoline. Oxy case 1 is also included for comparison purposes. ASU: air separation unit. Manufacture of reformulated gasoline generates approximately 4% more GHG emissions during the refining stage and approximately 1% in WTP emissions (ANL, 2012), but insufficient information is available in McKellar et al. (2009) to adjust their GHG emissions to a basis of conventional gasoline.

extraction and upgrading life-cycle stages based on the water consumption of the associated processes. The electricity required to treat the water is not included in the analysis.

Steam generation. Steam required in various processes is produced with an 81% efficient natural gas boiler. The hydrogen plant generates excess high-quality steam, which is used to offset steam requirements in other processes in the upgrading/pre-processing stages.

Electricity. All baseline and high GHG cases use electricity from Utah's electricity grid (82% coal, 15% natural gas, and 3% renewables) with an emission rate of 1864 g CO_2 e/MJ (EPA, 2012). For the oxy cases 2 and 3, we considered oxyfiring with CO_2 capture for a NGCC plant to provide all electricity from extraction through the upgrading stage at 12 g CO_2 e/kWh (Davison, 2007).

2.11. Fuel combustion

When considering WTW life-cycle emissions, combustion of gasoline with associated GHG emissions of 75.2 g CO_2 e/MJ is added to each case.

2.12. Net energy return

The net energy return (NER) and the net external energy return (NEER) are useful metrics for comparing fuel sources. The NER is the ratio of usable energy gained from an energy resource to the energy used (directly and indirectly) to obtain that resource. The NEER is the ratio of usable energy gained from an energy resource to the direct energy used (excluding e.g., any produced fuel consumed while producing the resource). For the oil shale cases presented in this study the NER and NEER are the same. For the oil sands cases, the NER includes the gases generated in the delayed coker, and NEER excludes these gases. The NER and NEER presented are at the point of consumption, the fuel pump.

3. Results

3.1. Baseline

Fig. 6 illustrates the baseline and sensitivity analysis of WTP GHG emissions for conventional gasoline production from in situ and ex situ oil shale (baseline 87.4 and 52.8 g CO_2 e/MJ, respectively) and ex situ oil sands (30.5 g CO_2 e/MJ baseline). For comparison purposes, Fig. 6 includes reported WTP GHG emissions from ex situ production of Canadian oil sands (ANL, 2012) and US conventional crude oil (US EPA, 2009) as well as the GHG emissions for oxy case 1. Although this study uses ANL's ex situ oil sands WTP GHG emissions and US EPA's WTP GHG emission as points of comparison, other ranges of WTP life-cycle GHG emissions have been reported, as illustrated by the error bars in Fig. 6. The figure also illustrates the importance of the extraction and upgrading steps to the lifecycle WTP GHG emissions from unconventional fuels. GHG emissions from transport to the pump are the same for all cases. The GHG contributions associated with transport to the refineries are lower for the Utah cases than either the Canadian oil sands or US conventional crude because the transport distances are shorter.

The sensitivity analysis shows the importance of the resource quality (all scenarios), the retort process (ex situ shale), shale permeability (in situ shale), and project lifetime (in situ shale) on life-cycle GHG emissions. The range of WTP GHG emissions (low to high) estimated for in situ (60.4–120 g CO_2 e/MJ) and ex situ (45.2–80.9 g CO_2 e/MJ) production of gasoline from oil shale is greater than the range of emissions for ex situ sand (25.6–37.5 g CO_2 e/MJ), Canadian oil sands (29–35 g CO_2 e/MJ), or conventional crude (16–33 g CO_2 e/MJ). The variation between the low GHG and high GHG cases are greater for the oil shale scenarios than for the sand scenario because commercial processing of shale is not widely established and greater uncertainty is associated with the process selection and resource recovery.

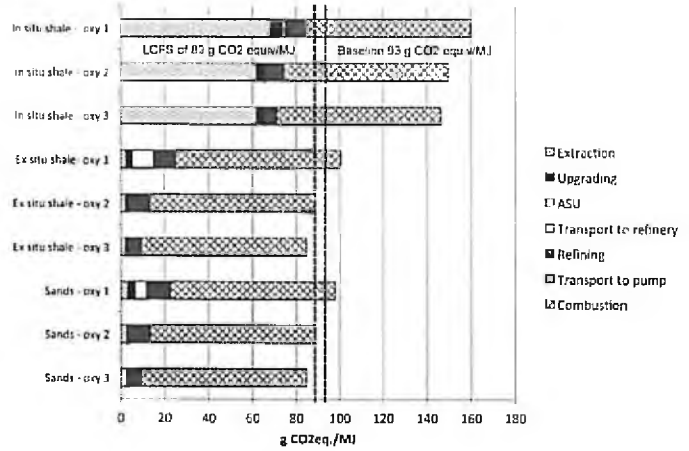

Fig. 7. Comparison of estimated WTW GHG emissions for ex situ Utah oil sands and shale with the California LCFS of 89 g CO_2 e/MJ and the baseline GHG emissions associated with the Energy Independence and Security Act. Note that WTP GHG emissions can be obtained by subtracting 75.2 g CO_2 e/MJ from the WTW GHG emissions.

Fig. 6 also illustrates the large potential for oxyfiring with CO_2 capture to reduce GHG emissions. It is worthwhile to note that the additional GHG emissions associated with air separation and CO_2 compression are less than the overall GHG emissions savings associated with oxyfiring and CO_2 capture.

3.2. Oxyfiring to meet a LCFS

Fig. 7 presents the WTW life-cycle GHG emissions for the three scenarios (3 cases each) with oxyfiring and CO_2 capture. Fig. 7 presents these emissions along with the California LCFS and the Energy Independence and Security Act benchmark. The figure illustrates that it is possible to meet a LCFS through oxyfiring with carbon capture for the ex situ oil sands and shale scenarios.

For the ex situ shale and sand cases, oxyfiring with CO_2 capture in the extraction and upgrading life-cycle stages can reduce WTW GHG emissions by 22–34% and 7–20%, respectively. Because natural-gas generators used to heat the in situ shale cases are not suited to oxyfiring, WTW GHG emissions can only be reduced by 2–10%. In addition, oxy case 1 GHG reductions are insufficient for any of the three scenarios to meet the baseline average GHG emissions of 93.3 g CO_2e/MJ (US EPA, 2009) or California's LCFS. Additional GHG reductions could be achieved by supplying all of the electricity in the extraction through upgrading stages from an oxyfired NGCC plant with CO_2 capture (oxy case 2). These additional steps would allow conventional gasoline produced from Utah oil shale and sand (ex situ scenarios) to meet the California LCFS. Fuels produced from in situ processing of oil shale are unlikely to meet an LCFS.

3.3. Net energy return

The baseline NERs for in situ and ex situ shale at the point of consumption are 0.48 and 2.19, respectively. The baseline NEER for oil sands is 3.01, and the baseline NER is 2.37. For comparison purposes, the point-of-consumption EROI (energy return on investment) for gasoline produced from conventional crude ranges from 6 to 10 (Cleveland, 2005), and the NER for fuel produced from Canadian oil sands is 2.81 (Brandt et al., 2013).

Oxyfiring with carbon capture does reduce the NERs as shown in Fig. 8. For the baseline ex situ oil shale case, applying oxyfiring with CO_2 capture decreases the NER by 6.8–11% for a corresponding reduction of 22–34% of WTW GHG emissions for oxy cases 1–3, respectively (52–82% for WTP GHG emissions). The application of oxyfiring with CO_2 capture to the baseline oil sands case decreases the NER by 4.2–7.7% with corresponding reductions in WTW GHG emissions of 7–20% for oxy cases 1–3, respectively (25–69% reduction in WTP GHG emissions). The ex situ shale scenario has a greater quantity of GHG emissions that are amenable to CO_2 capture than the sand scenario. Specifically, CO_2 emissions from the extraction and transport of the resource and overburden with diesel-powered equipment (assumed not capturable) are greater for the oil sands scenario than the ex situ shale scenario because the oil shale scenario does not require removal of overburden. Oxyfiring with CO_2 capture can also reduce in situ shale WTW GHG emissions by 2–10%. Because CO_2 from the generators that heat the shale formation are not capturable and this is responsible for the majority of the WTP GHG emissions, oxyfiring with CO_2 capture has a smaller effect on the in situ shale scenario than on the other scenarios.

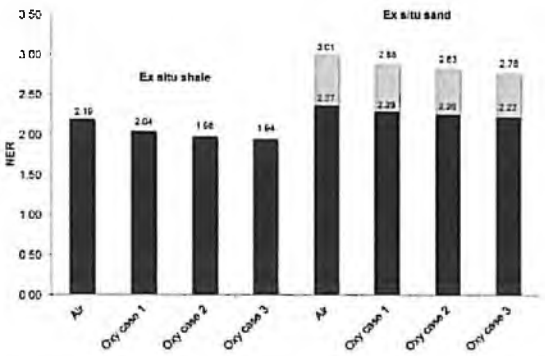

Fig. 8. Point-of-consumption NER and NEER estimates for the air-fired baseline and three oxyfired cases. For the shale cases, NER and NEER are equal, but for the sand cases NER (lower value) and NEER (higher value) are both presented. In situ sand is excluded because the baseline NER is less than 1.

4. Discussion

4.1. Baseline and sensitivity – comparison with other studies

WTP GHG emissions for the two oil shale scenarios exceed the range reported for US conventional crude oil, and the emissions for the oil sands scenario exceeds the average WTP GHG emissions for conventional crude oil (Fig. 6).

Although studies of GHG emissions from production of oil shale are limited, employ different assumptions, and have different final products, this study's WTP GHG emissions from ex situ oil shale of 52.8 g CO_2 e/MJ (baseline, 45.2–80.9 g CO_2 e/MJ range) are in the range of values reported for other ex situ shale processes: 45 g CO_2 e/MJ for a hot-solids recycle process (estimated from Burnham and McConaghy, 2006), a range of 54–83 g CO_2 e/MJ (reformulated gasoline) for the ex situ Alberta Taciuk retorting process (ATP) in the Green River Formation (estimated from Brandt, 2009), and 65 g CO_2 e/MJ for the OSEC ATP in the Uinta basin (estimated from US BLM, 2007). One might expect the ATP process discussed by Brandt et al. to have greater GHG emissions than this study because they produce much of the heat needed for their process by combusting the spent shale at 750 °C, which results in higher GHG emissions than combusting natural gas to heat the retort, as in this analysis. Their retort temperature also results in some release of CO_2 though carbonate decomposition. Our baseline and low GHG cases include a lower retort temperature of 480 °C and assume negligible carbonate decomposition.

The WTP GHG emissions from the in situ oil shale scenario (87.4 baseline, 60.4–120 g CO_2 e/MJ range) are dominated by the extraction stage – specifically the heating of the shale formation with natural-gas electrical heaters, which contributes 68 g CO_2 e/MJ of the 87 g CO_2 e/MJ WTP GHG emissions. The WTP GHG emissions are greater than those reported for the Shell in situ conversion process (ICP) of 38–63 g CO_2 e/MJ transportation fuel (Brandt, 2008) although they do fall within the wide range of values reported for ex situ oil shale (40–180 g CO_2 e/MJ gasoline, Brandt and Farrell, 2007). Likely sources of the differences between this study and the ICP results include differences in the heating well layout and assumptions about the properties of the rock. For example, this analysis uses a different well spacing and the STARS reservoir simulation tool to predict oil production curves as a function of heating time. The production curves obtained from the STARS simulations are very sensitive to permeability and porosity, and Brandt (2009) also reports that GHG emissions from shale production are sensitive to shale richness. Porosity is related to shale grade, and this analysis uses a porosity of 30.1% to match a Fischer Assay of 104 l/ton (assuming the porous space is initially filled with kerogen). Brandt's analysis uses a shale grade of 111 l/ton. Changes in the production curve for the same amount of heat input strongly affect CO_2 emissions per energy unit of fuel. Finally, in the Brandt study the ICP product did not require additional upgrading and required 33% less refining energy than conventional crude. This study's product required upgrading and approximately 20% less refining energy than conventional crude.

The Utah ex situ oil sands baseline WTP GHG emissions of 30.5 g CO_2 e/MJ are in the range of values (29–35 g CO_2 e/MJ for reformulated gasoline) reported by McKellar et al. (2009). In addition, the range of 25.6–37.5 g CO_2 e/MJ is close to the range reported by Mckellar et al.

4.2. NERs

The NERs for gasoline produced from the ex situ sands and shale, the baseline and oxyfired cases are lower than the US-average, point-of-consumption EROI of 6–10 (Cleveland, 2005). The NERs for these unconventional resources will likely be a significant barrier to their commercial production. The range of NERs in this study is generally consistent with other studies of unconventional fuels. Cleveland and O'Connor (2011) report an NER for refined fuel produced from in situ and ex situ production of oil shale of approximately 1.5. They also summarize EROIs at the point of consumption calculated for oil shale processes and report EROIs ranging from 1.2–7 for in situ shale and 1.1 to greater than 10 for ex situ shale. A direct comparison with some of these studies is difficult because system boundaries differ. Brandt (2008, 2009) is the most widely cited source regarding NERs and GHG emissions for oil sands and shale. He reports NERs ranging from 1.2 to 1.6 for in situ oil production of refined fuel from oil shale. Although the estimated NER for gasoline produced by in situ processing of shale in this study is lower than those reported by Brandt (2008), as discussed in Section 4.1, shale richness and permeability are critical factors in both the energy required and the associated GHG emissions from this scenario. Brandt (2009) also reports an NER for the ATP process (ex situ shale) of 1.1–1.8, and this study's baseline NER for ex situ shale of 2.19 is slightly higher. However, the NER is consistent with this study's lower GHG emissions, which are on the low end of those reported by Brandt. The baseline NER of 2.37 for gasoline produced from ex situ oil sand is close to the NER reported by Brandt et al. (2013) of 2.81 for point of consumption product produced from Canadian oil sands. Inman (2013) reports an EROI of 1.6 for Canadian oil sands.

Studies on the effect of oxyfiring with CO_2 capture on NER are limited. However, Corstena et al. (2013) recently summarized the effect of carbon capture and storage from several life-cycle assessments studies and report a 16–44% reduction in NER associated with the addition of CO_2 capture for coal-fired power plants and a lower reduction in NER for natural gas power plants for CO_2 capture of 88–95% of the CO_2. This study shows a reduction in NER of 4–11% associated with a 7–34% reduction in WTW GHG emissions. It is also worth noting that adding carbon capture to reduce GHG emissions increases other environmental impacts due to increased energy demand and fuel consumption (Zappa et al., 2012).

4.3. Opportunities for GHG reductions

Because the fuel-consumption life-cycle stage is responsible for the majority of WTW GHG emissions (Fig. 1), it generally presents the greatest opportunity for reducing the fuel cycle's carbon footprint, particularly for conventional sources of crude oil. For example, improving the average efficiency of a gasoline-powered passenger vehicle from 9.2 km/l (21.6 miles per gallon, MPG) to 12.2 km/l (28.5 MPG) reduces the life-cycle WTW GHG emissions by 20% – equal to the average WTP GHG emissions in the US (Gerdes and Skone, 2009).

For conventional crude oil, refining is generally the second most GHG intensive life-cycle stage (Fig. 1), and some incremental opportunities for improving the efficiency exist. For example, the efficiency of most refinery process heaters could be improved by 10% with air preheating and improved burner design (US DOE, 2007). However, the refining industry is mature, and these opportunities are limited (Gerdes and Skone, 2009). Carbon capture is also an option for reducing GHG refining emissions. As discussed in the Section 3, approximately 40% of CO_2 emissions from a world-scale refinery are suitable for CO_2 capture; these capturable emissions tend to come from the larger, more concentrated CO_2 sources such as boilers and process heaters (van Straelen et al., 2010; Allam et al., 2005).

The raw material extraction and processing (including upgrading) life-cycle stages can be important contributors to the carbon footprint for unconventional fuels, such as oil sands, oil shale, and heavy oil. Dooley et al. (2009) suggest that the development of unconventional fuels in the United States would significantly

increase GHG emissions, and Brandt and Farrell (2007) suggest that transitioning to low-quality crude sources, such as tar sands or coal-to-liquids, could raise upstream GHG emissions by several gigatonnes annually without mitigation strategies. Industry has focused on improving energy efficiency in the extraction and processing of unconventional fuels and has begun to consider carbon capture. Brandt et al. (2013) report that Canadian oil sands operations have become more efficient over the past 40 years, with net energy returns ratios increasing from 1 in 1970 to approximately 2.8 in 2013. As an example of the potential for CO_2 capture in conjunction with oil sands production, the Shell Quest project seeks to captures CO_2 emissions from their hydrogen production facilities in Alberta Canada and serves as an example of steps being taken to reduce GHG emissions.

5. Conclusions

GHG emissions for conventional gasoline produced from the unconventional resources examined in this study are greater and NERs are lower than the corresponding emissions and NERs for conventional sources of crude. Furthermore, GHG emissions and NERs from the ex situ production oil shale and sands are in the range of those reported in other studies. GHG emissions from the in situ production of shale are greater than those reported in other studies although fewer studies have considered this production method than ex situ production of shale. The sensitivity analysis shows the importance of the resource quality (all scenarios), the retort process (ex situ shale), and shale permeability (in situ shale).

The use of oxyfiring with CO_2 capture could significantly reduce WTW GHG emissions from the ex situ scenarios: by 22–34% (shale) and 11–23% (sand). Applying oxyfiring and CO_2 capture to the electricity generation and the appropriate processes in the extraction through upgrading life-cycle stages would allow these two fuels to meet a LCFS. The in situ oil shale scenario is less amenable to CO_2 capture with potential reductions of 2–11%, which would not allow compliance with a LCFS. The application of oxyfiring with CO_2 capture is energy intensive although the GHG benefit exceeds the GHG penalty associated with air separation and CO_2 compression. However, this does reduce the NERs for the ex situ scenarios by 4–11%, which could place unconventional fuels at a competitive disadvantage compared to less GHG-intensive resources.

Acknowledgments

This material is based upon work supported by the Department of Energy under Award Number DE-FE0001243. Many thanks to Adel F. Sarofim, Presidential Professor, University of Utah, deceased, for his numerous contributions. Thanks to Jesse Dumas, undergraduate research assistant, for help with data gathering.

Appendix A. Supplementary data

Supplementary data associated with this article can be found, in the online version, at doi:10.1016/j.ijggc.2014.01.002.

References

Advanced Resources International, 2008. Greenhouse Gas Life-cycle Emissions Study: Fuel Life-cycle of U.S. Natural Gas Supplies and International LNG. Advanced Resources International, Arlington, VA http://www.adv-res.com/pdf/ari_lca_nov_10_08.pdf

Allam, R., White, V., Ivens, N., Simmonds, M., 2005. The oxyfuel baseline: revamping heaters and boilers to oxyfiring by cryogenic air separation and flue gas recycle. In: Thomas, D.C. (Ed.), Carbon Dioxide Capture for Storage in Deep Geologic Formations: Results from the CO_2 Capture Project. Capture and Separation of Carbon Dioxide from Combustion Sources. Elsevier, pp. 451–475 (Chapter 26).

Amann, J.M., Kanniche, M., Bouallou, C., 2009. Natural gas combined cycle power-plant modified into an O_2/CO_2 cycle for CO_2 capture. Energy Conservation and Management 50, 510–521.

ANL, 2012. The Greenhouse Gases, Regulated Emissions, and Energy Use in Transportation (GREET) Model. http://greet.es.anl.gov/

Blackett, R.E., Open File Report 355 1996. Tar-Sand Resources of the Uinta Basin, Utah: A Catalog of Deposits. Utah Geological Survey, Salt Lake City, UT http://ugspub.nr.utah.gov/publications/open_file_reports/OFR-335.pdf

Brandt, A.R., Farrell, A.E., 2007. Scraping the bottom of the barrel: greenhouse gas emission consequences of a transition to low-quality and synthetic petroleum resources. Climatic Change 84, 241–263.

Brandt, A., 2008. Converting oil shale to liquid fuels: energy inputs and greenhouse gas emissions of the Shell in situ conversion process. Environmental Science & Technology 42 (19), 7489–7495.

Brandt, A.R., 2009. Converting oil shale to liquid fuels with the Alberta Taciuk processor: energy inputs and greenhouse gas emissions. Energy & Fuels 23, 6253–6258.

Brandt, A.R., 2012. Variability and uncertainty in life-cycle assessment models for greenhouse gas emissions from Canadian oil sands production. Environmental Science & Technology 46, 1253–1261.

Brandt, A.R., Englander, J., Bharadwaj, S., 2013. The energy efficiency of oil sands extraction: energy return ratios from 1970 to 2010. Energy 55, 693–702.

British Columbia Parliament, 2010. Bill 16-2008, Greenhouse Gas Reduction (Renewable and Low Carbon Fuel Requirements Act. 4th Session, 38th Parliament). http://www.leg.bc.ca/38th4th/1st_read/gov16-1.htm

Buhre, B.J.P., Elliott, L.K., Sheng, C.D., Gupta, R.P., Wall, T.F., 2005. Oxyfuel combustion technology for coal-fired power generation. Progress in Energy and Combustion Science 31 (4), 283–307.

Burnham, A.K., McConaghy, J.R., 2006. Comparison of the acceptability of various oil shale processes. In: Presentation at 26th Oil Shale Symposium, volume UCRL-CONF-226717, Golden, CO. Lawrence Livermore National Laboratory.

Campbell, J.H., 1978. The kinetics of decomposition of Colorado oil shale: II. Carbonate minerals. Lawrence Livermore Laboratory, Livermore, CA, UCR-52089, Part 2.

Cleveland, C.J., 2005. Net energy from the extraction of oil and gas in the United States. Energy 30 (5), 769–782.

Cleveland, C.J., O'Connor, P.A., 2011. Energy Return on Investment (EROI) of oil shale. Sustainability 3, 2307–2322.

Corstena, M., Ramírezа, L., Shena, L., Koornneef, J., Faaija, A., 2013. Environmental impact assessment of CCS chains – lessons learned and limitations from LCA literature. International Journal of Greenhouse Gas Control 13, 59–71.

Dooley, J.J., Dahowski, R.T., Davidson, C.L., 2009. The potential for increased atmospheric CO_2 emissions and accelerated consumption of deep geologic CO_2 storage resources resulting from the large-scale deployment of a CCS-enabled unconventional fossil fuels industry in the US. International Journal of Greenhouse Gas Control 3, 720–730.

CARB, 2012. Final Regulation Order with Ammendments Subchapter 10. Climate Change Article 4. Regulations to Achieve Greenhouse Gas Emission Reductions Subarticle. 7. Low Carbon Fuel Standard. http://www.arb.ca.gov/fuels/lcfs/CleanFinalRegOrder112612.pdf

Cleveland-Cliffs Iron Company, Development Engineering, Inc., Arthur G. McKee & Company, Sohio Petroleum Company, 1976. Paraho Final Report, Commercial Evaluation. Paraho Development Corporation, Grand Junction, CO.

CMG Ltd, 2013. STARS – Advanced Processes Reservoir Simulator. http://www.cmgl.ca/software/soft-stars

Davison, J., 2007. Performance and costs of power plants with capture and storage of CO_2. Energy 32, 1163–1176.

European Union, 2008. Monitoring and reduction of greenhouse gas emissions from fuels (road transport and inland waterway vessels).

Energy Independence and Security Act of 2007, 2007. Pub. L. No. 110-140, 121 Stat. 1492, § 201 (codified at 42 U.S.C. § 7545.(o).

Fuel and Mineral Resources, 1983. Process Engineering Data on the Unit Operations of the Paraho-Ute (direct retorting) and Union B (indirect retorting) oil shale processes. Fuel & Mineral Resources, Inc, Reston, VA.

Gerdes, K.J., Skone, T.J., DOE/NETL-2009/1362 2009. An Evaluation of the Extraction, Transport and Refining of Imported Crude Oils and the Impact on Life Cycle Greenhouse Gas Emissions.

Higginbotham, P., White, V., Fogash, K., Guvelioglu, G., 2011. Oxygen supply for oxyfuel CO_2 capture. International Journal of Greenhouse Gas Control 5S, S194–S203.

Inman, M., 2013. The true cost of fossil fuels. Science American 308, 58–61.

ICSE (Institute for Clean and Secure Energy), 2013. A Market Assessment of Oil Shale and Oil Sands Development Scenarios in Utah's Uintah Basin. ICSE, Salt Lake City, UT http://www.icse.utah.edu/leftnavid3sublistnavid10subpage115

Johnson, H.R., Crawford, P.M., Bunger, J.W., Technical Report 2004. Strategic Significance of America's Oil Shale Resource: Volume II – Oil Shale Resources, Technology and Economics. AOC Petroleum Support Services, LLC, Chantilly, VA.

Johnson, R.C., Mercier, T.J., Brownfield, M.E., Self, J.G., 2010. An assessment of in-place oil shale resources in the Eocene Green River Formation, Uinta Basin, Utah and Colorado. In: U.S. Geological Survey Oil Shale Assessment Team (Ed.), Oil shale resources of the Uinta Basin, Utah and Colorado, Chapter 1, U.S. Geological Survey Digital Data Series DDS-69-BB. U.S. Geological Survey, Reston, VA http://pubs.usgs.gov/dds/dds-069/dds-069-bb/

McKellar, J.M., Charpentier, A.D., Bergerson, J.A., MacLean, H.L., 2009. A life cycle greenhouse gas emissions perspective on liquid fuels from unconventional Canadian and US fossil sources. International Journal of Global Warming 1 (1/2/3), 160–178.

Oblad, A.G., Bunger, J.W., Hanson, F.V., Miller, J.D., Ritzma, H.R., Seader, J.D., 1987. Tar sand research and development at the University of Utah. Annual Review of Energy and the Environment 23, 283–356.

Ritzma, H.R., 1979. Oil-impregnated rock deposits of Utah, Map 47, Scale 1:750,000. Geological and Mineralogical Survey, Salt Lake City, UT.

Singh, D., Croiset, E., Douglas, P.L., Douglas, M.A., 2003. Techno-economic study of CO_2 capture from an existing coal-fired power plant: MEA scrubbing vs. O_2/CO_2 recycle combustion. Energy Conversion and Management 44, 3073–3091.

Spath, P.L., Mann, M.K., 2000. Life Cycle Assessment of a NG Power Generation System. National Renewable Energy Laboratory, Golden, CO.

Snarr, D.G., 2008. Presentation to the Western U.S. Oil Sands Technology Transfer Meeting, Salt Lake City, UT.

Nelson, L., 2012. Red Leaf Resources: overview and update. In: Presentation at University of Utah Unconventional Fuels Conference, Salt Lake City, UT http://www.icse.utah.edu/assets/archive/2012/ucl_agenda.htm

United Kingdom Renewable Fuels Agency, 2009. The Renewable Transport Fuel Obligations Order, amended 15 April 2009.

US BLM, 2007. Oil shale research, development, and demonstration project, White River Mine, Uintah County, UtahC Environmental Assessment UT-080-06-280.

US DOE, 2007. Mining Industry Energy Bandwith Study. BCS, Inc.

US EPA, 2012. Emissions & Generation Resource Integrated Database (eGRID) eGRID2012 Version 1 for Year 2012 summary tables. http://www.epa.gov/cleanenergy/energy-resources/egrid/index.html

US EPA, Docket ID: EPA-HQ-OAR-2005-0161-0938 2009. Lifecycle Greenhouse Gas (GHG) Emissions Results Spreadsheets. www.regulations.gov

Vanden Berg, M.D.V., Special Study 128 2008. Basin-wide Evaluation of the Uppermost Green River Formation's Oil-Shale Resource, Uinta Basin, Utah and Colorado. Utah Geological Survey, Salt Lake City, UT http://geology.utah.gov/online/ss/ss-128/ss-128txt.pdf

van Straelen, J., Geuzebroek, F., Goodchild, N., Protopapas, G., Mahony, L., 2010. CO_2 capture for refineries, a practical approach. International Journal of Greenhouse Gas Control 4, 316–320.

Weiss, M.A., Klumpar, I.V., Peterson, C.R., Ring, T.A., (DOE Report # DOE/ER/30013) 1982. Shale-Oil-Recovery Systems Incorporating Ore Beneficiation. Energy Laboratory, Massachusetts Institute of Technology, Cambridge, MA.

Zappa, P., Schreiber, A., Marx, J., Haines, M., Hake, J.F., Gale, J., 2012. Overall environmental impacts of CCS technologies: a life cycle approach. International Journal of Greenhouse Gas Control 8, 12–21.

CHAPTER 4

EVALUATING UNDERGROUND COAL THERMAL TREATMENT AS A POTENTIAL LOW-CARBON ENERGY SOURCE

In preparation for submission to International Journal of Greenhouse Gas Control. K.E. Kelly, D. Wang, M. Hradisky, G.D. Silcox, P.J. Smith, E.G. Eddings, D.W. Pershing

4.1 Abstract

Although methane recovery from coal seams is a common industrial practice, in situ pyrolysis of the resource to produce a syngas or liquid fuel is not a commercial technology. Coalbed methane produces less than 1% of the energy content of the coalbed, and in situ pyrolysis (underground coal thermal treatment, UCTT) offers the potential for substantially more energy recovery than coalbed methane. This evaluation assesses the life-cycle energy and greenhouse gas (GHG) impacts of UCTT, including drilling wells, heating the formation, recovery, cleanup, and transportation of the product. It is based on experimental results at two scales, a simple heat-transfer model and literature results. The results show that UCTT can produce a high-quality liquid product and a gas mixture. However, heating the formation, much of it to low temperatures, results in limited product formation and requires significant energy. Consequently, the GHG emissions are high, at the upper end of the range reported for in situ processing of oil shale. Net energy returns (NERs) are in the range reported for in situ production of oil shale. Product yield at low temperatures and the moisture content of the coal are the two key factors in determining the feasibility of the UCTT process.

4.2 Introduction

With current coal mining technologies and production rates, the US has approximately 270 years of coal reserves (BP 2014). In addition to recoverable coal reserves, the US has vast coal resources, which are currently unrecoverable due to their depth, access, and other factors (US EIA 2013). This provides an opportunity for an in situ technology to recover otherwise unrecoverable energy from coal. Although 2014

natural gas prices are at historic lows in the United States, price increases are projected, and prices will increase more rapidly with US natural gas exports (US EIA 2014). Furthermore, methane recovery from coal seams is common, but coalbed methane (CBM) produces less than 1% of a coal bed's energy content (Flores 1998). In situ pyrolysis offers the possibility of substantially more energy recovery from the resource and the potential to convert the high-carbon content fuel into a lower carbon content, higher heating value syngas or liquid fuel.

A novel in situ pyrolysis process, UCTT, is proposed and evaluated. By slowly heating coal in situ, the coal is transformed from long chain geopolymers to a synthetic gas stream containing hydrogen and low molecular-weight hydrocarbons, liquid fuel, and char. The coal contains native moisture as well as ash, and these components are also heated but do not transform into valuable products. This process has the potential to leave large portions of the carbon from the coal in the ground in the form of char. Although UCTT requires additional energy input compared to CBM, the added resource utilization and carbon management may make this process worthwhile and motivates its evaluation. UCTT differs from underground coal gasification – it does not inject oxygen and foster coal combustion; rather, it involves heating coals to pyrolysis temperatures. Figure 4.1 shows an example of the UCTT concept.

Although peer-reviewed studies of a UCTT-type process are limited, studies evaluating other in situ fossil fuel processes report life-cycle GHG emissions for the production of transportation fuel. These studies include thermal treatment of heavy oil, in situ production from oil sands, and the Shell in situ conversion process (ICP) for oil shale conversion. As conventional sources of crude oil become scarce, transportation

fuels are increasingly being produced from lower quality resources, like heavy oil and oil sands, and potentially oil shale. Brandt and Unnsach (2010) examined the energy intensity of thermally enhanced (steam injection) oil recovery of heavy oils in California. They report well-to-pump (WTP) greenhouse gas (GHG) emissions of 32 – 47g CO_2 e/MJ for gasoline produced from this resource (lower heating value). In comparison, well-to-wheels GHG emissions from conventional petroleum sources in the US are 18.1 g CO_2 e/MJ (US EPA 2009). Brandt and Unnsach (2010) found that the GHG emissions vary with energy demand of the heavy oil treatment (i.e., steam to oil ratio), choice of fuel used for steam generation, co-generation of electric power, and the electricity mix.

Brandt (2008) evaluated GHG emissions from the production of gasoline using the Shell ICP. This process heats an oil-shale field in situ, releasing liquid- and gas-phase fuels. Due to concerns over potential groundwater contamination, the process also requires a freeze wall to isolate the processing area from the water table. First, heater and producer wells are drilled. In the heating wells, electrical heaters heat the oil shale to 340 – 370°C over a period of several years. The liquid and gas fuels flow to the production wells for recovery. These products are then upgraded, transported, and refined into gasoline. The study reports GHG emissions of 38 – 63 g CO_2 e/MJ gasoline. Work began on ICP in western Colorado in the 1980s, but activities in the US appear to have ceased. However, work on this process continues in Jordan and Israel (Josco 2014, IEI 2014).

In addition to studies of in situ processes to provide transportation fuels, researchers have proposed electricity production from oil shale with in situ carbon capture (EPICC). This method employs a solid fuel cell underground to heat a shale

formation (Mulchandani and Brandt 2011). The produced gas from this process flows back to the fuel cell to provide additional energy to generate electricity and to heat the formation. They report that EPICC's GHG emissions are 51 – 99 kg CO_2/MWh compared to 92-145 kg CO_2/MWhr for pulverized coal with carbon capture. This work appears to be in the conceptual stages, and the authors cite EPICC's potential drawbacks including uncertain operation of subsurface fuel cells, potential geologic impacts without pressure management, and economic concerns associated with the value of stranded energy left in the formation and the long time period for retorting.

The goal of this study is to begin to understand the feasibility of a UCTT process, specifically by estimating UCTT's cradle-to-gate, life-cycle energy, and greenhouse gas (GHG) emissions. The analysis includes the impacts of well drilling, heating the formation, recovery, cleanup, and transportation of the UCTT products. The energy required and product yields are based on experimental results and simulations that rely on the properties from the experiments.

4.3 Material and methods

This study uses a simplified process model life-cycle assessment approach to determine energy and GHG emissions associated with UCTT. All results are presented on a lower heating value (LHV) of the coal and products. Figure 4.2 shows the processes considered in the UCTT analysis. It is envisioned as a cradle-to-gate analysis with final products being transportation fuel (conventional gasoline) and electricity generated from the gas-phase products. The evaluation does not include the energy and GHG emissions associated with the construction of the refineries and power plant or the manufacture of

the drilling rig, the well casing, the well cement, or the associated fittings and equipment. The UCTT process transforms coal in the ground into char and two product streams: a liquid and a gas stream containing hydrogen, low molecular-weight hydrocarbons. While several options for heating a formation candidate formation exist, this analysis focuses on electrical heating of the formation. The gas-phase products are burned to reduce the purchased electricity needed to heat the formation. The liquid products are refined into a transportation fuel, conventional gasoline. As discussed in Section 4.3.2, UCTT will not likely produce sufficient gas-phase products to permit the sale of excess electricity.

The following subsections describe the resource, life-cycle stages, and other related processes.

4.3.1 Resource

This evaluation, including the experimental and simulation studies, is based on a Utah Sufco coal, a high-volatile, low-moisture bituminous coal. Table 4.1 shows the coal properties. The Sufco coal mine is located in Sevier County, UT in the Blackhawk Formation of the Wasatch Plateau coalfield; it is one of the longest continuously running underground long-wall mines in the US. It has approximately 126 million tons of recoverable resource and its annual production in 2012 was 5.7 million tons (BSNF 2013). Its average thickness is approximately, 3.5 m, although thicker portions of the seam exist, and the overburden depth ranges from 100 – 600 m (Keith 1989, 1991).

The evaluation assumes a 10 m thick seam of coal at a depth of 333 m; this hypothetical coal seam that is sufficiently contiguous in the radial direction for the heat to be completely absorbed by the coal over the time period of interest.. The seam is heated

with a 10 m long, 0.25 m diameter heater. Only one well is drilled for the analysis; the heating well is also assumed to be the producing well. The analysis assumes a formation pressure of 30 bar and a formation temperature of 20°C.

4.3.2 Drilling

For drilling the vertical well (a heating and producing well), diesel fuel consumption and well depth come from the Utah Division of Oil Gas and Mining Well Reports (UDOGM 2012), and the average of 12.4 l/m for wells less than 3300 m deep is used. This value is in the range of reported fuel consumption of 18.6 l/m (Advanced Resources International 2008).

4.3.3 Heating the formation

A preliminary analysis revealed that the energy needed to heat the formation and product yield are critical to the feasibility of UCTT, and these depend on the coal, char, and product properties. Consequently, much of this study focused on gathering experimental results to understand these key parameters. Literature data provided energy requirements and GHG emissions for the other life cycle stages.

4.3.3.1 Experimental measures and properties

UCTT experiments were performed at two scales: scoping studies in a high-temperature, high-pressure 1.9 cm diameter, fixed-bed reactor and larger scale studies in a 15 cm diameter, high-pressure, high-temperature rubblized-bed reactor (Smith et al. 2015). The scoping studies identified the most promising conditions as well as data for

development of a yield model. The larger scale studies allowed for more representative product generation.

The composition of the gas- and liquid-phase products comes from GC and GC/MS analysis, respectively, of the products from the larger scale reactor. Although additional species are present in limited amounts, the gas-phase products are represented by: H_2 (3%), H_2O (7%), CO (10%), CH_4, (35%), C_2H_4 (7%), C_2H_6 (10%), and CO_2 (28%) (by weight). The liquid products contain approximately 85% carbon, 11% hydrogen, 0.5% nitrogen, and 2% sulfur (by weight). The elemental composition of the liquid is in the range of that reported for conventional crude oil (Beychok 2011). The Appendix shows the product's simulated distillation and single carbon number profile, and illustrates that the UCTT product is "light-crude like".

Additional measurements were performed to determine the heat capacity (C_p) and thermal conductivity of the coal and char. These properties are used in the simulations and discussed in the following subsection. Heat capacity for the coal and char were measured with a TA DSC-Q20 differential scanning calorimeter. The measured C_p values were 1.25 ± 0.04 J/g°C for the coal and 1.41 ± 0.359 J/g°C for the char. Details of the heat capacity measurements can be found in the Appendix. Thermal conductivity was inferred from the larger scale experimental results, as described in the Appendix. As a function of temperature, the thermal conductivity of the aggregate char, product mixture is:

$$k = 3.37 \times 10^{-4} T + 0.19$$

where,

T= temperature, K.

k = thermal conductivity, W/m K.

All properties of interest − density, heat capacity, thermal conductivity, and thermal diffusivity − change as a function of temperature and coal conversion, which is also a function of temperature. The temperature simulation and yield estimates assume that properties remain constant until 234°C, one degree above the temperature at which water boils at 30 bar. As coal is converted to char and liquid and gas products, the properties in the temperature simulation changed as a weighted average of the aggregate composition. Due to the difficulty in obtaining properties for all species at UCTT temperatures and the formation pressure, the properties of the gas product are assumed to be a simplified mixture of 30% CH_4, 30% CO_2, 30% C_2H_6, and 10% water (by weight). The liquid properties were based on the single-carbon number analysis of the liquid product (Appendix). The Peng-Robertson Polar properties in the ProMax™ process simulator provided the liquid and gas properties as a function of temperature at 30 bar. The coal and char properties are based on the experimental measurements for heat capacity and thermal conductivity, described above. The coal and char specific gravities are 1.31 and 0.99, respectively (Gloyn et al. 2003). Relationships for each of the properties as a function of temperature can be found in the supplementary material (Appendix).

Thermal diffusivity was calculated using:

$$\alpha = \frac{k}{\rho C_p}$$

where,

k = thermal conductivity, W/m K.

ρ = density, kg/m^3.

C_p = heat capacity, J/kg°C.

The thermal diffusivity for coal is 1.76 x 10^{-7} m^2/s at temperatures below 234 °C when it begins to transform into char. The thermal diffusivity of the coal, char, and product aggregate at 600°C is 1.14 x 10^{-6} m^2/s. Literature values for thermal diffusivity of coal and char vary widely. Clendenin et al. (1949) summarize the effect of coal treatment temperature on coal/char properties and report the diffusivity of raw coal, approximately 1 x 10^{-7} m^2/s, and char treated to 600°C, 3.5 x 10^{-7} m^2/s. They also report that coal/char thermal diffusivity is constant until approximately 300°C, and then it increases with temperature in the range of temperatures of interest to a UCTT process. The Appendix shows the coal, char, product aggregate thermal diffusivity as a function of temperature.

The evaluation also considers an enhanced thermal conductivity case, in which the coal thermal conductivity is 0.87 W/m K (Wellington et al. 2000) and the char thermal conductivity is 1.7 W/m K (Chern and Hayhurst 2006). Wellington et al. (2000) reported that coal in situ had a higher conductivity than pulverized coal. This results in a coal diffusivity of 5.31 x 10^{-7} m^2/s and a weighted average coal, char, product diffusivity of 1.64 x 10^{-6} m^2/s at 600°C.

4.3.3.2 Yield model

A sigmiodal function was fit to the experimental scoping data (Figure 4.3), and this function was used to predict yield as a function of temperature in the UCTT simulations, discussed in the following subsection. The scoping data provided more consistent temperature profiles compared to the larger scale studies where measuring the internal temperature of the coal was challenging. The experimental data were fit by

minimizing the least squares difference between the predicted and measured yields. For the baseline case, the yield was set at 0.4525 at temperatures of 950°C and above, from coal's proximate analysis, and at less than 0.03 at a temperature of 340°C.

The baseline sigmoidal fit is given by:

$$Yield = \frac{Yield_{max}}{1 + e^{0.02096(472 - Temp)}}$$

where,

Yield = the fraction of the coal that is volatilized on an as-received basis.

$Yield_{max}$ = the maximum yield, from the proximate analysis, 0.4525 (as received).

Temp = temperature, °C.

Table 4.2 shows the minimum and maximum yield functions that were used in the sensitivity analysis (described in Section 4.3.9), and the Appendix provides additional detail on the yield function. Based on the experimental results, the model assumes a 50:50 split between liquid and gas-phase products for the baseline cases.

4.3.3.3 Temperature simulations

Temperatures were predicted as a function of time and distance from the heater using a one-dimensional unsteady heat conduction in cylindrical coordinates, given by:

$$\frac{1}{r}\frac{\partial}{\partial r}\left(r\frac{\partial T}{\partial r}\right) = \frac{1}{\alpha}\frac{\partial T}{\partial t}$$

where,

r = radius, m, with radial steps of 0.25 m.

t = time, s. The time step for the baseline case is 4750 s.

T = temperature, °C.

α = thermal diffusivity, m^2/s. See Appendix.

The equation was solved using an explicit finite-difference method where the initial temperature of the outside surface of the 0.25 radius heater was 800°C. This was consistent with the larger scale experimental studies. The far-field background temperature of the formation was 20°C. The initial temperatures of the system were: the heater at 800°C and the coal formation at 20°C. Each cylindrical element occurred at intervals of 0.25 m away from the heater and the elements extended 17.25 m from the heater, and each time step was 4750 s. This temperature prediction did not include the energy needed to heat and evaporate the water, although this energy was considered, as discussed in Section 4.3.4.4. The energy needed to vaporize the pyrolysis products was neglected. Above, 233°C the thermal diffusivity changed as a function of temperature (Appendix). These predicted temperatures were used in the yield model and in estimating the energy required to heat the coal, char, and product mixture.

4.3.3.4 Energy requirements

The energy requirement was calculated for the coal and water separately. For the coal, the energy required for each element at each time step in the simulation was calculated using:

$$Q = m\, C_p\, (T - T_{(t-\Delta t)})$$

where,

m= mass of material remaining within each element, kg. Above a temperature of 233 °C, coal transforms into the product mixture, and the product leaves the system.

C_p = heat capacity of coal at the average temperature of the element. Above a temperature of 233°C. See Appendix.

$T_{(t-\Delta t)}$ = average temperature at the previous time step at the midpoint of the element, °C.

T = midpoint temperature at time t, °C.

The cumulative energy required to heat the coal was calculated by summing the required energy at each time step.

The cumulative energy required to heat the water is given by:

$$Q = m\Delta H_{vap,\ H2O} + mC_p\ (T - T_o)$$

where,

Q = energy, kJ.

m= mass of water in each element.

T_o = 20°C, background temperature.

T = Final midpoint temperature at each element, °C. If the final temperature exceeded the boiling point of water at the formation pressure, the temperature was 233°C (boiling point of water @ 30 bar).

C_p = 4.18 kJ/kg.

$\Delta H_{vap,\ H2O\ (@30\ bar)}$ = 1,794 kJ/kg. This was included only if the final temperature of the element exceeded 233 °C.

The energy requirements for heating the water in each element to its final temperature were then summed.

During the UCTT process, an operator might choose to heat the formation for a given time period and then collect the product, or he could choose to produce continually. If products are collected continually, energy leaves the system continually. It is unclear how such a process would operate; consequently, this energy is included because it is considered more conservative, i.e., requiring more energy. This energy is given by:

$$Q = m\ C_p\ (T - T_o)$$

where,

m = cumulative mass of material leaving the system from each element, kg.

C_p = heat capacity of product mixture, kJ/kg.

T_o = initial temperature of the element, °C.

T = midpoint temperature at time t, °C.

4.3.4 Liquid products and refining

Because the hydrogen and carbon content are similar to that of conventional crude, US average refining GHG emissions and energy requirement are selected. These are 3.2 MJ/kg crude and 8.69 g CO_2e/MJ crude, respectively (ANL 2014). The mass of crude oil moved into a refinery is slightly less than the mass of the product leaving the refinery and the heating value of the liquid product and crude oil differ. Consequently, the method outlined in Wang et al. (2004) was used to adjust from a crude to gasoline basis.

4.3.5 Gas Products and processing

The product gas contains approximately 30% CO_2, and removing this prior to combustion is relatively expensive. Consequently, the gas product was presumed to be combusted in a 50% efficient natural-gas combined cycle (NGCC) turbine. This process generates 147 g CO_2 e/MJ of electricity (Spath and Mann 2000). Spath and Mann (2000) report on a 53% efficient NGCC, and the emissions were adjusted to 50% efficiency.

Because all of the gas is combusted in the NGCC to generate the electricity needed to heat the coal, no excess electricity is available for sale (see Section 4.3.2).

4.3.6 Liquid product transport

Energy and GHG emissions from transport of the liquid product are based on a US average of 6720 J/MJ product and 0.493 g CO_2 e/MJ product (ANL 2014).

4.3.7 Electricity generation and fuel combustion

Energy consumption and GHG emissions were assumed to be from a 50% efficient NGCC plant (Spath and Mann 2000). GHG emissions from combustion of gasoline were 75.2 g CO_2 e/MJ, and diesel emissions were 77.0 g CO_2 e/MJ. Natural gas combustion emits 56.6 g CO_2 e/MJ.

4.3.8 Net energy return

The net energy return (NER) and the net external energy return (NEER) are useful metrics for comparing fuel sources. The NER is the ratio of usable energy gained from an energy resource to the energy used (directly and indirectly) to obtain that resource. The NEER is the ratio of usable energy gained from an energy resource to the direct energy used (excluding e.g., any produced fuel consumed while producing the resource). For this analysis, the NER value assumes that the products are the refined liquid and gas product, and the NEER assumes that the gas is combusted to generate electricity to heat the formation. The NER and NEER presented are at the point of consumption, the fuel pump.

4.3.9 Sensitivity analysis

Table 4.2 summarizes selected emission factors, assumptions, and properties investigated for the sensitivity analysis. The preliminary analysis of UCTT identified the energy required to heat the formation and product yield as being key to the feasibility of this process. Recognizing this, the sensitivity analysis focused on several factors affecting the yield and heating of the formation. These included coal moisture content, thermal conductivity, yield model, refining energy requirements, and formation heating period.

4.4 Results

4.4.1 Experimental results

Analysis of the products from the larger scale studies revealed that carbon tends to partition to the char, while hydrogen tends to partition to the gas and tar products (Figure 4.4). Oxygen tends to be found in the water and gas products, while sulfur tends to partition to the char and tar products. The mass balance shown in Figure 4.4 uses average coal composition; however, inherent inhomogeneties in the coal exist. Consequently, the balance does not account for approximately 3% of the carbon and 6% of the hydrogen, and it slightly over-accounts for oxygen and sulfur.

4.4.2 Simulation results

Figure 4.5 shows the simulated temperature profile for baseline conditions. In this figure for a 2.5-year heating period, the edge of the element located 17 m away from the heater, which is next to the simulation boundary (17.25 m away from the heater), is

0.04°C above the background temperature of 20°C; at 5 years, this difference increases to 0.5°C. The temperature and yield profiles follow similar trends for all cases, with temperatures decreasing rapidly with distance from the heater.

For all cases except the maximum yield case, the produced gas contains less energy than that required to heat the formation. For the baseline case, the produced gas contains approximately 45% of the energy needed to heat the formation. For the 20% moisture case (Table 4.2), the produced gas contains only 23% of the energy needed to heat the formation (at 2.5 years). For the maximum yield case, the produced gas contains 50% more energy than that required to heat the formation (at 2.5 years). However, once the gas is combusted in a 50% efficient NGCC, it generates just enough energy to heat the formation. For the baseline case, 80% of the energy is needed to heat the coal, and 13% is needed to evaporate the water. In addition, 7% is needed to replace the energy leaving the system with the heated products (7%). This energy allocation indicates that, considering the life-cycle energy requirements, heating the formation requires the majority of the energy, greater than 90%, for all cases except for the maximum-yield case (83% at 2.5 years).

4.4.3 Net energy return

As time progresses, NER values decline since relatively small volumes of coal are treated to significant temperatures. Considering just the process of heating the formation, Figure 4.6 shows how NER declines over time. It also shows the energy required and the energy produced. It shows that the NER declines from 1.5 at 2.5 years to approximately

1.25 at 5 years. Figure 4.6 also confirms that the energy leaving the system with the products is small compared to the energy required to heat the coal and moisture.

Figure 4.7 shows that NERs decrease as a function of time for heating the formation for all cases. The maximum-yield model process exhibits the greatest NERs. Figure 4.7 illustrates the importance of the initial moisture content. As moisture content increases, NER decreases. At a 20% moisture content, heating the formation requires more energy than it produces in approximately 1 year, indicated by an NER of less than one. At 5 years, both the minimum yield and the 10% moisture case have process NERs of less than 1.

If the WTP lifecycle stages are considered, NER values are lower than those for just heating the formation. Table 4.3 summarizes the WTP NER and NEER values for each case. This suggests that the cases with a moisture content much greater than the baseline (3.2% moisture) are unlikely to be feasible, and the maximum-yield case is the only one that would likely be commercially viable.

4.4.4 CO_2 emissions

Of the life-cycle stages, heating the formation clearly drives the CO_2 emissions (Figure 4.8). The results presented in this figure assume that all of the natural gas is combusted to generate the electricity needed to heat the formation and that gasoline is the only remaining product. Transport and refining CO_2 emissions are similar to those for other sources of liquid fuels. On an energy content basis, well-to-pump (WTP) life-cycle CO_2 emissions are 176 g CO_{2e}/MJ baseline (56 – 367 g $CO_{2\,e}$/MJ range). This is several times greater than the US average WTP GHG emissions of 18.1 g CO_2 e/MJ (EPA 2009).

As with the NER values, the maximum-yield model provides the most attractive (lowest GHG emissions), and high moisture and minimum-yield models lead to the highest GHG emissions. The trends shown in Figure 4.8 are similar over the 5-year heating period, although the GHG emissions per unit of product are slightly higher than over the 2.5-year heating period.

4.4.5 Sensitivity analysis

Of the factors considered in the sensitivity analysis, the selected yield model and the moisture content of the coal had the greatest effect on both the GHG emissions and the NER. The maximum-yield case has a NER three-times greater than the baseline NER. Increasing the coal's moisture content from 3.2% to 10 and 20% increases the GHG emissions by a factor of 30 and 38%, respectively. Varying the refining energy requirement and GHG emissions by 10% has a less than 1% effect on overall NER and GHG emissions.

Although thermal diffusivity affects the time required to heat the coal seam and this property has a good deal of uncertainty, in the range considered in this evaluation, its effect on the NER and GHG emissions is limited. Consequently it is not included in the results. However, diffusivity may be an important consideration for the economics of a UCTT process.

4.5 Discussion

The experimental results show that UCTT can produce a high-quality liquid product and a lower energy content gas. The carbon in the coal tends to partition to the

char and would remain in the formation, while the hydrogen in the coal tends to partition to the liquid and gas products. This suggests that UCTT is worth further evaluation.

4.5.1 NERs

The baseline NEER for gasoline produced from the UCTT process is 1.1 (range of 0.4 – 4.3), and the baseline NER is 1.3 (range of 0.51– 3.2). NEER values are lower than NER values for all cases except for the maximum yield case, which has large gas yields relative to the energy required. Figure 4.9 compares the range of UCTT NERs to other sources of liquid transportation fuels and to electricity generated from coal. NERs for transportation fuels produced from corn ethanol vary because of challenges associated with estimating land-use change (Searchinger et al. 2008, Wang et al. 2012). Limited NERs are reported for oil shale. Recognizing that oil shale has a limited commercial production history, particularly in situ, a good deal of uncertainty is associated with oil shale NERs. The baseline NER for UCTT is less than half that for oil sands and in the range of that for oil shale (0.48 and 2.2, respectively, for in situ and ex situ production of crude from oil shale, Kelly et al. 2014). The in situ shale and coal processes face similar challenges with energy losses, i.e., waste energy to the formation. A number of factors would limit UCTT's feasibility including coals with high moisture content and/or low volatile yield.

NER declines with time. Consequently, the formation heating time would likely need to be a balance between the economics and NER. To overcome the fixed cost of well drilling and infrastructure, a minimum yield will be necessary. However, longer

formation heating times lead to larger volumes of coal that are heated to low temperatures, resulting in wasted energy and lower NERs.

4.5.2 CO_2 emissions

The WTP GHG emissions for the liquid fuel produced from the UCTT process with the low-moisture coal (56 – 367 g CO_2 e/MJ range) are dominated by the process of heating of the coal formation, which contributes 169 g CO_2 e/MJ of the 176 g CO_2 e/MJ WTP GHG emissions (baseline at 2.5 years of heating time). Literature values for GHG emissions from in situ recovery of coal resources are limited. However, in situ recovery of oil shale and sands can serve as useful benchmarks, as does coal-to-liquid conversion.

Figure 4.10 compares the range of WTP GHG emissions for gasoline produced by UCTT with GHG emissions from other transportation fuels. Note that a high WTP GHG emission estimate is less favorable; however, in Figure 4.9, a high NER is favorable. This evaluation's WTP GHG emissions are greater than those reported for the Shell in situ conversion process (ICP) of 38-63 g CO_2 e/MJ transportation fuel (Brandt 2008), although they are close to the wider range of values reported for ex situ oil shale operations (40-180 g CO_2 e/MJ gasoline, Brandt and Farrell 2007). They are also slightly higher than the range of values reported by Kelly et al. (2013) of 60.4-120 g CO_2 e/MJ for in situ production of crude from oil shale. These values are more than double those reported for production of reformulated gasoline from in situ recovery of Canadian oil sands (29 - 35 g CO_2 e/MJ) reported by McKellar et al. (2009). The comparatively low GHG emissions from Canadian oil sands reflects the relative ease in recovering bitumen from sands and the shallow depth of the sands. WTP GHG for transformations of coal to

liquid fuels via the Fischer Tropsch process (73-140 g CO_2 e/MJ, diesel product) are also in the range of those reported for the conceptual UCTT process described in this paper (Jaramillo et al. 2008). Those values range from 110-120 g CO_2 e/MJ (gasoline product).

This type of fuel resource, in situ coal, falls into the category of lower quality crudes that, if developed, would result in increased GHG emissions compared to conventional crude sources. Dooley et al. (2009) suggest that the development of unconventional fuels in the United States would significantly increase GHG emissions. Brandt and Farrell (2007) suggest that transitioning to low-quality crude sources, such as tar sands or coal-derived liquids, could raise upstream GHG emissions by several gigatonnes annually.

4.5.3 Sensitivity

The most important considerations in the UCTT process are product yield followed by the coal moisture content. Existing yield models focus on rapid heating rates, typical of pulverized coal combustion. Better models are needed to predict product yields at the low ultimate temperatures and the very low heating rates typical of a UCTT process (< 1°C/hr). This evaluation examined three yield models, all based on sigmoidal fits of the experimental data. These models produce yields that follow trends reported in the literature for coal devolatilization at higher heating rates >0.5°C/s (Smith et al. 1994). Because of the large volumes of coal heated to relatively low temperatures, using the maximum yield model resulted in more favorable NERs and GHGs than any of the other cases (Table 4.2).

Two subcomponents of the yield model are the ultimate yield and the product composition. The ultimate yield for the baseline coal is typical of a high-volatile bituminous coal (38 – 45%) (Smith et al. 1994). However, coal volatile content varies widely from 2 – 10% for anthracites, to 20 – 30% for low and medium-volatile bituminous coals and 40 – 50% for subbituminous and lignites (Smith et al. 1994). The product composition and the liquid-to-gas ratio are also related to the yield model. The liquid products have a greater heating value than the gas products. The LHV of the liquid products is 43,000 kJ/kg, and the LHV for the gas product mixture is 16,500 kJ/kg. The gas products contain approximately 30% by weight CO_2 and 7% H_2O, which contributes to the lower energy value of the gas products. Consequently, increasing the ratio of liquid to gas products improves the NER of the process.

Lower rank coals tend to exhibit high gas yields and low liquid yields, while high-volatile bituminous coals tend to exhibit high liquid and moderate gas yields (Smith et al. 1994). The coal selected for this analysis is a high-volatile bituminous coal with a low-moisture content. With these attributes, it a more likely candidate for the UCTT process than a lower rank, higher moisture coal or a low-volatile high rank coal.

Moisture has the second greatest effect on the viability of the UCTT process. The moisture content of the baseline coal is low. Different ranks of coal exhibit a wide variety of moisture contents, ranging from less than 5% for anthracites and bituminous/subbituminous coals to greater than 30% for lignites (Radovic 1992, Smith et al. 1994). Bituminious and subbituminous coals account for more than 90% of US coal production (US EIA 2011). Selecting a low-moisture resource would a key criterion of a UCTT process.

4.5.4 Other uncertainties

The sensitivity analysis began to address potential uncertainties in the UCTT process including formation and coal/product properties, and product yield. However, additional uncertainties will affect the feasibility of UCTT. These include, for example, whether water in the formation will flow into the heating zone as the product is recovered. Any additional water would continue to absorb energy and make the energy balance less favorable. If CMB was extracted from the formation, the coal seam would have been dewatered, thus limiting water flow into the formation. In addition to water, other light hydrocarbons may flow into the heating zone and be recovered, which would improve UCTT's feasibility.

The yield models explored in this evaluation do not cover the full range of possible models, such as Biagini and Tognotti (2014) or Kobayashi et al. (1976). Furthermore, the yield models considered in this analysis did not account for any recovery losses associated with gathering the products from the well and transporting these to the surface. Finally, it is unlikely that an operator would drill a single well. An array of closely spaced wells would be likely required. If the well spacing is sufficiently dense, product recovery per unit energy input may increase.

4.6 Conclusions

The experimental results suggest that UCTT may be promising because it can produce a high-quality liquid product as well as a gas that could help heat the formation. UCTT tends to leave the carbon in the ground and produce a lower carbon fuel than the parent coal. However, a large fraction of energy is "lost" to the formation; much of the

energy heats large volumes of coal to low temperatures, which results in limited product yield. Product yield at low temperatures and the moisture content of the coal are the two key factors in determining the feasibility of UCTT. Accurate low-temperature, low heating rate yield information is critical to further evaluation of UCTT. In spite of this limitation, this evaluation suggests that a high-volatile, low-moisture coal would be a good target for UCTT. The NER for the process is less favorable than that for oil sands and is in the general range of that for oil shale. CO_2 emissions follow a similar trend to NERs, with higher moisture and lower yields, resulting in more GHG emissions per unit product. Furthermore, the estimated CO_2 emissions are at the high end of those reported in the literature for oil shale and for production of liquid fuels from coal.

Given the NERs and GHG emissions associated with UCTT as well as the limited commercial adoption of in situ oil shale production and the low natural gas and liquid fuel prices, UCTT is unlikely to become commercially viable in the near term.

4.7 Acknowledgments

This material is based upon work supported by the Department of Energy under Award Number DE-FE0001243 and DE-NT0005015. The views and opinions of authors expressed herein do not necessarily state or reflect those of the United States Government or any agency thereof. Many thanks to Adel F. Sarofim, Presidential Professor, University of Utah, deceased, for his numerous contributions.

4.8 References

Advanced Resources, Int. 2008. Greenhouse Gas Life-Cycle Emissions Study: Fuel Life-Cycle of U.S. Natural Gas Supplies and International LNG, Technical Report November 10, 2008.

ANL (Argonne National Laboratory). 2014. The Greenhouse Gases, Regulated Emissions, and Energy Use in Transportation (GREET) Model, GREET 1 2014.

Beychok, M. 2011. Petroleum crude oil. In: *The Encyclopedia of Earth.* C.M Hogan (editor).

Biagini E., Tognotti, L. 2014. A generalized correlation for coal devolatilization kinetics at high temperature. Fuel Processing Technology 126, 513–520.

BNSF Railway. 2013. Guide to Coal Mines, BNSF Railway, Fort Worth, Texas, USA June 12, 2013.

Brandt, A.R., Farrell, A.E., 2007. Scraping the bottom of the barrel: greenhouse gas emission consequences of a transition to low-quality and synthetic petroleum resources. Climatic Change 84, 241–263.

Brandt, A., 2008. Converting oil shale to liquid fuels: Energy inputs and greenhouse gas emissions of the Shell in situ conversion process. Environ. Sci. Technol. 42 (19), 7489-7495.

Brandt A.R. 2009. Converting oil shale to liquid fuels with the Alberta Taciuk processor: energy inputs and greenhouse gas emissions. Energ. Fuel. 23, 6253-6258.

Brandt, A.R. Unnsach S. 2010. Energy intensity and greenhouse gas emissions from thermal enhanced oil recovery. Energ Fuel. 24, 4581-4589.

Brandt A.R., Englander, J., Bharadwaj, S., 2013. The energy efficiency of oil sands extraction: Energy return ratios from 1970 to 2010. Energy 55, 693-702.

British Petroleum (BP) 2014. BP Statistical Review of World Energy June 2014.

Chern, J-S., Hayhurst, A.N. 2006. A model for the devolatilization of a coal particle sufficiently large to be controlled by heat transfer. Combust. Flame 146, 553–571.

Clendenin, J.D., Barclay, K.M., Donald, H.J., Gillmore, D.W., Wright C.C. 1945. Thermal and electrical properties of anthracite and bituminous coals. Paper 1, Transactions of the 7th annual anthracite conference of Lehigh University, May 5 – 6. Bethlemehm, PA, 1945.

Cleveland, C.J., 2005. Net energy from the extraction of oil and gas in the United States. Energy 30(5), 769-782.

Flores, R.M, 1998. Coalbed methane: from hazard to resource. International Journal of Coal Geology, 35(1-4), 3-26.

Gloyn, R.W., Tabet, D.E., Tripp, B.T., Bishop, C.E., Morgan, C.D., Gwynn, J.W., Blackett, R.E. 2003. Energy, Mineral, and Ground-Water Resources of Carbon and Emery Counties, Utah. Utah Geological Survey, Bulletin 132.

Hucka, B.P. 1991. Analysis and Regional Implication of Cleat and Joint systems in Selected Coal Seams, Carbon, Emery, Sanpete, Sevier, and Summit Counties, Utah. Utah Geological Survey Special Study 74.

Israel Energy Initiatives (IEI). 2014.

Inman, M. 2013. The true cost of fossil fuels. Scientific American 308, 58-61.

Jaramillo, P., Griffin, W.M. Matthews, H.S. 2008. Comparative analysis of the production costs and life-cycle GHG emissions of FT liquid fuels from coal and natural gas. Environ. Sci. Technol. 7559-7565.

Jordan Oil Shale Company (JOSCO). 2014.

Kelly, K.E., Wilkey, J.E., Spinti, J.P., Ring, T.A., Pershing, D.W. 2014. Oxyfiring with CO_2 capture to meet low-carbon fuel standards for unconventional fuels from Utah. Int. J. Greenhouse Gas Control 22, 189–199.

Kobayashi, H., Howard, J.B., Sarofim. A. F. 1976. *Coal* devolatilization at high temperatures. Proceedings of the 16th International Symposium on Combustion. The Combustion Institute.

Keith, A.C. 1989. Coal Quality Characteristics of Utah's Coal Beds in and Near Potentially Producible Coal Tracts. Utah Geological Survey, Reports of Investigation 219.

Lee, A.L. 1968. Heat capacity of coal. In: ACS Annual Meeting, Fuel Section, Atlantic City, September 11, 1968.

MacDonald R.A., Callanan J.E., McDermott, K.M. 1987. Heat capacity of a medium-volatile bituminous premium coal from 300 – 530 K. Comparison with a high-volatile non-premium coal. Energ. Fuel 1, 535-540.

McKellar, J.M., Charpentier, A.D., Bergerson, J.A., MacLean, H.L., 2009. A life cycle greenhouse gas emissions perspective on liquid fuels from unconventional Canadian and US fossil sources. Int. J. Global Warming 1(1/2/3), 160-178.

Merrick D., 1983. Mathematical models of the thermal decomposition of coal. Fuel 62, 540 – 546.

Mulchandani, H., Brandt, A.R. 2011. Oil shale as an energy resource in a CO_2 constrained world: the concept of electricity production with in situ carbon capture. Energ. Fuel 25, 1633-1641.

Radovic, L.R. 1992. Energy and Fuels in Society, McGraw-Hill, New York.

Searchinger, T., Heimlich, R., Houghton, R.A., Dong, F., Elobeid, A., Fabiosa, J., Tokgoz, S., Hayes, D., Yu, T-H. 2008. Use of U.S. croplands for biofuels increases greenhouse gases through emissions from land-use change. Science 319, 1238-1240.

Spath P.L., Mann, M.K. 2000. Life Cycle assessment of a NG Power Generation System, National Renewable Energy Laboratory, Golden, CO.

Smith, K.L., Smoot, D.L., Fletcher T.H, Pugmire, R.J. 1994. The Structure and Reaction Processes of Coal. Plenum Press, New York.

Smith, P.J., Deo, M., Eddings, E.G., Hradisky, M., Kelly, K.E., Krumm, R., Sarofim, A.F., Wang, D. 2015. Underground Coal Thermal Treatment, Task 6 Topical Report, Utah Clean Coal Program. DOE Award Number: DE-NT0005015.

Utah Division of Oil Gas & Mining (UDOGM). 2014. Oil and gas well file search.

US Energy Information Administration (US EIA). 2014. Effect of Increased Natural Gas Exports on Domestic Energy Markets.

US Energy Information Administration (US EIA). 2013. Recoverable Coal Reserves.

US Energy Information Administration (US EIA). 2011. Subbituminous and bituminous coal dominate U.S. Coal Production, August 16, 2011.

US EPA. 2009. Lifecycle Greenhouse Gas (GHG) Emissions Results Spreadsheets, Docket ID: EPA-HQ-OAR-2005-0161-0938.

Wang, M., Lee, H., Molburg, J. 2004.Allocation of energy use in petroleum refineries to petroleum products implications for life-cycle energy use and emission inventory of petroleum transportation fuels. Int. J. LCA 9 (1) 34–44.

Wang, M., Han J., Dunn, J.B., Cai, H. Elgowainy A. 2012. Well-to-wheels energy use and greenhouse gas emissions of ethanol from corn, sugarcane and cellulosic biomass for US use. Environ. Res. Lett. 7, 045905.

Wellington, S., Vinegar, H., Berchenko, B., Maher, K., DeRouffignac, E., Karanikas, J., Zhang E. 2000. Emissionless energy recovery from coal, US Provisional Patent Application 33,482.

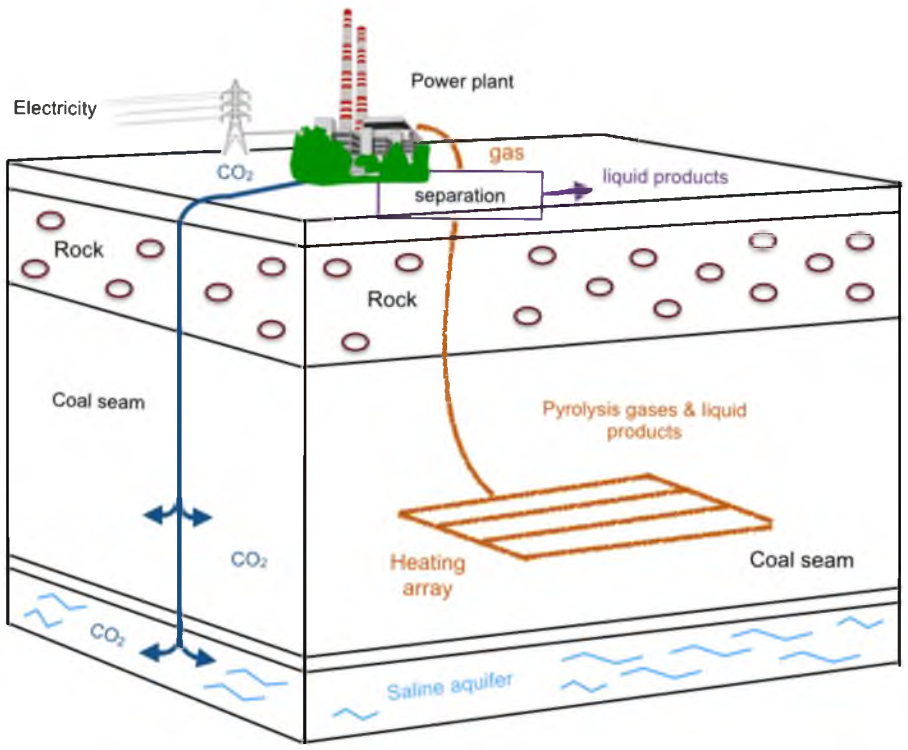

Figure 4.1 Example of a UCTT process.

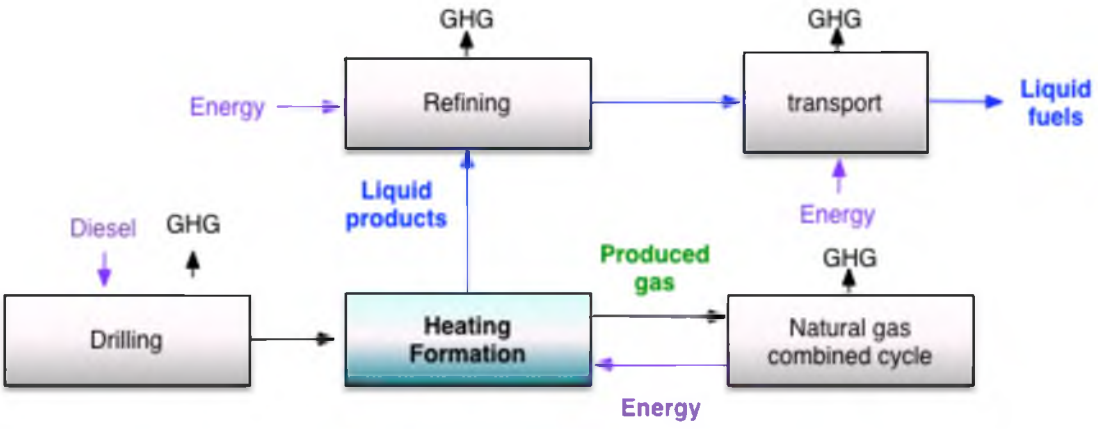

Figure 4.2 System boundaries for the analysis of UCTT. The colored box indicates that heating the formation is critical to the analysis.

Table 4.1 Sufco coal properties. These are presented on a dry ash free basis. This is based on the average of 6 samples. The average moisture content is 3.21% and the average ash content is 5.04%.

Fixed carbon (%)	Heating value (MJ/kg)	Carbon (%)	Hydrogen (%)	Nitrogen (%)	Oxygen (%)	Sulfur (%)
54.75	32.7	78.46	5.61	1.72	13.56	0.65

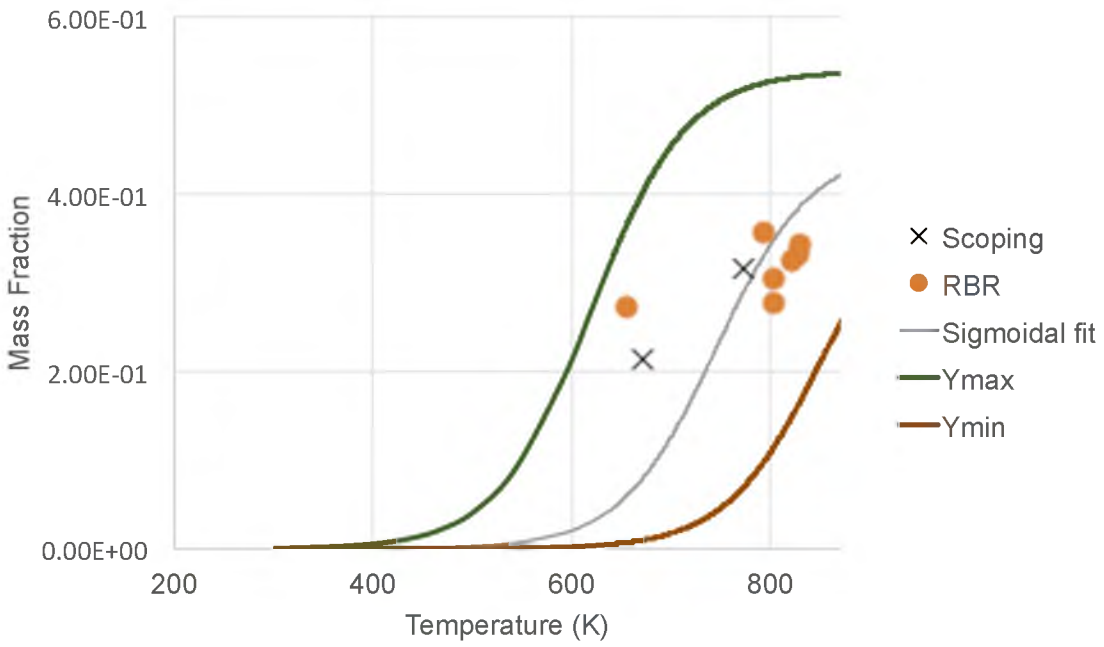

Figure 4.3 Sigmoidal fit of the scoping experimental results, with the larger scale (RBR) experiments, minimum yield (Ymin) and maximum yield (Ymax) functions also shown.

Table 4.2 Emission factors, coal properties, and selected parameters used in the sensitivity analysis.

Process	Baseline	Max NER	Min NER	Max Yield	Min Yield	10% water	20% water	Enhanced k
Coal moisture	3.2 %	3.2%	3.2%	3.2%	3.2%	10%	20%	3.2%
Background temperature (°C)	20	20	20	20	20	20	20	20
Drilling diesel fuel consumption (l/m)	12.4[1]	12.4[1]	12.4[1]	12.4[1]	12.4[1]	12.4[1]	12.4[1]	12.4[1]
Heating the formation								
k coal (W/mK)	0.29	0.29	0.29			0.29	0.29	0.87
k char (W/mK)[2]	0.484	0.484	0.484			0.484	0.484	1.7
Maximum yield (%)	45.25	50	40			45.25	45.25	45.25
Liquid product (%)	50	60	40			50	50	50
Yield model	3	4	5	6	7	3	3	3
Refining (MJ/kg crude)[8]	3.2	2.88	3.52			3.2	3.2	3.2
Transport (J/MJ)[8]	6720	6720	6720			6720	6720	6720
Efficiency of NGCC electricity generation	50%	50%	50%			50%	50%	50%

1 (UDOGM 2012).

2 At 600°C.

3 $Yield = \frac{0.4525}{1+e^{0.02096(472-Temp)}}$ (baseline yield model).

4 Baseline yield model (footnote 3) with a maximum yield of 0.5.

5 Baseline yield model (footnote 3) with a maximum yield of 0.4.

6 $Yield = \frac{0.54}{1+e^{0.02096(437-Temp)}}$ (maximum yield model).

7 $Yield = \frac{0.42}{1+e^{0.02096(577-Temp)}}$ (minimum yield model).

8 ANL (2014).

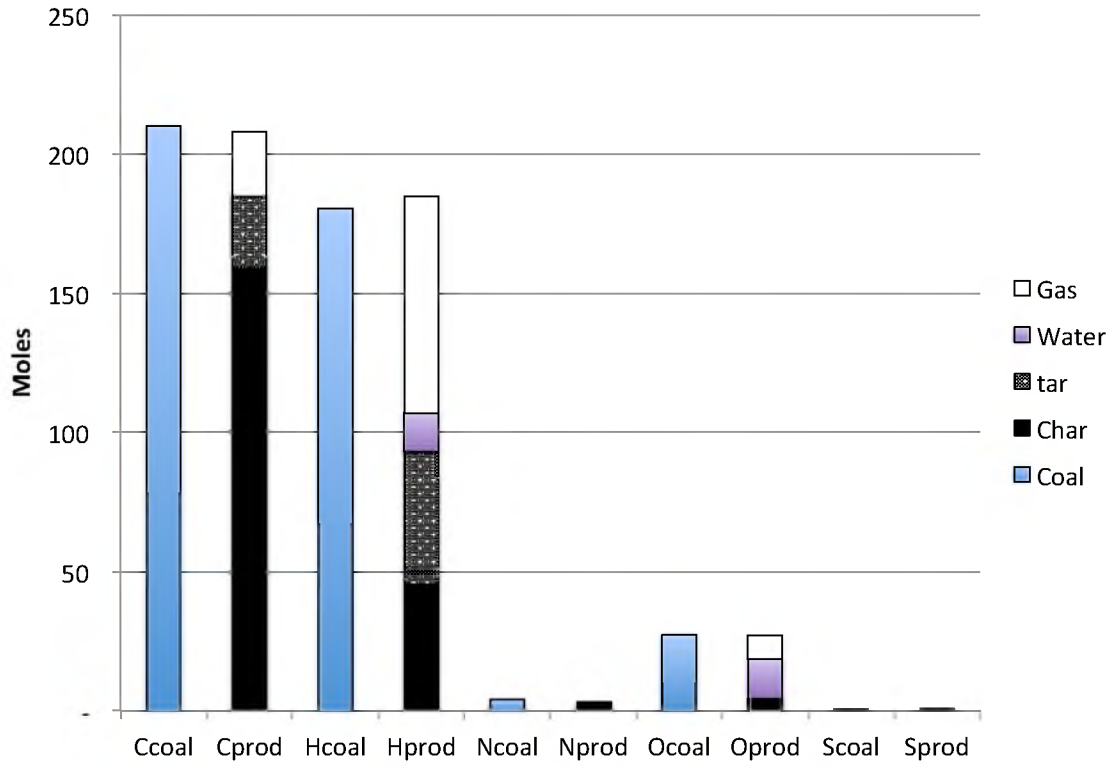

Figure 4.4 Moles of carbon (C), hydrogen (H), nitrogen (N), oxygen (O), and sulfur (S) in the original coal (as received) and in the char, tar, and gas. The coal was heated to an internal temperature of 540°C at ambient pressure and held for 3 hours.

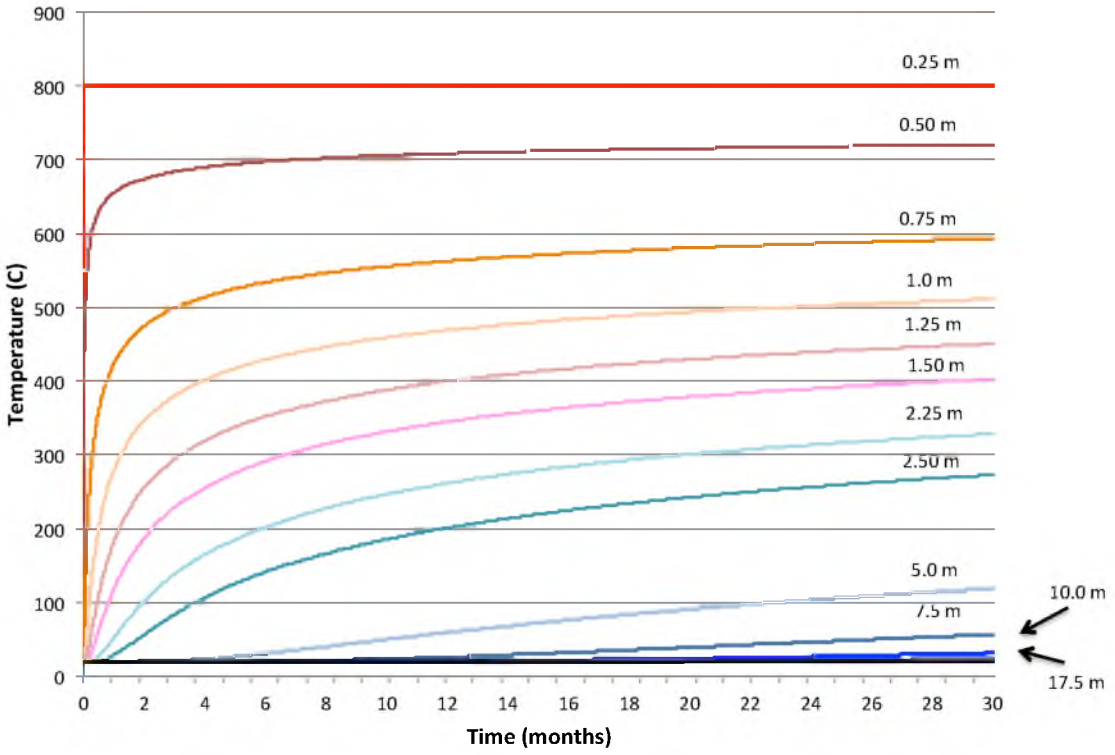

Figure 4.5 Temperature profile at various radial distances from the heater (distance 0.25 m increments) at a 2.5-year heating period for the baseline case.

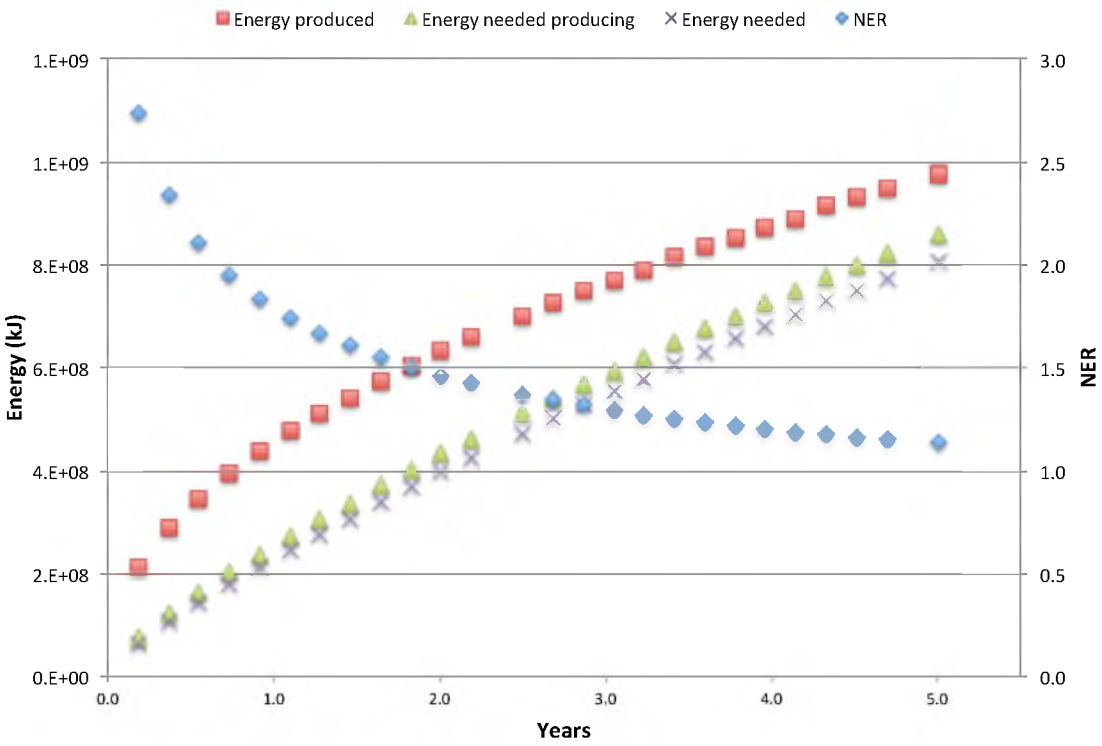

Figure 4.6 Energy produced, energy required, energy required with simultaneous production, and NER as a function of time for the process of heating the formation.

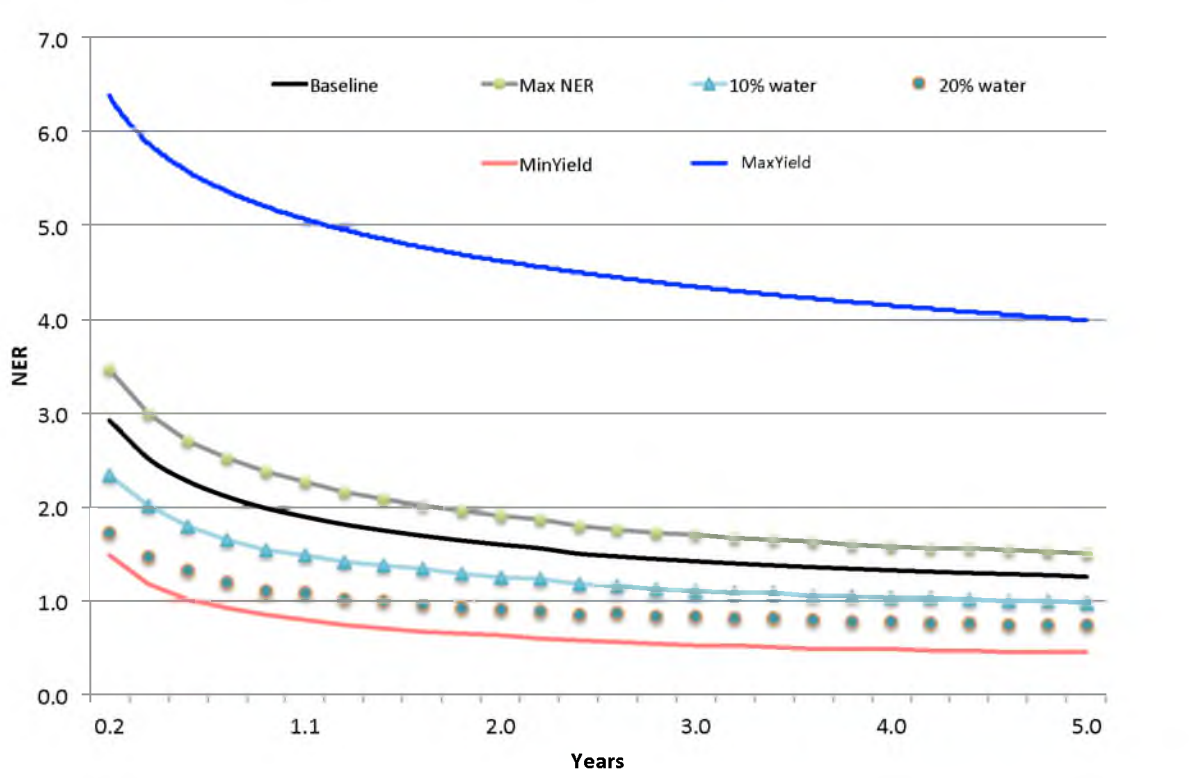

Figure 4.7 Comparison of NERs for the process of heating the coal formation.

Table 4.3 Summary of WTP NER and NEER values at 2.5 and 5 years of UCTT production.

	Baseline	Max NER	Min NER	10% Water	20% Water	Min yield	Max yield
2.5 years							
NER	1.26	1.58	1.04	1.01	0.75	0.51	3.22
NEER	1.11	1.51	0.82	0.86	0.61	0.40	4.24
5 years							
NER	1.06	1.13	0.87	0.84	0.62	0.39	2.96
NEER	1.01	1.27	0.74	0.77	0.54	0.3	3.66

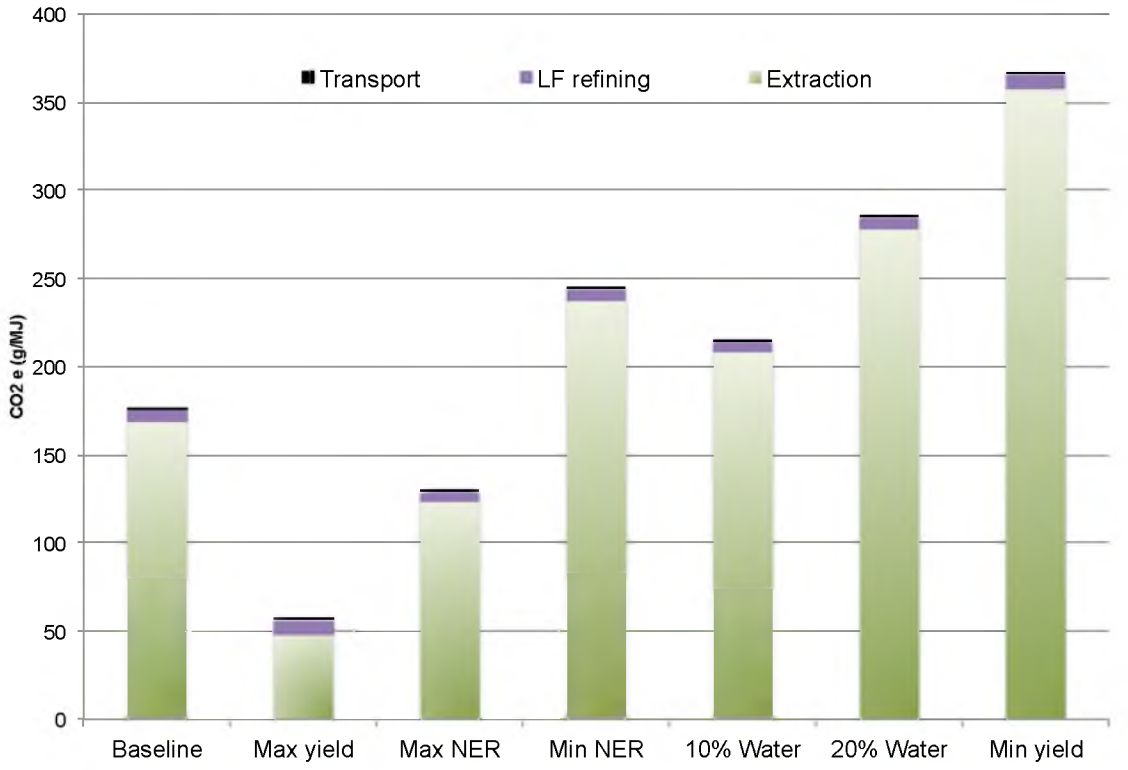

Figure 4.8 GHG emissions (CO_2 e) from baseline, maximum yield, NER max, NER min, 10% water, and 20% water cases at a 2.5-year heating period.

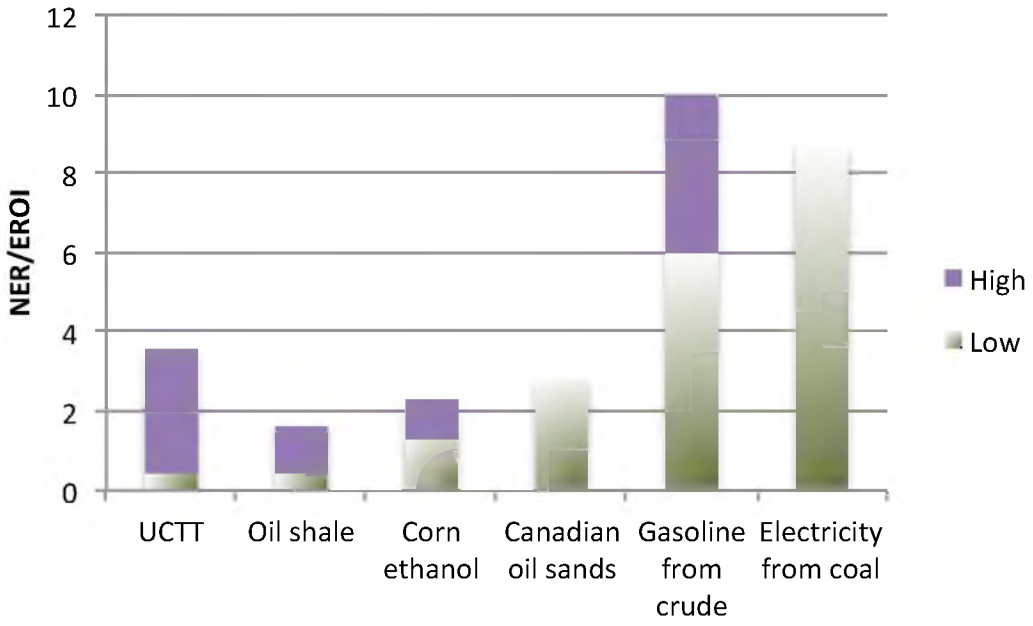

Figure 4.9. NER/EROI for gasoline produced from the UCTT process, oil shale (Kelly et al. 2014), corn ethanol (Wang et al. 2012, Inman 2013), Canadian oil sands (Brandt et al. 2013), conventional crude (Cleveland 2005), and electricity generated from coal (Inman 2013).

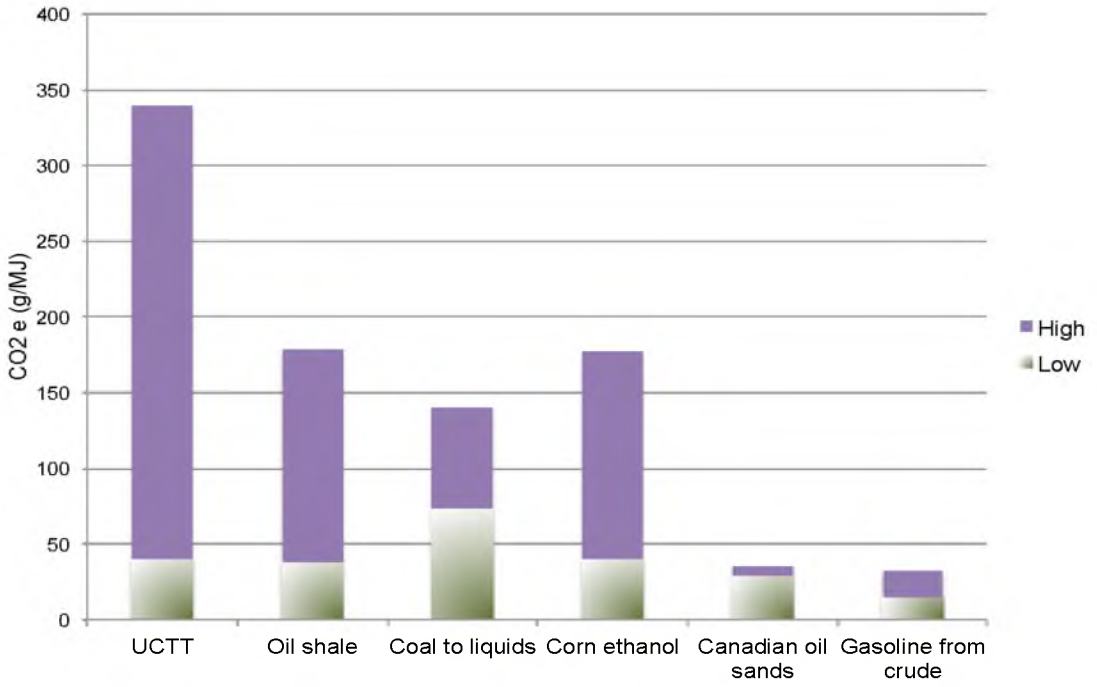

Figure 4.10. Range of CO_2 emissions per MJ of transportation fuel for UCTT, oil shale (low for Shell's in situ conversion process (Brandt 2008) and high for ex situ shale, (Brandt and Farrell 2007)), diesel produced from coal via the Fischer Tropsch process (Jaramillo et al. 2008), corn ethanol (Searchinger et al. 2008, Wang et al. 2012), Canadian oil sands (McKellar et al. 2009), and gasoline from crude oil (McKellar et al. 2009).

CHAPTER 5

CONCLUSIONS

This research evaluates three GHG mitigation strategies: (1) aqueous CO_2 mineralization, (2) oxyfiring for unconventional transportation fuels, and (3) UCTT. Each evaluation includes quantitative consideration of all major energy and GHG flows as well as a qualitative consideration of other potential environmental barriers.

5.1 Aqueous CO_2 mineralization

This first evaluation was based entirely on literature data. It indicated that once the full-life cycle material and energy balances are considered, this technology has limited near-term applicability on a large scale. It illustrates the importance of considering comprehensive system boundaries (in this case, including the manufacture of caustic) as well as the importance of the proposed process's scale to the evaluation.

5.2 Oxyfiring for CO_2 capture

The evaluation of oxyfiring to help unconventional crude sources meet a low-carbon fuel standard (2) showed that this strategy is feasible and could allow unconventional energy resources to meet a low-carbon fuel standard. However, it will

likely place these fuels at a competitive pricing disadvantage compared to more traditional sources of crude oil.

5.3 UCTT

The evaluation of UCTT relied heavily on experiments performed at the University of Utah. The results suggest that UCTT has a limited potential as a CO_2 mitigation strategy because of the large energy "losses" to the coal formation and consequently the large GHG emissions. This is primarily caused by large volumes of coal heated to low temperatures, which results in limited product. Furthermore, the feasibility of UCTT is highly dependent on the coal's low-temperature yields and its moisture content.

APPENDIX

SUPPLEMENTARY MATERIAL FOR CHAPTER 4

A.1 Measurements of coal/char heat capacity

Heat capacity measurements included four raw coal samples and six char samples that had been heated to approximately 540°C in the large-scale reactor at ambient pressure. Table A.1 presents the results. The raw coal samples were heated at 5°C /min from ambient temperature up to 350 °C. Because of the release of the volatiles, it is not possible to calculate heat capacity at temperatures above 80°C. For raw coals, the calculated heat capacities range from 1.21 – 1.28 J/g°C (Table A.1). For comparison purposes, MacDonald et al. (1987) report a heat capacity of 1.18 for a high-volatile bituminous coal from the Juanita C steam in Colorado. The char samples were heated at 5°C /min to a temperature of 500 5°C /min, and heat capacities of the char range from 1.01 – 1.92 J/g°C. This large variation may be due to heterogeneity in the coal/char samples as well as uncertainties associated with the measurement methods. The heat flow profiles periodically exhibited small excursions, which affect the calculated heat capacity. Consequently, we selected temperature ranges for the calculation of heat capacity in regions without excursions. It was difficult to obtain heat capacity measures at temperatures above 400 °C.

There are conflicting reports about the effect of temperature on heat capacity. Most studies suggest that heat capacity increases with temperature up to approximately 600 C (Merrick 1983, MacDonald et al. 1987), with heat capacity increasing from roughly 1.1 kJ/kg°C to slightly more than 2 kJ/kg C. However, Lee (1968) reports that heat capacity of coal decreases as temperature increases above 300°C. Measurements of heat capacity are complicated by the pyrolysis reactions.

A.2 Coal thermal conductivity

Figure A.1 shows the temperatures inside the coal chunks at two different distances from the heater in the rubblized bed reactor. These results are used to estimate thermal conductivity.

Assuming that the thermal conductivity is a linear function of temperature.

$$k = aT + b$$

where,

k = thermal conductivity, W/m K

T = temperature, K

a and b are constants

At ambient temperature (22°C), the thermal conductivity of raw coals range from 0.22 – 0.55 W/m K, and two Utah high-volatile subbituminous coals from Blind Canyon and Sunnyside ranged from 0.27 – 0.31 W/m K (Herrin and Deming 1996). These coals had low moisture content, 3.2 and 4.8%, respectively. Consequently, we use an initial k of 0.29 W/m K at 298 K, and $0.29 = 298a + b$

Heat transfer in the coal is given by:

$$Q = -kA\frac{dT}{dx}$$

Integrating

$$Q\int_{x_1}^{x_2} dx = -A\int_{T_1}^{T_2} (aT + b)dT$$

$$\frac{Q}{A} = \frac{\frac{a}{2}(T_1^2 - T_2^2) + b(T_1 - T_2)}{(x_2 - x_1)}$$

where, x = distance from the heater, x_1=0 cm, , x_2=3.8 cm, and , x_3=5.1 cm,

T= measured temperature, K, T1= 1073 K, T2 = 853, T3 = 817 K

At steady state, Q/A is constant and

$$\frac{\frac{a}{2}(T_1^2 - T_2^2) + b(T_1 - T_2)}{(x_2 - x_1)} = \frac{\frac{a}{2}(T_2^2 - T_3^2) + b(T_2 - T_3)}{(x_3 - x_2)}$$

$$\frac{\frac{a}{2}(T_1^2 - T_2^2) + (0.29 - 298a)(T_1 - T_2)}{(x_2 - x_1)} = \frac{\frac{a}{2}(T_2^2 - T_3^2) + (0.29 - 298a)(T_2 - T_3)}{(x_3 - x_2)}$$

solving for a yields 3.37 x 10^{-4} W/m K^2, and b = 0.19 W/m K.

$$k = 3.37 \times 10^{-4} T + 0.19$$

Thus, at a midpoint temperature of 963 K (half-way between the heater and the thermocouple located at 3.8 cm), k = 0.515 W/m K. This is slightly lower than ranges reported in the literature (Chern and Hayhurst 2006).

A.3 Yield model

This section provides details about the yield models selected for the yield analysis. Figure 4.3 shows the predicted yields for a sigmoidal function, the fitted Yamamoto model (fitted for Sufco coal at a heating rate of 5 x 10^{-3} K/s), and a maximum

and minimum yield model, with the overlaid experimental results. The RBR and scoping results in Figure 4.3 are final yields and are not a function of time. In each experiment, the coal is heated to its final temperature and held at this temperature for several hours (Smith et al. 2015). It should be noted that limited literature data exist for yields at the very low heating rates that would be used in the UCTT process. The lowest heating rates for typical pulverized coal devolatilization models are several orders of magnitude greater than those for the proposed UCTT process. The sigmoidal fit was:

$$Yield = \frac{Yield_{max}}{1 + e^{0.02096(472 - Temp)}}$$

where,

Yield = the fraction of the coal that is volatilized on an as received basis.

$Yield_{max}$ = the maximum yield, from the proximate analysis = 0.4525 (as received).

Temp = temperature, °C.

For the sensitivity analysis, a minimum and maximum yield function were considered. The minimum yield function was:

$$Yield = \frac{Yield_{max}}{1 + e^{0.02096(577 - Temp)}}$$

$Yield_{max}$ = the maximum yield, from the proximate analysis = 0.42 (as received).

Temp = temperature, °C.

The maximum yield function was:

$$Yield = \frac{Yield_{max}}{1 + e^{0.02096(437 - Temp)}}$$

$Yield_{max}$ = the maximum yield, from the proximate analysis = 0.54 (as received).

Temp = temperature, °C.

The fitted Yamamoto 1-step devolatilization model (Yamamoto et al. 2011) is given by:

$$\frac{d_{vol}}{dt} = Fk_0 \exp\left(\frac{-E_v}{RT_p}\right) m_{vol}$$

and

$$F = \exp\left(\sum_{i=0}^{5} c_i G_v^i\right)$$

where k_o is the frequency factor, E_v is the activation energy, R is the ideal gas constant, T_p is the particle temperature, and m_{vol} is the mass fraction of volatiles. F is the modification factor of the frequency factor and is a function of the fraction of the mass devolatilized. It is given by:

$$G_v = \frac{m_{vol,0} - m_{vol}}{m_{vol,0}}$$

where,

$m_{vol,0}$ = the initial mass of volatile matter, 0.4525 (measured).

The c_i terms are determined by Fletcher by minimizing the difference between the CPD model (Fletcher et al. 1992) developed for a Sufco Coal and the Yamamoto model at a heating rate of 5 x 10^3 K/s. The c_i parameters are 5.775, -31.25, 66.97, -71.74, 24.76, -3.5 x 10^{-7}. We then obtained the k_o and E_v terms to best fit the scoping experimental data (k_o = 1 x 10^6 and E_v = 1870 J/mol).

A.4 Liquid product quality

Figure A.2 shows the simulated distillation results from the liquid product sample (heater set at 800°C and coal internal average temperature of 540 C) from the RBR, and

Figure A.3 shows a crude reference simulated distillation results obtained by the same method. The liquid products were collected in a series of bubblers filled with isopropyl alcohol. The figures illustrate that the UCTT product is light-crude like, but it contains doublets, which means that many of the carbon peaks show both a single and double-bonded species, i.e., decane and decene, whereas the crude reference sample does not tend to show doublets, i.e., only decane. Consequently, the UCTT product is less saturated and more reactive than conventional crude, which is not unexpected from a thermally derived product.

Figure A.3 shows that the most common species in the product mix range from c8-c15. Although the single-carbon number results indicate assume that 100% detection, and the sample likely contains 20% residual, it still provides a good indication of the product composition.

A.5 Properties of the coal, char, and UCTT product

In the simulations, all properties of interest - density, heat capacity, thermal conductivity, and thermal diffusivity - change as a function of temperature and coal conversion, which is also a function of temperature. The properties remain constant until 234 C, one degree above the temperature at which water evaporates at 30 bar. Coal is converted to product, and yield is given by the following relationship (Section A.3):

$$Yield = \frac{Yield_{max}}{1 + e^{0.02096(472 - Temp)}}$$

where,

Yield = the fraction of the coal that is volatilized on an as received basis.

$Yield_{max}$ = the maximum yield, from the proximate analysis = 0.4525 (as received)

Temp = temperature, °C

At full conversion, approximately 55% char is present along with 22.5% gas and 22.5% liquid. As coal is converted to char and liquid and gas products, the properties change as a weighted average of the composition. The gas product is assumed to be a mixture of 30% CH4, 30% CO_2, 30% C_2H_6, and 10% water, based on the experimental results. The liquid properties are based on the single-carbon number analysis of the liquid product (Figure A.4). The Peng-Robertson Polar properties from ProMax™'s process simulator provided the liquid and gas properties as a function of temperature at 30 bar. The ultimate liquid product is not necessarily a liquid at the temperatures and pressure present in the heated formation, and the distribution between gas and liquid phase is also considered automatically in the aggregate properties of the liquid product from ProMax™.

A.5.1 Density

The density of the coal is constant at 1310 kg/m^3 until 234°C, when density is given by (Figure A.5):

$$\rho = 0.00281 \times T^2 - 4.54 \times T + 2345$$

where,

ρ = density, kg/m^3.

T = temperature, °C.

A.5.2 Thermal conductivity

For the baseline case, the thermal conductivity of the coal/char was extracted by the experimental results and is given by (described above):

$$k = 3.37 \times 10^{-4} T + 0.19$$

where,

T= temperature, K.

k = W/m K.

The thermal conductivity of the aggregate is given by (Figure A.6):

$$k = -6.13 \times 10^{-7} T^2 + 4.67 \times 10^{-4} T + 0.281$$

where,

T= temperature, °C

k = W/m K.

For the enhanced conductivity case, the coal thermal conductivity is 0.87 kJ/kg°C (Wellington et al. 2000) and the char thermal conductivity is 1.7 kJ/kg°C (Chern and Hayhurst 2006).

A.5.3 Heat capacity

The measured heat capacity of the coal/char is 1.25 J/g°C at 25°C and it increases to1.41 J/g°C at 540°C. Above 233°C, the heat capacity of the aggregate is given by (Figure A.7):

$$C_p = 2.61 \times 10^{-6} T^2 - 1.03 \times 10^{-4} T + 1.23$$

where,

T= temperature, °C.

C_p = heat capacity, J/g°C

A.5.4 Diffusivity

Diffusivity is calculated from density, heat capacity, and thermal conductivity by:

$$\alpha = \frac{k}{\rho C_p}$$

where,

k = thermal conductivity, W/m°C.

ρ = density, kg/m^3.

C_p = heat capacity, kJ/g°C.

α = thermal diffusivity, m^2/s.

Above the 233°C, the diffusivity of the aggregate is given by:

$$\alpha = 4.12 \times 10^{-12} T^2 - 1.15 \times 10^{-9} T + 2.31 \times 10^{-7}$$

See Figure A.8.

A.6 References

Chern, J-S., Hayhurst, A.N. 2006. A model for the devolatilization of a coal particle sufficiently large to be controlled by heat transfer. Combust. Flame 146, 553–571.

Fletcher, T.H., Kerstein, A.R., Pugmire, R.J., Solum, M.S., Grant, D.M. 1992. A chemical percolation model for devolatilization: 3. chemical structure as a function of coal type. Energ. Fuels, 6, 414-422.

MacDonald, R.A., Callanan, J.E., McDermott, K.M. 1987. Heat capacity of a medium-volatile bituminous premium coal from 300 – 530 K. Comparison with a high-volatile non-premium coal. Energ. Fuels 1, 535-540.

Lee, A.L. Heat Capacity of Coal. ACS Annual Meeting, Fuel Section, Atlantic City, September 1968.

https://web.anl.gov/PCS/acsfuel/preprint%20archive/Files/12_3_ATLANTIC%20CITY_09-68_0019.pdf

Merrick D. 1983. Mathematical models of the thermal decomposition of coal. Fuel 62, 540-546.

Smith, P.J., Deo, M., Eddings, E.G., Hradisky, M., Kelly, K.E., Krumm, R., Sarofim, A.F., Wang, D. 2015. Underground Coal Thermal Treatment, Task 6 Topical Report, Utah Clean Coal Program. DOE Award Number: DE-NT0005015.

Wellington, S., Vinegar, H., Berchenko, B., Maher, K., DeRouffignac, E., Karanikas, J., Zhang E. 2000. Emissionless energy recovery from coal, US Provisional Patent Application 33,482.

Yamamoto K., Murota, T., Okazaku, T., Tangiguchi, M. 2011. Large eddy simulation of a pulverized coal jet flame ignited by a preheated gas flow. Proc. Comb. Inst. 33, 1771-1778.

Table A.1. Heat capacities for coal and char samples and the temperature range over which these heat capacities are calculated.

Sample	Range	Cp (J/g C)
Raw coal	45-75	1.28
Raw coal	35-60	1.21
Raw coal	30-68	1.25
Average		**1.25 ± 0.04**
Char block	200-320	1.04
Char block	280-420	1.92
Char block	80-220	1.32
Char block	200 – 400	1.01
Char block	200 – 400	1.68
Char block	180-360	1.48
Average		**1.41 ± 0.359**

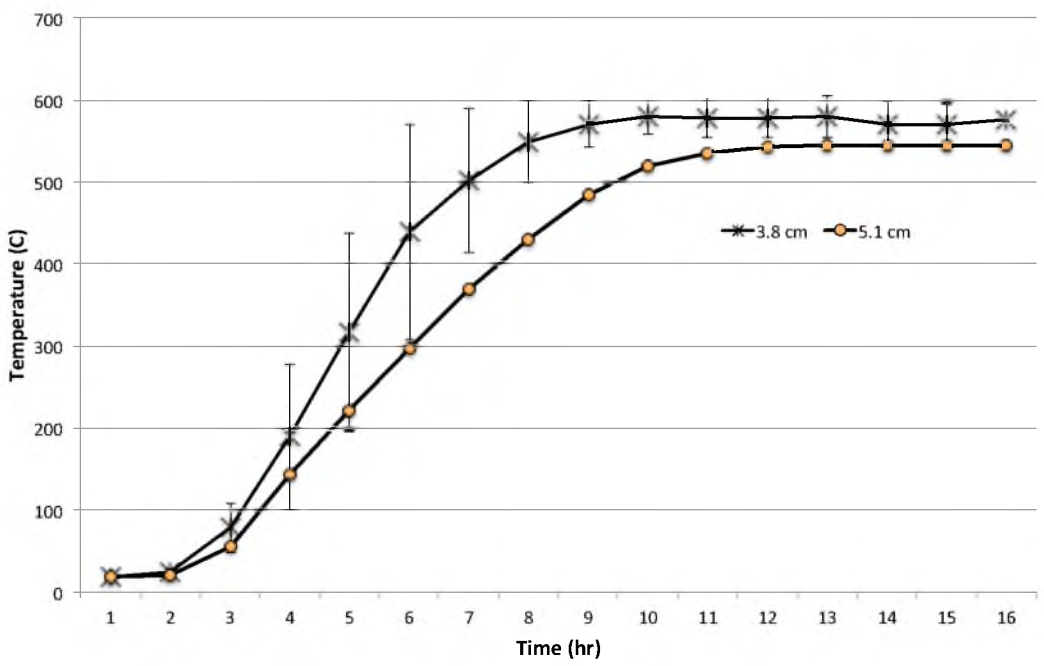

Figure A.1. Temperature measurements at two different distances from the heater. The measurements collected 3.8 cm above the heater are located in the coal chunk, nearest the heater cap, and the measurements collected 5.1 cm above the heater are located in the center coal chunk. Only one measurement was available at 5.1 cm, so error bars are not presented.

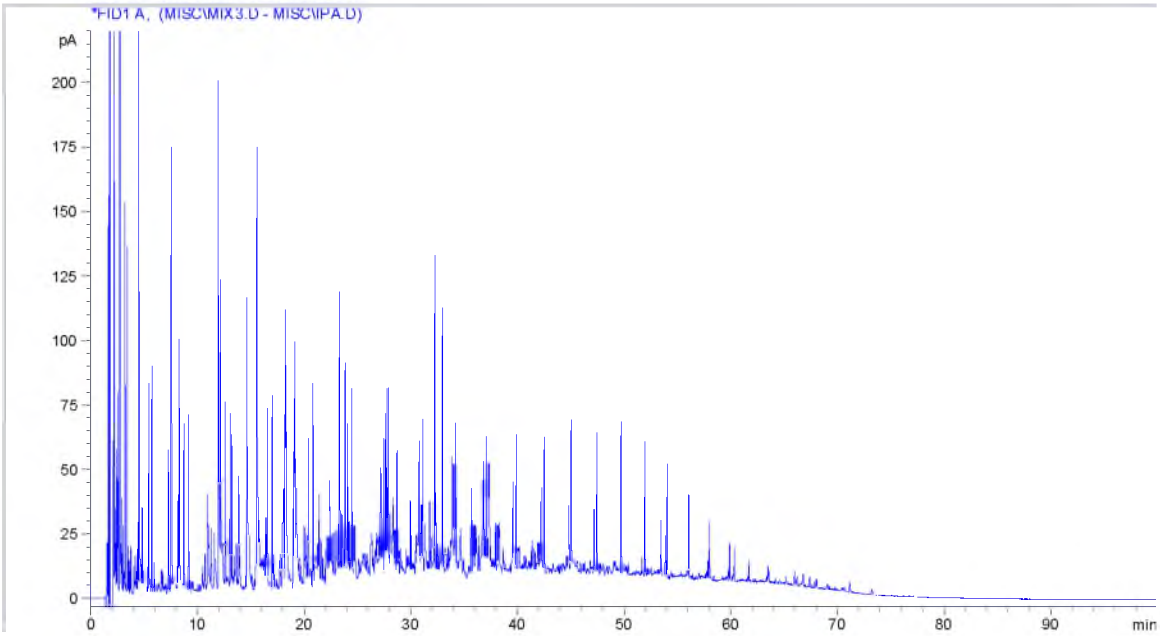

Figure A.2. Gas chromatograph flame-flame ionization detector (GC-FID) analysis of the liquid product from coal heated to an average internal temperature of 540°C. The isopropyl solvent from the bubblers is not shown.

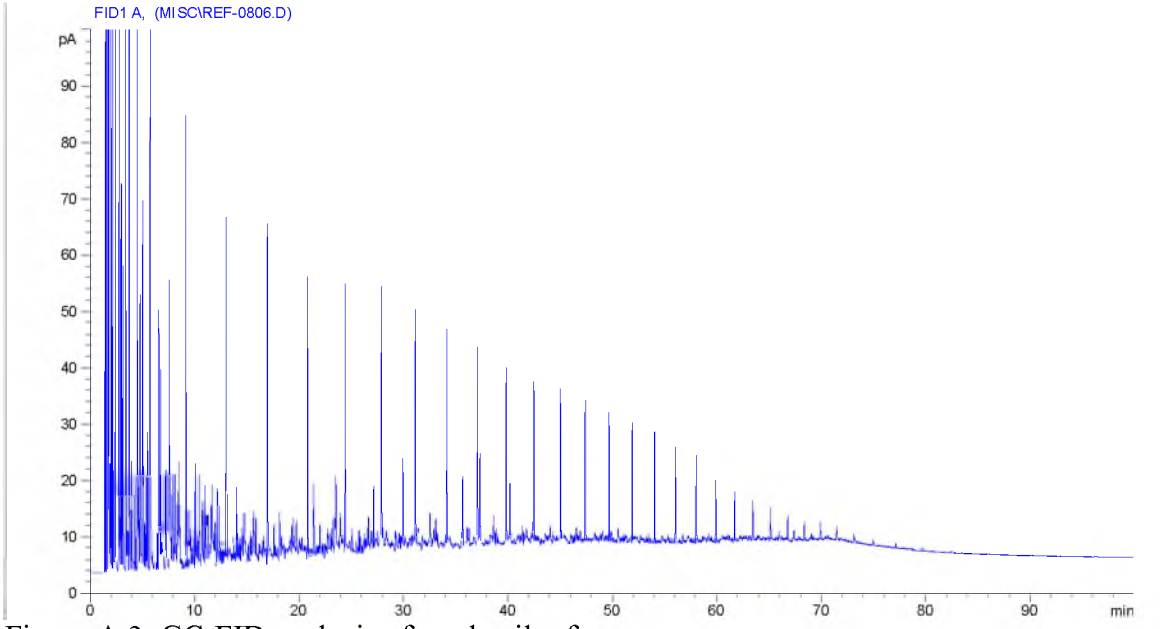

Figure A.3. GC-FID analysis of crude oil reference.

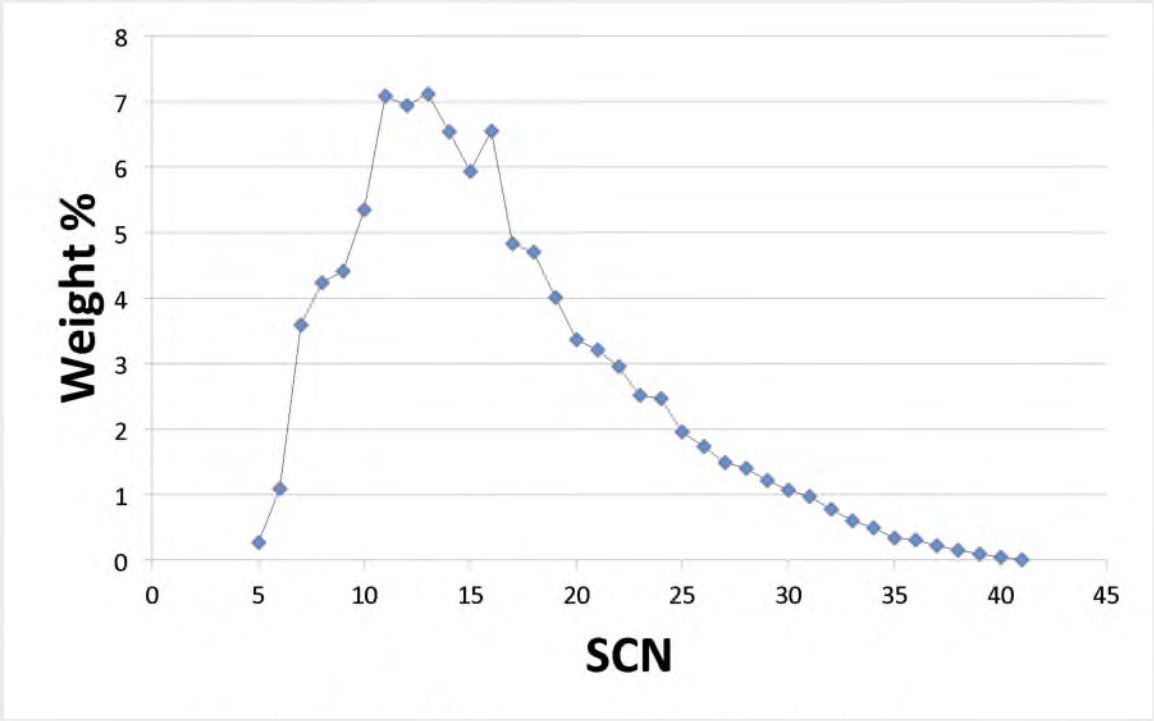

A.4. Single carbon number (SCN) weight distribution.

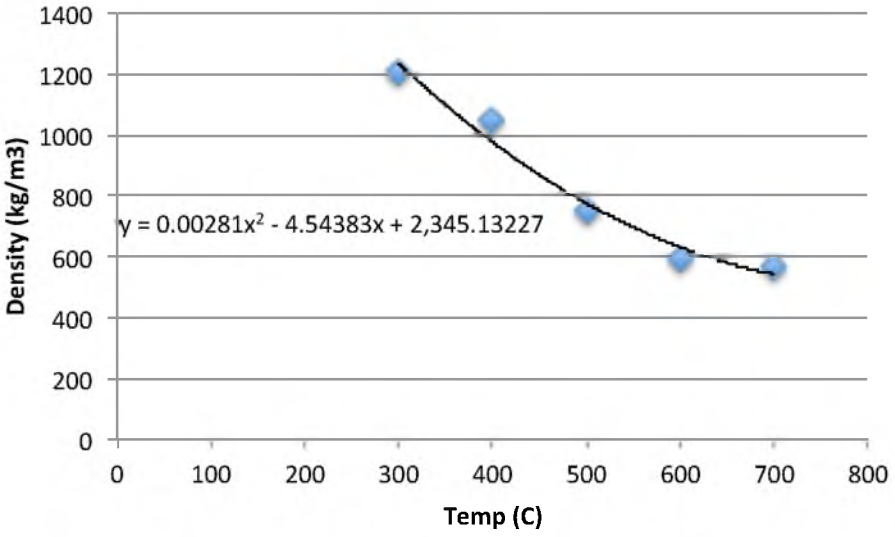

Figure A.5. Density of the coal, char, and product mixture versus temperature.

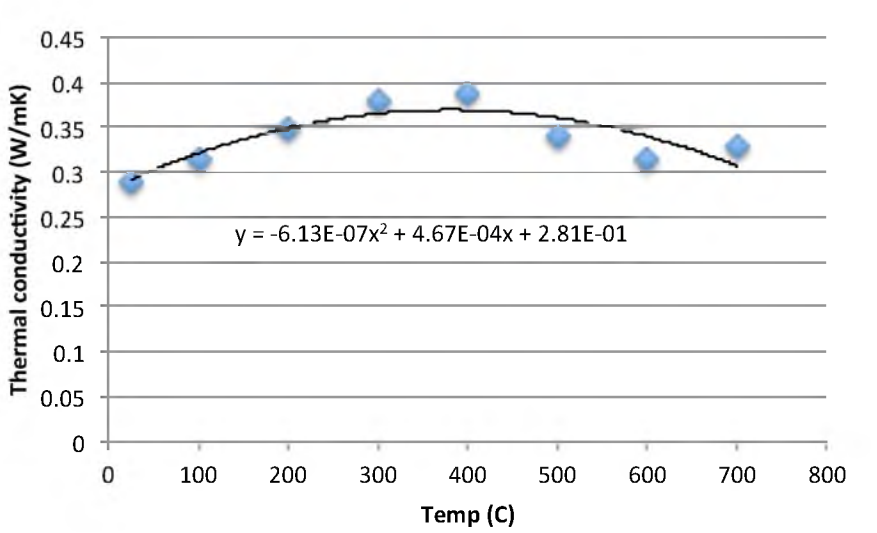

Figure A.6. Thermal conductivity of the coal, char, and product mixture versus temperature.

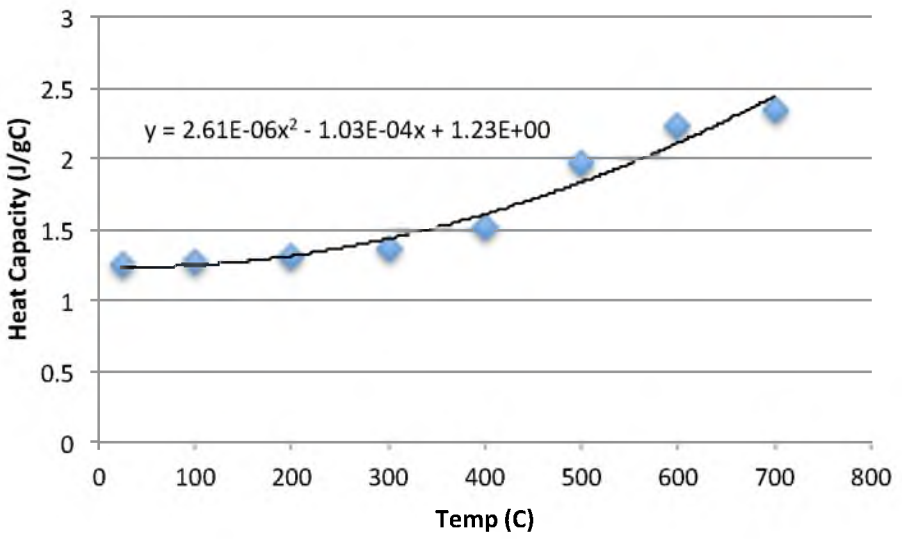

Figure A.7. Heat capacity of the coal, char, and product mixture versus temperature.

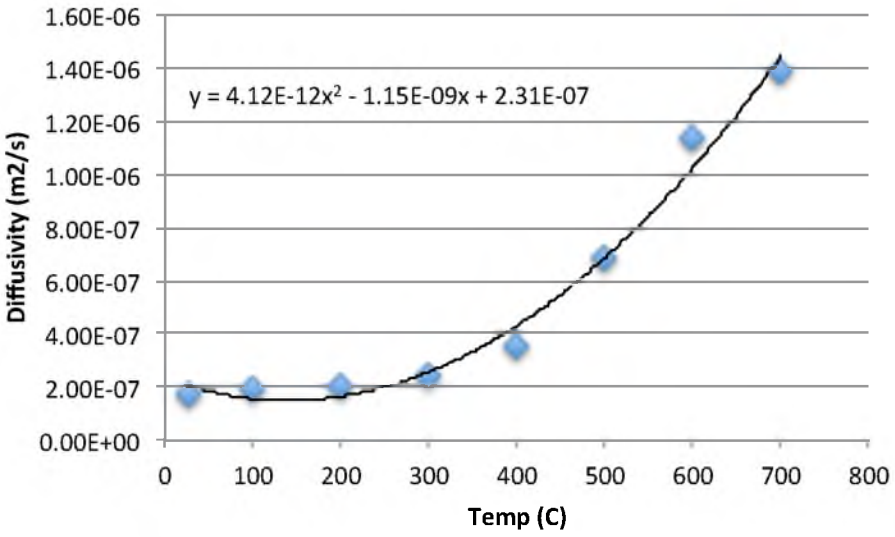

Figure A.8. Thermal diffusivity of the coal, char, and product mixture versus temperature.